Characterization of the Purkinje cell to nuclear cell connections in mice cerebellum

Orçun Orkan Özcan

Ecole Doctorale des Sciences
de la Vie et de la Santé

Albert-Ludwigs-Universität
Freiburg im Breisgau

THÈSE

Présentée par:

Orçun Orkan ÖZCAN

En vue d'obtenir le grade de docteur de l'université de Strasbourg et Freiburg

Spécialité: Neurosciences

Characterization of the Purkinje cell to nuclear cell connections in mice cerebellum

Caractérisation des connexions cellules de Purkinje - cellule des noyaux profonds dans le cervelet de souris

Soutenue le: 20 Mars 2017

THÈSE dirigée par:

Dr. Philippe ISOPE	INCI, Université de Strasbourg
Prof. Dr. Arvind KUMAR	KTH Royal Institute of Technology, Stockholm
Prof. Dr. Ad AERTSEN	Albert Ludwig University of Freiburg

RAPPORTEURS:

Prof. Dr. Chris I. DE ZEEUW	Erasmus Medical Center, Rotterdam
Dr. Yann HUMEAU	IINS, Université de Bordeaux

AUTRES MEMBRES DE JURY :

Dr. Romain GOUTAGNY	LNCA, Université de Strasbourg

This study was carried out as a joint project of the following research institutes:

Physiology of Neural Networks (group of Dr. Philippe Isope)

Institut des Neurosciences Cellulaires et Intégratives, UPR 3212 CNRS

Université de Strasbourg

5 rue Blaise Pascal, 67084 Strasbourg, France

and

Bernstein Center Freiburg (group of Prof. Dr. Ad Aertsen)

Albert-Ludwigs Universität

Hansastrasse 9a, 79104 Freiburg, Germany

TABLE OF CONTENTS

Acknowledgements

I want to thank my primary thesis supervisor, Dr. Philippe Isope gratefully. Since I changed my field, the whole journey of this study was very easy for me and I was lucky to work with Philippe all this time. His support during all the phases of this study made it possible for me to complete it. He was both a good supervisor and a good teacher. He never hesitated to deal with details whenever I needed, from welcoming arrangements to his very valuable reviews on the thesis manuscript.

I want to thank my supervisors, Prof. Dr. Arvind Kumar and Prof. Dr. Ad Aertsen for their important contributions to this study. Their advice and input helped a lot to improve the project. Arvind welcomed me many times in Freiburg and in Stockholm, our meetings always gave new ideas for the analyses. Ad's supervision was also essential to conclude on the findings of this study.

I want to thank my current and previous colleagues who helped me tremendously and made it easier to work for long hours. I was lucky to be in the same team with Kevin, Ludovic, Alvaro, Joseph, Antoine, Anais, Francesca, Elise and Fernando. I will always remember this study together with the times we spent together. Especially, I want to thank Kevin and Ludovic for their support.

I also want to thank Dr. Didier De Saint Jan, Dr. Romain Goutagny and Prof. Dr. Bernard Poulain for their valuable comments on my work during several occasions.

I want to thank my friends Tina, Madalina, Ola, Esra, Gulebru, Semih, Verda and Seher for their support. We shared good and bad times together and their friendship was very important for my life in Strasbourg.

I want to thank the organizers of the NeuroTime program, Dr. Paul Pevet and Dr. Domitille Boudard, who made the necessary funding available for this study.

Summary in French (Résumé)

Le cervelet intègre les commandes motrices ainsi que les informations sensorielles vestibulaires, visuelles et auditives qui interviennent dans les fonctions d'apprentissage et de coordination motrice. L'étape finale de cette intégration s'effectue au sein des noyaux cérébelleux profonds (DCN). Ces derniers reçoivent des projections neuronales des cellules de Purkinje (PC), mais également des fibres moussues et grimpantes. Nous avons étudié les connexions entre les PCs et les différents types cellulaires des DCN par une approche optogénétique *in vivo*, en stimulant le cortex cérébelleux de souris transgéniques L7-ChR2. Cette approche a été couplée à des enregistrements en multi électrode dans deux régions connectées; le lobule IV/V du cortex cérébelleux et le noyau DCN médian. Les cellules enregistrées dans le DCN *in vivo* ont été classées en fonction de la forme et la fréquence de décharge de leurs potentiels d'action, celles-ci correspondant aux propriétés des cellules GABAergiques et non-GABAergiques précédemment décrites par d'autres études *in vitro*. Des potentiels de champ locaux de différentes durées ont été observés. Cependant, les cellules des DCN sont synchronisées uniquement au sein des bandes de fréquence bêta, gamma et hautes fréquences. La stimulation optogénétique a conduit à l'excitation des PCs et à l'inhibition des cellules des DCN (codage en fréquence). D'un point de vue temporel, seul la décharge des cellules non-GABAergiques était affectée par la stimulation. De plus, nous avions prédit l'inhibition locale de la part des cellules GABAergiques, mais ce phénomène n'a pas pu être observée lors des mes expériences *in vivo*. Au final, synchroniser les PCs entraine un codage temporel au sein des réseaux de neurones en sortie du cervelet. La circuiterie neuronale propre au DCN favorise ce phénomène car les cellules GABAergiques responsables de l'inhibition locale n'affectent pas le codage temporel des neurones en sortie des DCN.

Mots clés: Cervelet, optogénétique, Noyaux cérébelleux profonds, cellules de Purkinje, inhibition locale, inter neurones GABAergiques, Cellules de projection glutamatergiques, électrophysiologie *in vivo*, codage temporel, codage de fréquence, souris transgénique L7-ChR2

Summary

The cerebellum integrates motor commands with somatosensory, vestibular, visual and auditory information for motor learning and coordination functions. The final step of this integration is done in the deep cerebellar nuclei (DCN) that process inputs from Purkinje cells (PC), mossy and climbing fibers, the two main excitatory inputs of the cerebellar cortex. We investigated the properties of PC connections to the different DCN cell types using optogenetic stimulation in L7-ChR2 mice combined with *in vivo* multi electrode extracellular recordings in lobule IV/V of the cerebellar cortex and in the medial nuclei. We identified two groups of DCN cells with significant differences in their action potential waveforms and firing rates which matched with the properties of GABAergic and non-GABAergic cells discriminated *in vitro*. The discharge of the DCN cells was correlated to the local field potentials and we found that DCN cells were phase locked to oscillations in the beta, gamma and high frequency bands. Although optogenetic stimulation of PCs resulted in the inhibition of the two groups of DCN cells (rate coding), spike times were controlled only for non-GABAergic cells. Moreover, local inhibition onto non-GABAergic cells was not observed in our *in vivo* experiments. Our results suggest that synchronized PC inputs drive the output of cerebellum by temporally controlling only non-GABAergic cells. Also, the internal DCN circuitry supports this phenomenon since GABAergic cells are not temporally controlled and the local inhibition they provide does not alter the time-locked output of the DCN.

Keywords: Cerebellum, optogenetic stimulation, deep cerebellar nuclei, Purkinje cells, local inhibition, GABAergic interneurons, Glutamatergic projection cells, in vivo electrophysiology, rate coding, temporal coding, L7-ChR2 mice

Abbreviations

-A-
AMPA: 2-amino-3-(3-hydroxy-5-methylisoxazol-4-yl)
propanoic acid
AP: Action potential

-B-
BC: Basket cell

-C-
CF: Climbing fiber
ChR2: Channelrhodopsin-2

-D-
DAO: Dorsal Accessory Olive
DCN: Deep Cerebellar Nuclei
dIH: Dorsolateral hump of anterior interposed nuclei

-E-
EPSCs: Excitatory Postsynaptic Currents
EPSPs: Excitatory Postsynaptic Potentials

-G-
GABA: *gamma*-Aminobutyric acid
$GABA_AR$: GABA A-type receptor
GAD67: glutamic acid decarboxylase
GFP: Green fluorescent protein
GlyT2: Glycine transporter 2

-I-
IFF: Instantaneous Firing Frequency
IntP: Posterior Interposed Nuclei
IntA: Anterior Interposed Nuclei
IPSCs: Inhibitory Postsynaptic Currents
IPSPs: Inhibitory Postsynaptic Potentials
ISI: Inter spike interval

-L-
Lat: Lateral Nuclei
LFP: Local Field Potentials
LTD: Long term depression
LTP: Long term potentiation

-M-
MAO: Medial Accessory Olive
Med: Medial Nuclei
MedDL: Medial Nuclei Dorsolateral protuberance

-N-
NMDA: *N*-Methyl-D-aspartate

-P-
PBS: phosphate-buffered saline
PC: Purkinje cell
PO: Principal Olive

-S-
SC: Stellate cell

Table of Figures and Tables

1 INTRODUCTION

1.1 A short history of cerebellar physiology and function

The first sources distinguishing the cerebellum from the rest of the brain date back to Aristotle (384-322 B.C.) and Erasistratus (304-250 B.C.). They used the name paracephalon (meaning "similar to brain") without giving functional details (Malomo et al., 2006). Later, structure and role of the cerebellum was defined by Galen (129-201), stating that it is positioned behind the brain and gives rise to the cranial nerves and the spinal cord. In accordance with the dominant Greek theory of the time, Galen proposed that the cerebellum regulates the animal spirit which flows through the body. Due to the influence of this holistic approach, progresses in neuroanatomical investigations were delayed.

New methodological approaches were introduced by Andreas Vesalius and the structure of human cerebellum was presented in his book in 1543. Further advancements followed his work and, soon after, Costanzo Varolio introduced more details describing connections of the cerebellum to the brain stem. First, the cerebellar cortex and its possible links to spinal cord through white matter was noted by Marcello Malpighi (1665). Later, the deep cerebellar nuclei (DCN) were observed by Raymond de Vieussens as an ash gray area. Detailed descriptions of the lobules of the cerebellar cortex was given by Vincenzo Malacarne in 1776 in his book devoted to the cerebellum. With later contributions from his contemporaries, the gross anatomical description of the cerebellum was completed in the 19th century.

Hypothesis on the role of the cerebellum based on experimental findings also came in the 19th century. Luigi Rolando (1809, 1823) and Jean Pierre Flourens (1924) made successive observations following the ablation of the cerebellum: movements were still possible in general but they were not regular or coordinated, and sensory and cognitive functions were not affected. Later, Luigi Luciani (1891) compiled his observations of several symptoms due to cerebellar lesions and classified them as muscular weakness, lack of muscular tone and unstable muscular contraction. This classification was further developed by Joseph Babinski (1902) by identifying related impairments in rapid and complex

movements. With the reports of Gordon Holmes (1917, 1922) from many patients, the general implications of the cerebellum in human pathology were confirmed.

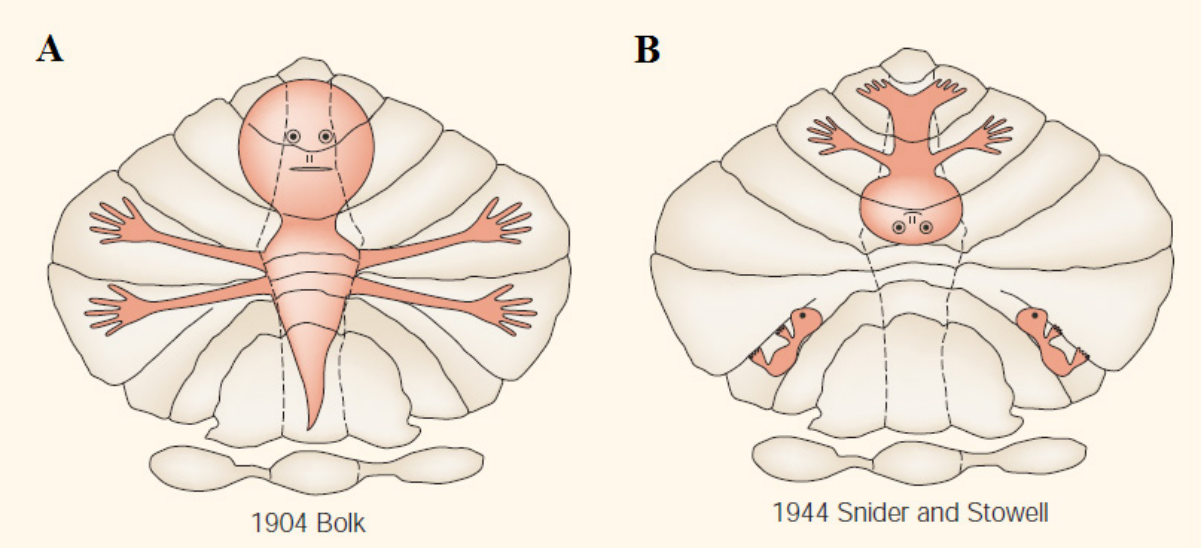

Figure 1: Early somatotopic maps in the cerebellum. Very simplified representations of body parts were given by Bolk (**A**), and Snider and Stowell (**B**), the first approaches within the historical context (adapted from Manni and Petrosini, 2004)

Further progress in deriving anatomical definitions of the cerebellum during this period was a different line of research. Lodewijk Bolk compared several mammals and described four regions: anterior and posterior vermis and two hemispheres having foliations. Together with Olof Larsell, they introduced most of the nomenclature that we use today. Bolk also proposed the first single somatotopic map on the surface of the cerebellum which represented different parts of the body (Figure 1 A) while the following studies challenged this idea with different maps. Snider and Stowell suggested an inverted mapping of gross body parts (Figure 1 B) and also bilateral afferents. Further information regarding historical development of functional localization in the cerebellum can be found in Manni & Pertosini (2004).

A clearer picture of the cerebellar macroscopic architecture was revealed through precise drawings of the cells and their connections by Santiago Ramon y Cajal (1911). With later advancements in microscopy techniques, Palay and Chan-Palay (1974) provided further information. Similarly, electrophysiological techniques were developed after the first electrical recording of cerebellar activity by Adrian (1935), and a functional architecture of cerebellar network was described by

Eccles, Ito and Szentagothai (1967) in their seminal book "The cerebellum as a Neuronal Machine". A very influential model of cerebellar cortex was given by David Marr in 1969. He described the input layer of the cerebellar cortex (i.e. granular cell layer which will be described later) as a pattern discriminator where discriminated patterns are then learned by the Purkinje cell (PC) layer (also described later) as evidenced by long term plasticity. This model had been further improved by James Albus (1971) and soon after it was partially validated by Ito and Kano (1982) that discovered long term depression at the granule cell to PC connection. It was suggested that cerebellar computations are carried out in the DCN that integrate all the input from the cerebellar cortex into a relatively small volume (Ito, 1984). Up to now, our knowledge about cerebellar somatotopy and cellular populations has improved a lot, however, we are still missing an accurate description of computations carried out by the cerebellum. Notably, rules governing the integration of information in the DCN are poorly known, and this area of research will be my focus in following chapters of my thesis.

1.2 Functions of the cerebellum

The cerebellum collects sensory and motor information from the body via the brainstem and the spinal cord, and from the cerebral cortex. With this collection of information, the cerebellum coordinates and adjusts movements, maintains posture and balance. It also functions as an adaptive filter involved in the gain of some reflexes (for a review, see Dean et al., 2010). Similar computational mechanisms are employed in the cerebellum during voluntary and involuntary tasks for accurate timing of actions (for a review, see De Zeeuw et al., 2011). In the case of a voluntary movement, the cerebellum receives a copy of the efferent motor command (Von Holst, 1954; Wolpert et al., 1998). As the movement proceeds, the updated state of the whole body is continuously delivered from somatosensory, vestibular, visual and auditory systems to the cerebellum where they are integrated, and a prediction about the next sensory state during the movement is generated. The difference between predicted and actual sensory feedback is determined and motor errors are detected (Wolpert et al., 1998; Bastian, 2006). Such a "prediction – error control" mechanism sequentially checks whether the intended movement is correctly executed (Thach et al., 1992; Jueptner and Weiller, 1998).

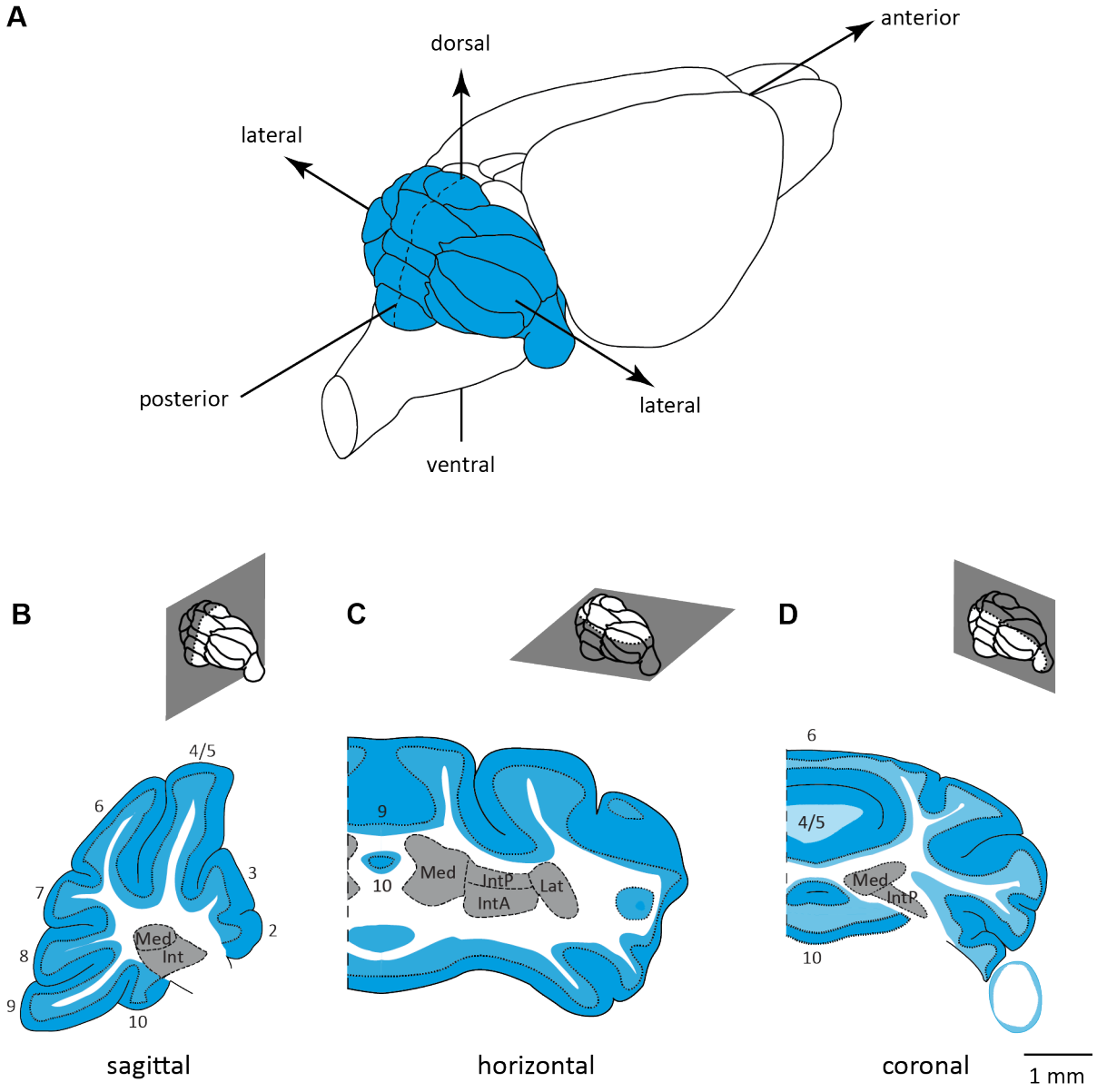

Figure 2: Anatomical planes of the cerebellum. Representation of a mouse brain in anteroposterior, ventrodorsal, and mediolateral axes with the cerebellum (in blue) (**A**). Midline is given in dotted lines. Sagittal (**B**), Horizontal (**C**) and Coronal (**D**) planes are given with the cerebellar cortex (in blue) and the DCN (in gray). Medial (Med), Anterior Interposed (IntA), Posterior Interposed (IntP) and Lateral (Lat) nuclei are shown. Slicing orientations shown in the upper right corners.

There is also evidence suggesting that the cerebellum takes part in cognitive tasks as well, which previously were attributed only to cerebral cortex (Ivry et al., 1988; Ito, 2008). Consequently, it is proposed that the cerebellum functions as a co-processor, working in parallel with the rest of the brain (D'Angelo and Casali, 2012). According to this theory, the cerebellum can take part in many different

tasks, operating in loops with specific parts of the brain related not only to sensory-motor processing but also to cognitive functions.

1.3 Anatomical organization of the cerebellum

1.3.1 Gross anatomy of the cerebellum

The cerebellum consists of a foliated cortex, with inner part containing mostly white matter that carries axons from/to the cortex, and three nuclei (DCN) that lie below the cortex inside the white matter bilaterally (Figure 2). The cerebellar cortex is divided into different numbers of lobules across species. In mammals, including humans, there are always 10 lobules that vary in size (Larsell, 1952). Lobules lie parallel to each other, extending from the vermis to the sides of the hemispheres (Figure 3 A). Lobules are separated from each other by superficial fissures, and two deep fissures group lobules into 3 lobes: anterior and posterior lobes are separated by the primary fissure while the secondary (posterolateral) fissure divides the flocculonodular lobe from the posterior lobe. Anterior lobe includes lobules I – V, posterior lobe includes lobules VI – IX, and flocculonodular lobe includes last lobule X (Figure 3 B).

The cerebellum has a symmetric structure along the midline: medial part of its cortex is called the vermis and the two lateral parts connected to the vermis are called the hemispheres (Figure 3 C). The hemispheres are also divided into two parts: the lateral hemisphere, and a more medial part, the paravermis (Figure 3 C). The DCN in rodents have 3 parts: medial, interposed and lateral nucleus.

The cerebellum is connected to the brainstem with three pairs of cerebellar peduncles: namely, inferior, medial and superior cerebellar peduncles. The inferior cerebellar peduncle carries cerebellar afferents arriving from the spinal cord and medulla oblongata. The medial cerebellar peduncle, which lies rostrolateral to the inferior one, carries afferents arriving from the pontine nuclei. The last cerebellar peduncle, the superior one, lies medial to the inferior peduncle and carries cerebellar efferents from the DCN rostrally. Uncinate tract and bulbar connections transfer cerebellar efferents to the brainstem (Carleton and Carpenter, 1983).

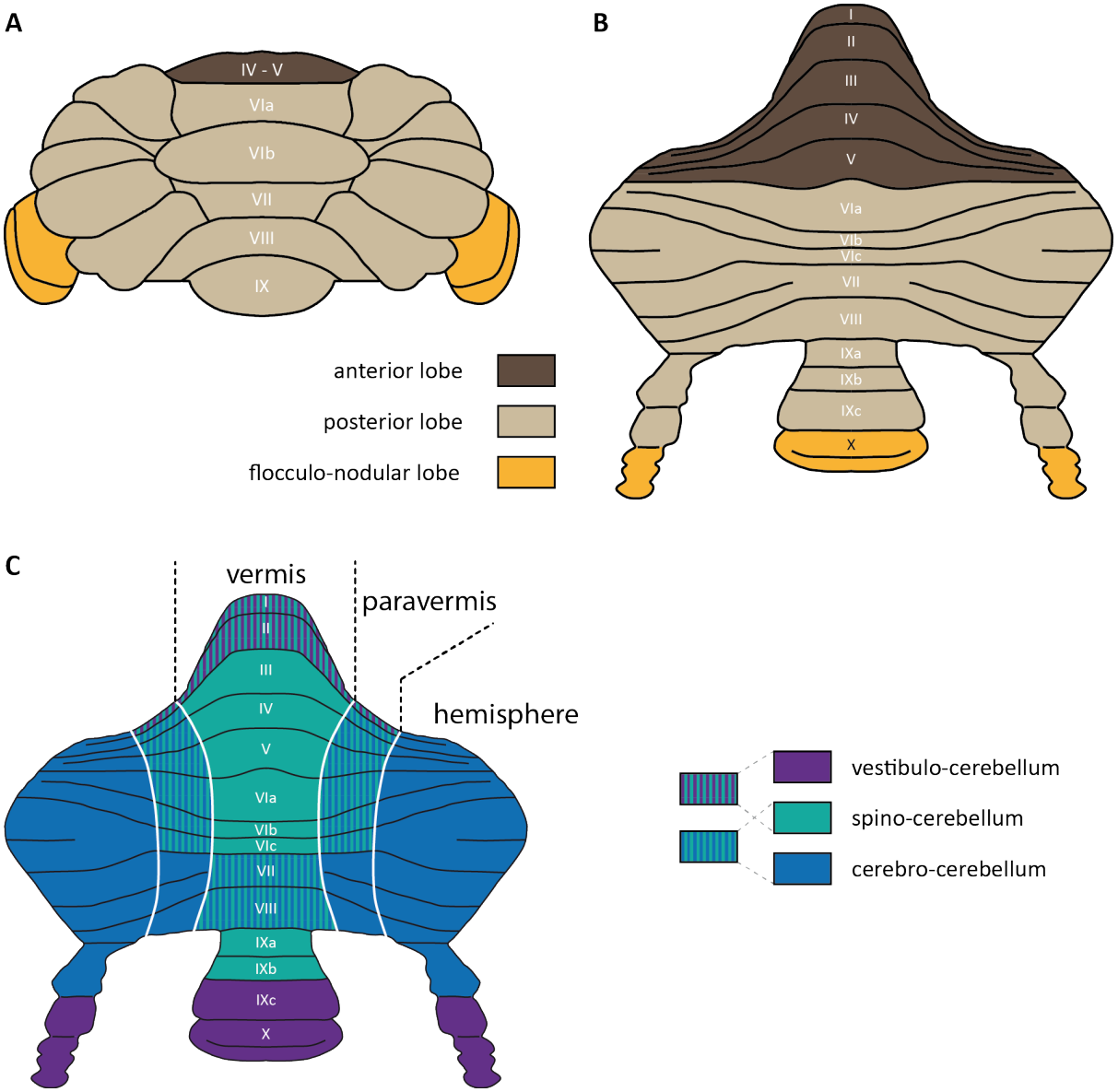

Figure 3: General anatomy and functional divisions of the cerebellar cortex (**A**) Lobes and lobules in the anteroposterior segmentation (**B**) Cerebellar cortex unfolded in anteroposterior axis, showing lobule numberings (**C**) Mediolateral segmentation into vermis, paravermis and the hemisphere, together with functional divisions given in colors (Figure modified from J. Chaumont)

1.3.2 Gross functional divisions of the cerebellum

The architecture of the cerebellar cortex was considered isotropic across lobules. Same groups of cells are repeatedly located at their respective places in different layers of the cortex. However, some differences in cell structure and patterned molecular expressions have been recently reported (for a

review, see Cerminara et al., 2015). These differences highlight smaller regions within the cerebellar cortex that will be explained in the following parts of the thesis.

Inputs from different parts of the body divide the cerebellar cortex into bigger functional regions (Brodal, 2004) and this topographical organization of cerebellar inputs determines the functional divisions of the cerebellum. First, the flocculonodular lobe receives mostly primary vestibular afferents and projects to extracerebellar vestibular nuclei. This is the most primitive part of the cerebellum that controls eye movement and balance in higher vertebrates. Due to its function, it is called vestibulocerebellum (Figure 3 C, purple).

In the mediolateral classification, the vermis and the paravermis receive somatosensory inputs from the spinal cord and are therefore together functionally called spinocerebellum (Figure 3 C, green). Spinocerebellum also receives visual, auditory and vestibular inputs for the integration. Vermis receives input from the head and proximal parts of the body and controls posture, locomotion and gaze. Paravermis receives input from more distal parts of the body, the limbs and controls movements of these areas. The vermis and the paravermis mainly project to the medial and the interposed nuclei, respectively. The lateral parts of the cerebellar cortex, the hemispheres, are functionally called cerebrocerebellum since they receive information mainly from the cerebral cortex (Figure 3 C, blue). Cerebrocerebellum, which is more developed in humans and apes, is associated with the planning of motor actions. It projects back to the cerebral cortex via the lateral nuclei and the thalamus.

1.3.3 Cerebellar inputs

Proprioceptive and exteroceptive information together with the efferent copy of the motor commands are delivered to the cerebellum through two input pathways: 1) the climbing fibers and 2) the mossy fibers. Climbing fibers arrive solely from inferior olive, which is the largest nucleus situated in the medulla of the hindbrain. Mossy fibers, originate from several nuclei of the brainstem and the spinal cord which are commonly called precerebellar nuclei.

The inferior olive integrates sensory motor information from different parts of the brain like cerebral cortex, spinal cord and precerebellar nuclei, and generates climbing fibers that connects to the cerebellar cortex and to the DCN. It also receives feedback from the output of the cerebellum. Inferior olive is divided into three subnuclei: namely, principal olive, dorsal accessory olive, medial accessory olive, and four smaller subnuclei. The function of inferior olive is not clearly known, but current theories suggest that it takes part in movement error detection and movement timing control (De Zeeuw et al., 1998; Llinás et al., 2004; Mathy & Clark, 2013).

Numerous precerebellar nuclei target parts of the cerebellar cortex via the mossy fibers. Briefly flocculus receives inputs from the nucleus intercalatus, the medial vestibular nucleus, supragenual nucleus, nucleus prepositus hypoglossi, nucleus reticularis tegmenti pontis, and lateral reticular nucleus. Vermis and hemispheres receive connections from the pontine nucleus, lateral reticular nucleus, the nucleus intercalatus, nucleus reticularis tegmenti pontis, and external cuneate nucleus. There are also direct inputs that arrive from spinal cord that carry sensory information to cerebellar cortex without any relays.

1.3.4 Cerebellar outputs

The output gate of the cerebellum is the DCN. All processed information from the cerebellar cortex is sent to the DCN where it is integrated with collaterals of cerebellar inputs, mossy and climbing fibers. In addition to the DCN, a fourth nuclei, the vestibular nuclei, lie in the brainstem can be included in the output of the cerebellum. The vestibular nuclei seem to lie anatomically outside of the cerebellum, however, they receive similar inputs and generate an integrated output like the other cerebellar nuclei.

The cerebellum projects to brain regions like the brainstem, diencephalon and the spinal cord. More specifically, the medial nuclei project mainly to the vestibular nuclei and also send projections to spinal cord, midbrain and thalamus. The interposed nuclei have a different main target, the red nucleus of the midbrain, while they also project to the vestibular nuclei and thalamus. Lastly, lateral nuclei predominantly project to thalamus by crossing the superior cerebellar peduncle. This connection takes part in the cerebellar thalamic cortical loop involved in error based control of complex movements. The cerebellum also sends feedback connections to inferior olive (for a review, see Brodal, 2004).

1.4 The cerebellar cortex

1.4.1 Information flow in the cerebellar cortex

The cerebellar cortex has a surprisingly uniform structure within each lobule in terms of cell structure and organization, as briefly mentioned earlier. It has been separated into three layers. The most inferior part is the granular layer which accommodates the most numerous cells of the brain, the granule cells. Within the granular layer there are also Golgi cells and other interneurons, namely, unipolar brush cells and Lugaro cells, all of which are much less numerous compared to granule cells. Mossy fibers terminate in this layer in a special structure called the glomerulus (Jakab and Hámori,

1988). Here, mossy fiber terminals, granule cell dendrites and the Golgi cell axon terminals make a ~10 μm spherical junction shielded by a glial sheet. Granule cell dendrites can be excited by mossy fiber terminals and inhibited by the Golgi cell axons (Figure 4 Ai).

The activation of Golgi cells, on the other hand, can happen through two direct synapses: 1) those from different mossy fibers (Kanichay and Silver, 2008) and/or 2) those from granule cells (Midtgaard, 1992; Dieudonne, 1998; Cesana et al., 2013). Consequently, Golgi cells can evoke feedforward and/or feedback inhibition onto granule cells; this inhibitory control shapes the excitatory input on granule cells in a glomerulus (Hamann et al., 2002).

Granule cells send their axons to the uppermost layer, the molecular layer, where they form parallel fibers and excite the PCs (Figure 4 Aii). A large information transfer happens in the molecular layer where a PC can receive inputs coming from about 175000 granule cells fibers (Napper and Harvey, 1988). In addition, there are around 10 molecular layer interneurons contacting each PC, and they provide feedforward inhibition on them (Eccles et al., 1967).

The second cerebellar input, the climbing fibers, directly target PCs and introduce a very strong excitation (Figure 4 B). PCs generate a complex spike which is formed of a spike and several spikelets. This input also affects interneurons through glutamate spillover in the molecular layer (Szapiro and Barbour, 2007). Therefore, the two excitatory inputs from mossy fibers and climbing fibers, and inhibitory inputs from molecular layer interneurons converge on the PCs and strongly modify ongoing PC activity according to their timings with respect to each other.

When climbing fiber and parallel fiber inputs arrive to a PC at the same time, parallel fiber-to-PC synapses are durably depressed (long term depression, LTD, Ito and Kano, 1982). The same synapses can go through a potentiation (long term potentiation, LTP) when parallel fiber inputs arrive without a climbing fiber input (Lev-Ram et al., 2002 and Coesmans et al., 2004). Consequently, there are LTD and LTP mechanisms mutually working at the granule cells to PC connections. Finally, PCs integrate excitation and inhibition that they receive, produce the sole output of the cerebellar cortex and send projections to the DCN.

The PC layer lies between the two layers described above, where PC somas position in one plane and define the layer. In total, there are seven types of neurons that I will briefly describe in the following paragraphs: the granule cells, Golgi cells, Lugaro cells and unipolar brush cells (in the granular layer), PCs (in PC layer), basket and stellate cells (in molecular layer).

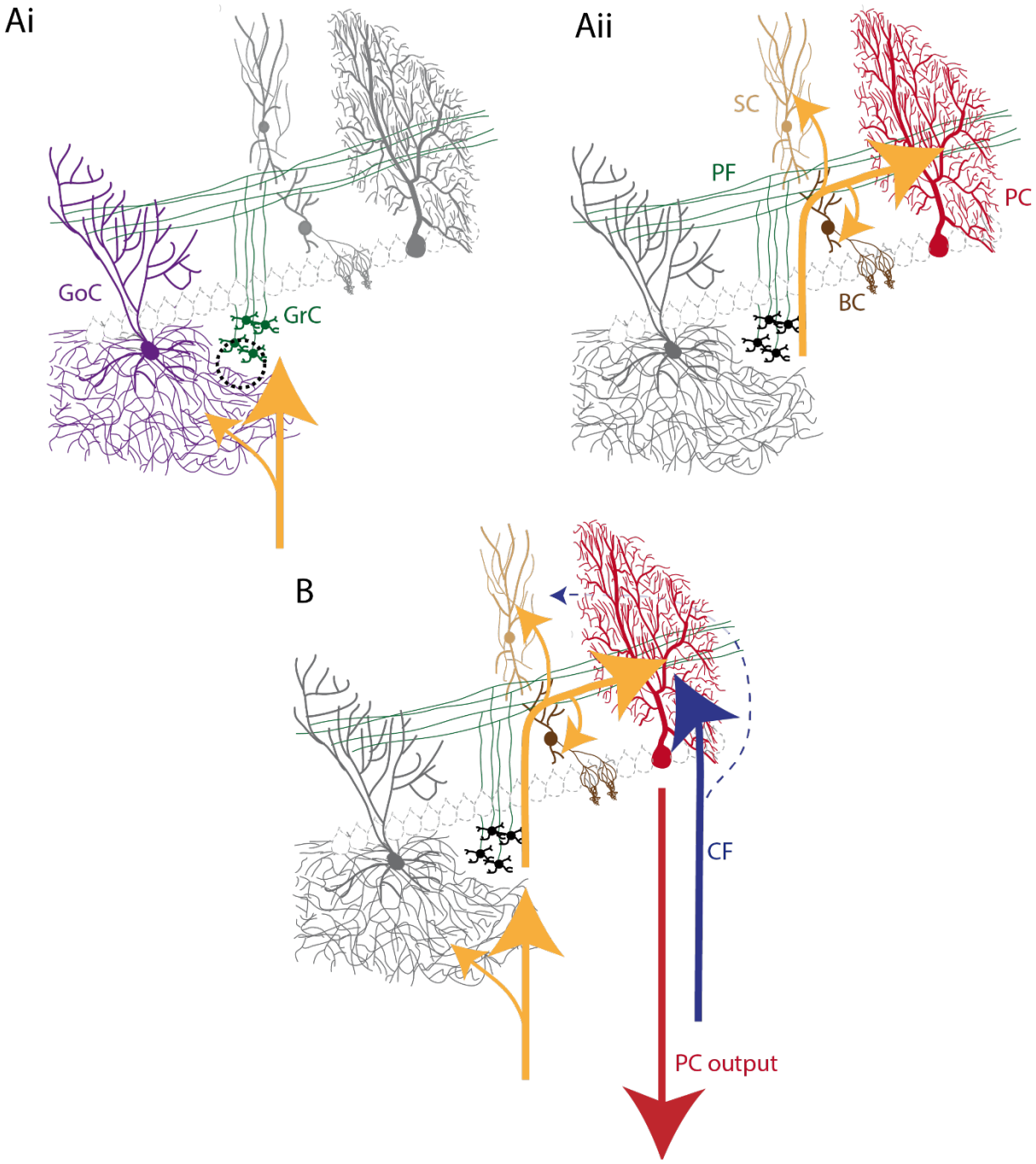

Figure 4: Information flow in the cerebellar cortex (**Ai**) Mossy fiber inputs (yellow arrow) excite granule cells (GrC) and Golgi cells (GoC) within a glomerulus (black dashed area). Golgi cells provide feedforward and/or feedback inhibition to granule cells in this structure (**Aii**) Granule cell axons give parallel fibers (PF) to excite Purkinje cell (PC) dendrites which also receive feedforward inhibition from molecular layer interneurons, namely stellate cells (SC) and basket cells (BC) (**B**) Climbing fibers (CF, blue arrow) induce strong excitation in PCs and also modify plasticities of in the cerebellar cortex. PC output (red arrow) is generated by the combination of these inputs. (Figure modified from A. Valera)

1.4.2 Cellular structure of the cerebellar cortex

1.4.2.1 The Purkinje cell

The Purkinje cell (PC) is the principal cell of the cerebellar cortex and it has been described by the physiologist Johannes Purkinje in 1837. PC dendrites make a planar arborisation in the molecular layer, where a single PC receives around 175000 excitatory synapses from parallel fibers (Napper and Harvey, 1988). Conversely, a single adult PC receives only one unique input from climber fibers.

PCs' big planar dendritic arborisation lays in a sagittal plane orthogonal to the plane of the parallel fibers (Figure 5 A-B). This dendritic arborisation generally has one primary trunk that forms secondary and tertiary dendrites with thinner branchlets, resembling in a tree structure. Parallel fibers contact PCs on dendritic spines located on branchlets, and each dendritic spine receives only one parallel fiber connection most of the time (Napper and Harvey, 1988; O'Brien and Unwin, 2006). Differently to a single contact made by many parallel fibers, climbing fibers make a single connection to each PC with hundreds of release sites that cover PC's dendritic trunk (Palay and Chan-Palay, 1974) (Figure 5 B-yellow). This exceptionally strong input results in complex spikes formed by one spike and several spikelets (Figure 5 C).

PCs send their projections to the DCN and make GABAergic inhibition in a projection area containing several different cell types in the DCN. Projection areas of different PCs overlap (Trott et al. 1998a, 1998b; Panto et al. 2001) and, consequently, each nuclear cell receives inhibition from several PCs. This connection has high divergence and convergence ratios and will be further explained in the next chapter. PC axons also make collaterals, and can contact different cell types in the cerebellar cortex: other PCs (Palay and Chan-Palay, 1974; Bornschein et al., 2013), Lugaro cells (Palay and Chan-Palay, 1974; Hirono et al., 2012), molecular layer interneurons (Palay and Chan-Palay, 1974; O'Donoghue et al., 1989) and also Golgi cells (Palay and Chan-Palay, 1974; Hirono et al., 2012). However, the distribution of these collaterals has not been extensively described. Recent studies suggest that they are distributed mostly in the parasagittal bands and a few of them cross short distances laterally (Hawkes and Leclerc, 1989; Sugihara et al., 2009).

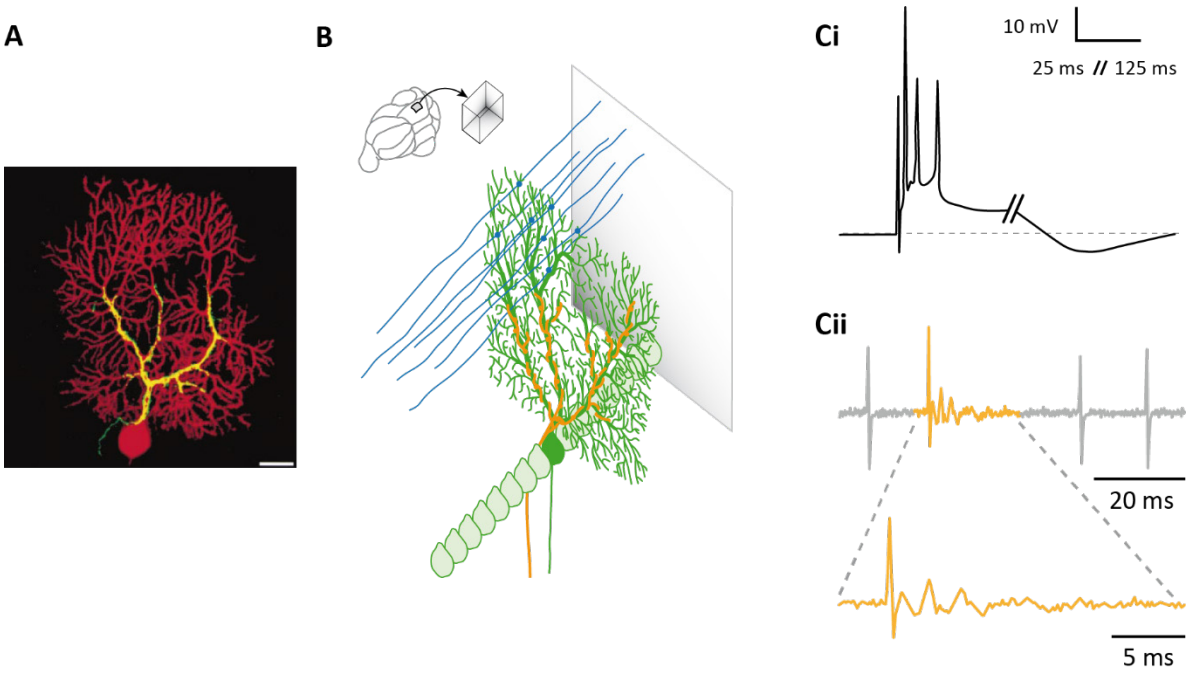

Figure 5: PC and its complex spike (**A**) Composite image of a climbing fiber (yellow) and a PC (red). Scale bar, 20 µm (adapted from Brenowitz and Regehr, 2012) (**B**) Dendritic arborisation of a PC (in green) in the sagittal plane, innervation of the parallel fibers (in blue) and the climbing fibers (in yellow) (**Ci**) Complex spike recorded *in vitro* current clamp mode (adapted from De Zeeuw et al., 2011) (**Cii**) Juxtacellular recording of simple spikes (gray) and a complex spike (yellow) of a PC (recorded by J. Chaumont)

1.4.2.2 The granule cell

The granule cells are the biggest number of cells in the brain, estimated roughly 100 billion in humans (Andersen et al., 1992). They fill up the volume between PC layer and the white matter in the cerebellar cortex. Granule cells are very small in somatic size, 4.82 µm on average (Harvey and Napper, 1991). This makes a very high density of granule cells in the most inferior layer, the input stage, of the cerebellar cortex (Harvey and Napper, 1988).

Granule cells have a few short dendrites that end as a dendritic claw, where they receive excitatory input from mossy fibers (Llinas et al., 2004) in the glomerulus. Unlike their dendrites, granule cells have long axons. They first ascend into the molecular layer of the cerebellar cortex and then bifurcate to give parallel fibers, expanding in both directions in the mediolateral axis. The ascending part and the parallel fibers both make synapses with PCs.

The ascending axon of the granule cells makes less synapses than the parallel fiber part of the same axon which is due to the difference in the length of these compartments. However, synapses are more densely found in the ascending axon than the parallel fibers. The percentage of the ascending axon

inputs per total granule cell inputs on PCs is estimated to be 7-24 % (Gundappa-Sulur et al., 1999), which actually makes more than 10000 synapses.

1.4.2.3 The Golgi cell

The Golgi cell is the second important cell in the granular layer. It receives excitation from mossy fibers and granule cells, and then it inhibits the granule cells in the glomerulus as described in the information flow.

The Golgi cell is named after the inventor of the silver nitrate method of staining, Camillo Golgi (1873). He described the morphology of the cells which was further extended by Ramon y Cajal (1911). Marr (1967) suggested that Golgi cells were driven by parallel fibers and mossy fibers. More detailed descriptions from Palay and Chan-Palay (1974) postulated that Golgi cells receive inputs not only from granule cells and mossy fibers but also from climbing fibers, PCs and molecular layer interneurons. The axonal part of the Golgi cell makes a big plexus, which extends in the sagittal plane and mediolateral plane. It sends projections to several glomeruli in its plexus. Between Golgi cells there are also gap junction connections that synchronize their activity (D'Angelo and De Zeeuw, 2009; Vervaeke et al., 2012; Szoboszlay et al., 2016) and impose a network inhibition on the excitatory inputs to the cerebellar cortex.

The last two cell types in the granular layer are Lugaro cells and unipolar brush cells are, and their properties are not extensively described (for more information, see Palay and Chan-Palay, 1974; Altman and Bayer, 1977; Geurts et al., 2001; Lainé and Axelrad, 2002; Mugnaini et al., 2011; Hirono et al., 2012).

1.4.2.4 Molecular layer interneurons

The upper layer of the cerebellar cortex is mostly filled with a huge dendritic tree structure arising from PCs in the parasagittal plane, and with long parallel fibers arising from granule cells that travel orthogonal to PCs' dendrites. In between these structures, there are also molecular layer interneurons: stellate and basket cells. They locally inhibit PCs and other molecular interneurons in the same layer.

Molecular layer interneurons are contacted and excited by parallel fibers, and they provide feedforward inhibition to PCs. They have dendrites in the parasagittal plane, like PC dendrites, but it is known that they can also inhibit neighboring PCs laterally that do not receive the same beam of parallel fibers (Eccles et al., 1967; Llinas and Sugimori, 1980; Cohen and Yarom, 2000).

The distinction between the two types of molecular layer interneurons, stellate and basket cells, is not totally clear and a smooth transition between the cell types was suggested by several studies (Sultan and Bower, 1998; Mittmann and Häusser, 2007; Schilling et al., 2008). However, differences in the short-term dynamics of parallel fiber connections to stellate and basket cells have been shown in Bao et al. (2010). In response to 50 Hz train stimulation of parallel fibers, synapses to stellate cells facilitate while synapses to basket cells were just slightly depressed. The two cell types differed in their respective locations as well: stellate cells were found to be located mostly on the superior part of the molecular layer, while basket cells were found mostly on the lower part. Basket cells have a special axonal extension which is found to cover the soma and initial part of PC axons. This special structure affects the spike initiation zone of PCs and it was hypothesized that it delivers electric field potentials to inhibit PC firing (Korn and Axelrad, 1980); this was further investigated and defined as ephaptic inhibition (Blot and Barbour, 2014).

1.4.3 Functional microzones in the cerebellar cortex

While the gross functional divisions of the cerebellum are determined by the coarse topography of cerebellar inputs, the precise synaptic arrangements in the cerebellum lead to a more specific functional organization similar to modular structures observed in the visual cortex (Callaway and Katz, 1993).

Modules in the cerebellum are distributed across the inferior olive, the cerebellar cortex and the DCN, and they function through the cooperation among these three regions. Boundaries of modules are determined by the projections between these regions, notably the climbing fibers contact PCs in precise parasagittal bands of cerebellar cortex matching with aldolase C compartments (Figure 6 B, small dots in color).

Since climbing fiber inputs are somatotopically organized, PCs in parasagittal bands share the same receptive fields. These bands can also be distinguished from each other by the expression of molecular marker zebrin II in PCs (Brochu et al., 1990) which represents the metabolic enzyme aldolase C (Figure 6 B white and gray areas, Ahn, 1994). PCs then project to specific regions in the DCN that generate the output of the cerebellum and also send feedback connections to the inferior olive. (Oscarsson, 1979; Sugihara and Shinoda, 2004; Voogd and Ruigrok, 2004; De Zeeuw et al., 2011). Consequently, a cerebellar module operates in an olivo-cortico-nuclear loop (Figure 6 A, Ruigrok, 2011), and its cortical element is called a microzone (for a review, see Apps and Hawkes, 2009).

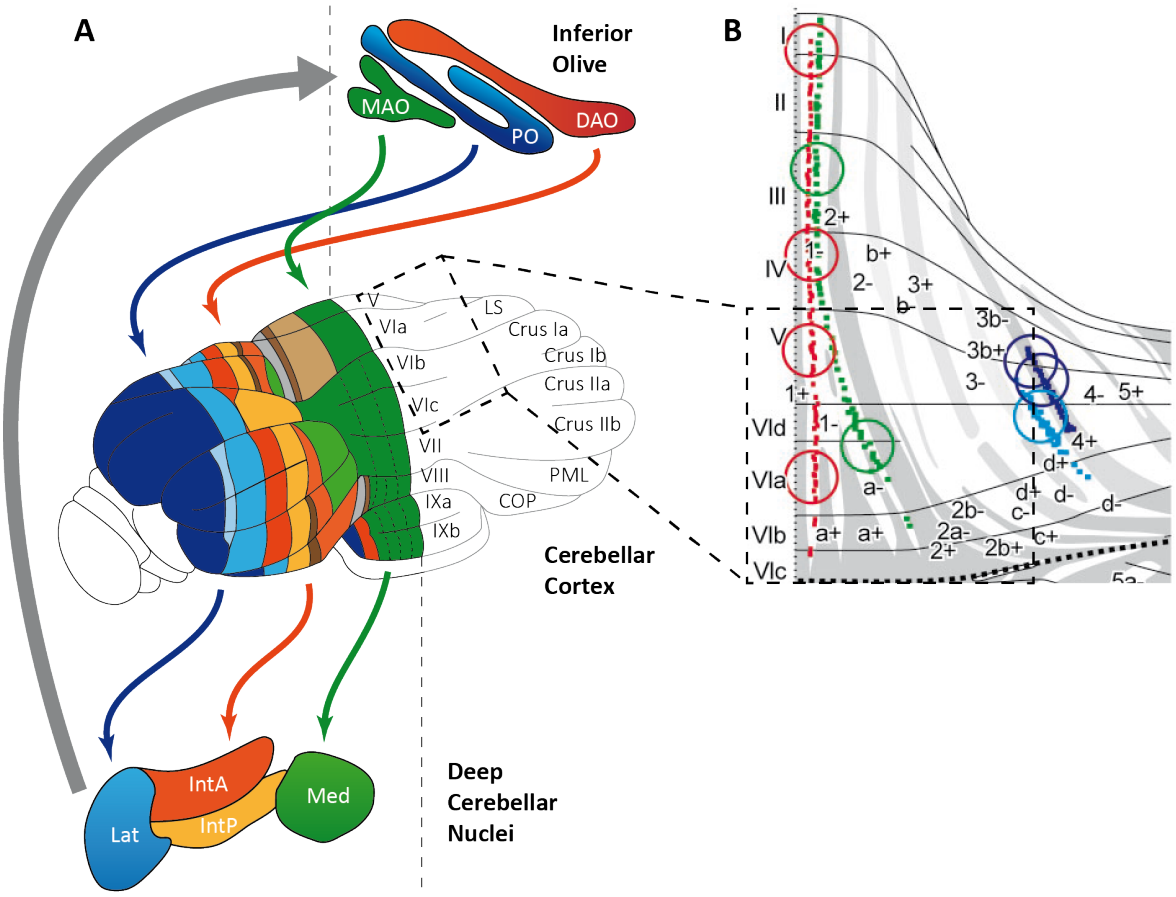

Figure 6: Olivo-cortico-nuclear loop in the cerebellum. (**A**) An overview of connected regions between the inferior olive, the cerebellar cortex and the DCN. Regions in the inferior olive: DAO (Dorsal accessory olive), PO (Principal olive), MAO (Medial accessory olive) and regions in the DCN Med (Medial Nuclei), IntP (Interposed Nuclei – posterior), IntA (Interposed Nuclei – anterior) and Lat (Lateral Nuclei). (adapted from Apps and Hawkes, 2009) (**B**) Climbing fiber projections in an unfolded cerebellar cortex within the loop operation. Red, green, blue and violet dots each show climbing fibers distributions from tracing experiments of small injections of BDA (Biotinylated dextran amine) to different subnuclei of the inferior olive. (adapted from Sugihara and Shinoda 2004).

In this network, mossy fiber and climbing fiber inputs that originate in the same body part partially match in microzones of the cerebellar cortex (Garwicz et al., 1998; Pijpers et al., 2006; Voogd et al., 2003) which suggests that microzones control a specific group of muscles (Apps and Garwicz, 2005; Thach et al., 1992). Mossy fiber inputs are relayed to local PCs through granule cells in the cortex (Ekerot and Jorntell, 2001; Isope and Barbour, 2002; Valera et al., 2016), however PCs of distant microzones are also targeted by the parallel fibers (Ekerot and Jorntell, 2003; Dean et al., 2010;

Valera et al., 2016). Consequently, local and/or distal granule cell inputs can be precisely selected in a PC through LTP and LTD mechanisms (Jörntell and Hansel, 2006; Gao, 2012b; Valera et al., 2016). Moreover, the recent study of our laboratory (Valera et al, 2016) focusing on lobules controlling locomotion discovered that the functional synaptic organization between microzones was conserved across animal. We therefore postulate that intermodular communication underlies the coordination between motor units.

1.4.4 Functional role of the cerebellar cortex and Purkinje cells

As mentioned in the very beginning, David Marr (1969) described the cerebellar cortex as a pattern discriminator, where PCs can learn the patterns of mossy fiber inputs that relay on granule cells. This theory was further improved by Albus (1971), Ito and Kano (1982). Now, I would like to introduce what information PCs transmit and how it is encoded. PCs discharge in correlation with different motor behaviors. For optokinetic reflex and vestibulo-ocular reflex in mice (De Zeeuw et al., 1995; Van Alphen et al., 2001; Katoh et al., 2015), and for reaching movements in monkey (Pasalar et al., 2006), detailed correlations of PC discharge with the motor activities were found. Similarly, the beginning of smooth pursuit eye movements were highly correlated with PC activity (Medina and Lisberger, 2007), and PCs, as a population, were found to encode temporal properties of saccade movements (Their et al., 2000; for a review see Ebner et al., 2011). In a recent study from Chen et al. (2015), it has been shown that specific groups of PCs represented the movements of whiskers in mice: a group of PCs increased their firing rate with whisker movements while another group of PCs decreased, and these changes were linear with the whisker position. Another encoding mechanism was also observed which was underlain by a synchronization of the activity of a group of PCs (De Zeeuw et al., 1997; Heck et al., 2007) under the control of climbing fiber afferents. Such examples show that PCs can encode several aspects of motor activities through modification of firing rates (rate coding) and/or specific discharge timings (temporal coding) together with possible synchrony in a group of PCs (Witter et al. 2011). The extent to which this information coding is preserved in the DCN depends on the details of the corticonuclear projections.

1.5 The deep cerebellar nuclei (DCN)

1.5.1 Anatomy of the DCN

The DCN lie in the inferior part of the cerebellum surrounded by the cerebellar cortex. As mentioned above, there are three nuclei: medial, interposed (anterior and posterior) and lateral nuclei, all having

bilateral pairs. They have a different nomenclature in humans: fastigial, emboliform, globose and dentate. The nuclei are located in the ventral part of the cerebellum where they are connected to the brainstem. PCs of the vestibulocerebellum project to another pair of nuclei outside of the cerebellum, the vestibular nuclei which is out of the scope of this study.

Anatomical properties of the DCN have been defined for different species. The medial nucleus (Med) is located next to the midline (Figure 7 A). A dorsolateral protuberance of medial nucleus (MedDL) is observed in rodents (Goodman et al. 1963). Interposed nucleus is separated in anterior (IntA) and posterior (IntP) parts. A similar dorsolateral hump of anterior interposed (dIH) nucleus is present next to lateral nucleus (Lat) in rodents (Voogd et al., 2013). In primates, lateral nucleus have a curved shape that extends in dorsomedial and ventrolateral directions. In humans, these two extensions are further developed with foliations and are called microgyric and macrogyric parts, respectively (Demole, 1927). In monkey and cat cerebellum, another group is recognized as Y nucleus which is the lateral extension of the vestibular nucleus and it was not defined in humans (Yamamoto et al. 1986, Stanton 1980). A group of cells, observed between medial and posterior interposed nuclei, can be grouped into the fifth nucleus defined as interstitial cell groups (iCG) which is present in rats (Buisseret-Delmas and Angaut, 1993) and other mammals (Voogd et al., 2013).

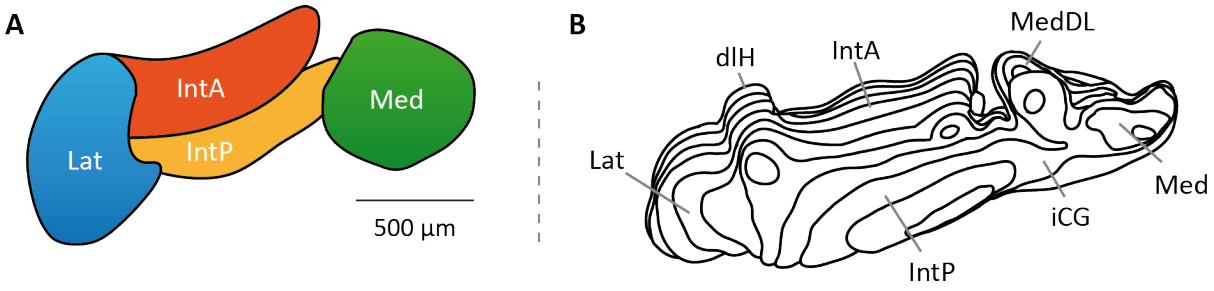

Figure 7: Anatomical structure of the DCN. (**A**) Division of cerebellar nuclei and (**B**) their three dimensional structure (adapted from Sugihara & Shinoda, 2007). Details are given in the text (adapted from J.Chaumont).

1.5.2 Functional role of the DCN

The final stage of cerebellar computation is carried out in the DCN. Excitatory connections of mossy fibers and climbing fibers plus inhibitory connections from a large number of PCs target the DCN (van der Want and Voogd, 1987; De Zeeuw et al., 1997, Ruigrok et al., 2015). Such a diverse input collection from the brainstem, the inferior olive, the spinal cord and the cerebellar cortex is combined and processed in the DCN. A specific study from Brooks and Cullen (2013) showed that the DCN

cells can differentiate an unexpected movement from a self-generated voluntary one. For an unexpected movement applied externally, the recorded DCN cell reliably represented the actual head velocity using sensory information (Figure 8 A, raster plots for ten trails and average firing rate). However, if the same movement was executed voluntarily, the incoming sensory information about the head velocity was cancelled with precision, and the same DCN cell did not respond at all (Figure 8 B, raster plots for ten trails and average firing rate). This precise cancellation shows the critical integration capabilities of the principal cells in the DCN where sensorimotor information is delicately processed. Distinguishing between unexpected and voluntary movements is one of the examples of the specific integration capabilities by the DCN.

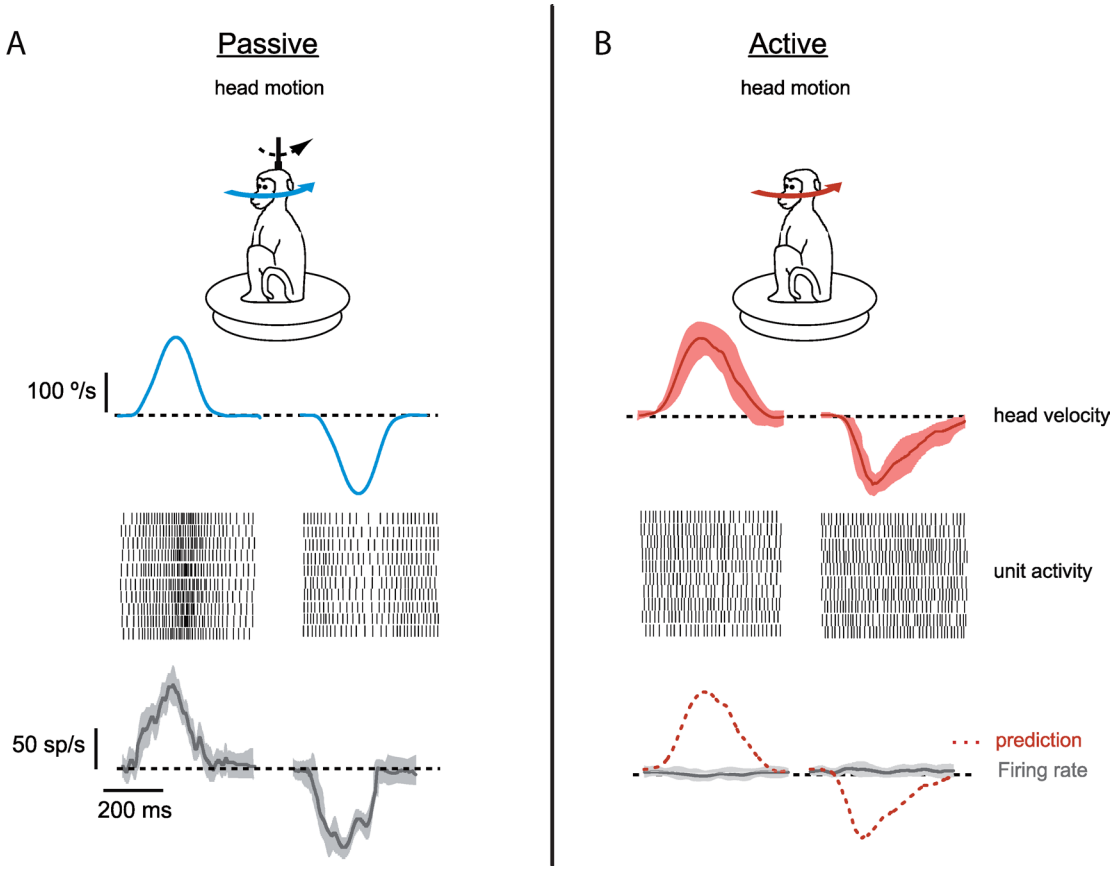

Figure 8: DCN cell responses to passive and active movement. *In vivo* recordings from medial nucleus in monkeys revealed different responses to the same movement (head motion). (**A**) Passive movement (externally applied, unexpected) was reliably represented by firing rate of a DCN cell. Raster plots illustrating spiking activity in ten trials and average change in the firing rate is given. (**B**) When the same movement was active (self-generated, voluntary), head velocity was not represented in raster plots and firing rate of the DCN cell didn't change. Shaded areas gives standard deviation between trials (adapted from Brooks and Cullen, 2013).

Previously, the DCN were thought to be a relay station, but two lines of research instigated a need to establish the functional role of the DCN. Firstly, an increasing body of studies describes the interplay between different inputs in the DCN (Ouardouz and Sastry, 2000; Gauck and Jaeger, 2003; Ohyama et al., 2003; Pugh and Raman, 2006; Person and Raman, 2010). Similarly to the example above, the DCN were shown to store some motor memories within their intrinsic connections (Chen et al., 1999; Wada et al., 2007). These studies suggested that information processing in the cerebellum is carried out not only in the cerebellar cortex but also in the DCN.

The second line of research that points to the information processing function of the DCN is a set of studies that describe different cell types. In a study from 2001, Czubayko and colleagues have characterized two types of the DCN neurons with respect to their intrinsic physiological properties. Later, studies by Uusisaari and colleagues (Uusisaari, et al., 2007; Uusisaari and Knöpfel, 2008; Uusisaari and Knöpfel, 2010; Uusisaari and Knöpfel, 2011), Bagnall and collegues (2009) characterized six different cells types in the DCN. After a recent study (Ankri et al., 2015), two of the proposed cell types have been joined, giving the result of five different DCN cell types described *in vitro*.

These five cell types are the following: 1) large glutamatergic projection cells, 2) GABAergic and glycinergic nucleo-cortical cells with local collaterals, 3) non-inhibitory interneurons, 4) GABAergic nucleo-olivary cells, and 5) glycinergic premotor projection cells. Discussions are still open about cell types, since the specifications of different cells were given by *in vitro* studies mostly and not all of the cell types were identified *in vivo*. However, the observed varying intrinsic properties of these cells may have particular importance for the computations in the DCN. Especially, local inhibition in the DCN (Wassef et al., 1986; Husson et al., 2014) is very likely to modulate the output; this topic will be further explained.

A recent *in vivo* whole cell recording study from Canto et al. (2016) also compared DCN cells and I will elaborate on it in the discussion.

1.5.3 Cellular structure of the DCN

1.5.3.1 The principal projection cell

The principal projection cells are the biggest cells of the nuclei and are the best described amongst DCN cells. Being the principal cells of the nuclei, they received most of the attention. Making use of their big size, most of the *in vitro* studies had targeted specifically them over the other DCN cell

types. (Telgkamp and Raman, 2002; Pedroarena and Schwarz, 2003; Person and Raman, 2011). The principal projection cells have a special importance since they generate and convey the main output of the cerebellum to the brainstem, the spinal cord, several premotor areas and cortical areas via the thalamus in the brain (Asanuma et al., 1980; Sultan et al., 2012; Ruigrok and Teune, 2014).

The principal cells are glutamatergic projection cells with soma diameter of 20-35 μm. Uusisaari and Knöpfel (2013) suggested that they vary considerably in terms of morphology, and that further subtypes could be described. However, distinctive physiological properties have not yet been found to define the subgroups. These cells have big dendritic structure which extends to a big portion of each nucleus (Chan-Palay, 1973). Dendritic surface area was shown to be around 25000 – 50000 μm^2, which accommodates a large number of synapses: estimated to be 850 – 1700 (Matsushita and Iwahori, 1971c; Bengtsson et al., 2011). It has been found that axon terminals from PCs and collaterals of climbing and mossy fibers converge onto these cells (Matsushita and Iwahori, 1971c), covering as high as 50 % of cell surface with synaptic buttons (Angaut and Sotelo, 1973). Uusisaari et al. (2011) suggested that cell bodies of the principal cells are mostly covered by GABAergic presynaptic terminals of PC axons. The convergence of mossy and climbing fiber inputs was shown solely for the principal cells, but their relative input strength is unknown (Uusisaari et al., 2011).

A fourth afferent to the principal projection cell comes from another DCN cell: collaterals of the inhibitory nucleo-cortical cells (Ankri et al., 2015), with fewer connections to proximal and distal dendrites. It was shown that collaterals of the inhibitory nucleo-cortical cells had significant local inhibitory effect on the principal cells with mixed GABA/glycinergic transmission *in vitro* (Husson et al., 2014). Such intra-nuclear interactions are likely to have critical importance, especially for the principal projection cells that generate the output of the cerebellum (Wassef et al., 1986; Husson et al., 2014). Properties of local inhibition in DCN will be further investigated in the following chapters.

In terms of output, the principal cells of the DCN were also found to project collaterals to the cerebellar cortex (Houck and Person, 2015). In a recent study, this circuitry was shown to take part in motor learning tasks in the cerebellum (Gao et al., 2016) by transmitting an efference copy of the cerebellar output back to the cerebellar cortex, which supports and enhances cerebellar learning.

The principal projection cells of the DCN were shown to have short action-potential half-widths (Uusisaari et al. 2007: Large GAD - cells). A baseline firing rate of 29.9 ± 5.8 Hz (Uusisaari et al. 2007) was observed when recording *in vitro* at 24 °C, and much higher rates of 91.59 ± 7.4 Hz when recording at physiological temperature *in vitro* at 36 °C (Person and Raman, 2011a). These cells can keep their spontaneous firing even under high convergence of PC inhibitory axons, however

experiments performed at lower temperatures masked their firing capabilities (Person and Raman, 2011a). *In vivo* recordings show that the principal projection cells discharge around 60 Hz (Rowland and Jaeger 2005), and that this value can go up to 160 Hz for short periods during cerebellar behaviors (Thach, 1968). These principal projection cells were also observed to exhibit a weak frequency adaptation in response to direct current injections so that they can keep spiking at different frequencies sustainably and transfer information reliably (Uusisaari et al., 2013). Their intrinsic tendency to preserve spontaneous firing enables these neurons to respond to excitatory or inhibitory inputs by increase or decrease in their firing rates without being strongly affected by any of the inputs continuously. Considering together with the patterns in the spontaneous firing of PCs (Shin et al., 2007), the cerebellum can use temporal signatures to encode activity. Consequently, the output of the cerebellum is given by spontaneously active principal projection cells which delicately integrate inputs from four different sources, namely PCs, inhibitory local collaterals, climbing and mossy fibers.

1.5.3.2 The inhibitory nucleo-cortical cell

The inhibitory nucleo-cortical cells of the cerebellar nuclei were initially thought to be small in number (Matsushita and Iwahori 1971a, b), however now they are considered to be as numerous as the principal projection cells (Husson et al., 2014). They are spread out together with the other DCN cell types, with their small soma size (10-20 μm) and dendritic extensions of around 150 μm (Uusisaari and Knöpfel, 2013). They project to the cerebellar cortex and also have collaterals providing local inhibition (Matsushita and Iwahori, 1971c, Chan-Palay, 1973a). The inhibitory nucleo-cortical cells release both GABA and glycine (Husson et al., 2014).

Compared to the principal cells of the DCN, the inhibitory nucleo-cortical cells have significantly different action-potential waveforms. They have longer action-potential half-widths, ranging between 0.7 and 1.2 ms, while principal cells have half-widths <0.6 ms at room temperature (Uusisaari and Knöpfel, 2013). These two cell groups also have significantly different firing rates: the principal cells fire around 30 Hz, while the nucleo-cortical cells fire slower than 12 Hz *in vitro* at 24 °C (Uusisaari and Knöpfel, 2013). The observed lower firing rate is probably due to the intrinsic membrane properties: inhibitory nucleo-cortical cells have less Kv3.1b and Kv3.3 potassium channels at their somatodendritic membrane segments (Raman et al., 2000; Alonso-Espinaco et al., 2008) compared to the principal cells. This leads to weaker afterhyperpolarization (Uusisaari at al., 2007) and probably decreased recruitment of depolarizing currents. Difference in this mechanism probably have important contribution to the difference in the firing rates between these two DCN cell types.

Another observed difference between these two DCN cell types was the spiking in response to injected current. The principal cells can spike up to 200 Hz with increasing injected current steps, while inhibitory nucleo-cortical cells spike up to 50 Hz only. Their spiking frequency accommodation was also found to be high compared to the principal cells. When a step depolarization evoking 40 Hz spiking was applied to the two groups of cells, the principal cells kept spiking at 70 % of this frequency but inhibitory nucleo-cortical cells could only keep spiking at around 40 % of this frequency (Uusisaari and Knöpfel, 2011). Consequently, the inhibitory nucleo-cortical cells appear to have limited capabilities to spike sustainably above their baseline frequency, and they operate in a smaller range of frequencies compared to principal cells. This difference between the groups is likely to be important for the computation within the DCN through the local inhibition. Since inhibitory nucleo-cortical cells with local collaterals cannot keep spiking at high frequencies, local inhibition that they provide would also be limited and it would have a restricted effect on their targets, the principal cells of the DCN.

1.5.3.2.1 The local collaterals of inhibitory nucleo-cortical cell

In a study from Uusisaari et al. (2010), glycinergic neurons were targeted in the lateral DCN using transgenic mice that expressed a fluorescent protein under the control of the glycine transporter (GlyT) 2 gene (Zeilhofer et al., 2005). It was found that a portion of glycinergic cells were not spontaneously active (Glycinergic inactive (Gly-I): Uusisaari and Knöpfel, 2010), they have long axons that leave the DCN in slices. This portion of cells was observed to spike bursts of action potentials only, and cannot keep their spiking regularly. Being purely glycinergic, they were characterized as a separate population in the mouse lateral cerebellar nucleus. These purely glycinergic cells were reported to have shorter action potentials compared to mixed GABAergic/glycinergic type nuclear cells (Uusisaari and Knöpfel, 2010).

However, this distinction was challenged in a recent study were both GABAergic and glycinergic markers were complementarily used (Ankri et al., 2015). It has been found that the nucleo-cortical projections actually arrived from the mixed-type inhibitory interneurons (Husson et al. 2014) that were thought to be responsible for only local inhibition. Finally, two types of cells, which were defined differently as Gly-I (Uusisaari and Knöpfel, 2010) and the mixed GABA-glycinergic neurons (Husson et al., 2014), are now proposed to belong to the same type according to the latest study (Ankri et al., 2015). These cells were also found to target a specific subset of Golgi cells in the cerebellar cortex in the same study, therefore they were called inhibitory nucleo-cortical cells with the local collaterals.

1.5.3.3 The non-inhibitory interneurons

In addition to the inhibitory interneurons described above, the DCN are likely to contain some non-inhibitory interneurons that were classified as such because of their small soma size (15-25 μm) and lack of GABAergic transmission. Using the glutamate decarboxylase (GAD) 67-green fluorescent protein (GFP) knock-in mouse model, Uusisaari and colleagues (2007) defined them as GADnS (GAD negative Small) neurons, and findings regarding this group of neurons are restricted only to this study to the best of my knowledge.

The non-inhibitory interneurons (GADnS) were defined to be putatively glutamatergic and were distinguished from the principal projection cells (defined as large GAD negative cells (GADnL), Uusisaari at al., 2007) by having the membrane capacitance <100 pF. This distinction is somewhat arbitrary since the reason for choosing a 100 pF threshold is not clear. Uusisaari et al. used other electrophysiological, but not morphological, measures for this classification, especially for cells with a capacitance of approximately 100 pF. Such a post-hoc classification might be biased since the electrophysiological criteria were chosen arbitrarily. Consequently, the existence of a distinct group of GADnS, the non-inhibitory interneurons, should be evaluated more carefully.

GAD negative population (GADnL & GADnS, Uusisaari at al., 2007) showed two clusters for the distribution of membrane capacitance versus action-potential width, however this does not exclude the possibility of two different types of glutamatergic projection neurons that send axons to different extracerebellar targets. This possibility should be tested with tracing studies before establishing GADnS group as interneurons, since we still lack information about their axonal extensions, which might not be observed from cell fillings in slices.

They exhibit similar morphological properties with the inhibitory interneurons with small soma size and limited dendritic extensions. However their electrophysiological properties *in vitro* were distinct from the two groups described so far. They had medium duration action potential (AP) widths of 1.15 ± 0.18 ms which was between the short AP of the principal cells and the long AP of inhibitory interneurons. Their AP peak amplitude was the biggest among the three with 27.1 ± 1.1 mV where the inhibitory interneurons were the second with 21.0 ± 2.3 mV, and the principal cells had the smallest peak amplitude of 9.0 ± 4.4 mV. These two properties were found to be significantly different among the three groups in-vitro by Uusisaari at al. (2007), however they were not observed by another study so far.

1.5.3.4 The Nucleo-olivary projection cell

In addition to the principal cells, another well-defined group of projection cells of the DCN is the GABAergic nucleo-olivary cells. This group of cells have a separate projection pathway to the inferior olive (De Zeeuw et al., 1988; Angaut and Sotelo, 1989). They had been thought to have a medium soma size (Ruigrok 1997) earlier, however a recent study using retrograde tracing (Najac and Raman, 2015) found that nucleo-olivary cell somatic area (108 ± 4 μm^2) is the smallest amongst the DCN populations. Interestingly, in the study of Uusisaari at al. (2007), nucleo-olivary cells were pooled together with the GABA/Glycinergic nucleo-cortical cells where the somatic area of the population was given as 150 μm^2 on average. A reciprocal connection between inferior olive and ventromedial cerebellar nuclei was found in mice, supporting the GABAergic feedback mechanism (De Zeeuw et al., 1997). The role of nucleo-olivary cells in the cortico-nucleo-olivary loop was also observed *in vivo* for the effective control of climbing fiber discharge (Witter et al., 2013; Chaumont et al., 2013).

Nucleo-olivary cells are found mostly in the interposed and the lateral nuclei, also in the vestibular nuclei. A small number of cells was located in the medial nuclei in rats (Fredette and Mugnaini, 1991). More specific nucleo-olivary cell localization was provided in another study in rats (Teune et al., 1998), listing the following areas: dorsolateral hump/horn, the rostral posterior interposed nuclei, the lateral part of the caudal anterior interposed nuclei, and the ventromedial part of the lateral cerebellar nuclei. Medial nuclei was also shown to contain these neurons extensively in cats (Dietrichs and Walberg, 1985). One recent study in mice did not observe nucleo-olivary cells in the medial nuclei (Najac and Raman, 2015), and another study did (Zhang et al., 2016). According to many studies, nucleo-olivary cells are nonuniformly distributed across different nuclei among species, and they are not always observed in the medial nuclei (Tolbert et al., 1976; Kalil, 1979; Najac and Raman, 2015).

1.5.3.5 The glycinergic premotor projection cell

The last population of the DCN is the glycinergic projection cell of the medial nucleus. This cell type was observed only in the rostral part of medial nucleus and it is similar to the principal glutamatergic cells as it projects to premotor areas (Bagnall et al. 2009). Glycinergic projection cells were found to receive inhibitory input from PCs efficiently. Moreover, these cells were observed to have big soma diameter of around 20 μm, which is significantly bigger than other glycinergic neurons in the DCN.

Electrophysiological properties of glycinergic projection neurons are different from the smaller glycinergic neurons. They exhibited smaller action potential width and higher maximum firing rates. This group of cells is interesting, since they were shown to have same targets with the principal projection cells. However, glycinergic projection cells were observed to send ipsilateral projections instead of contralateral ones. Excitatory/inhibitory outputs of medial nuclei to contralateral/ipsilateral areas was suggested as a balancing circuitry for postural movement control. These outputs are generated by glutamatergic/glycinergic cells with similar physiological properties and similar afferent connections received (Bagnall et al., 2009).

1.5.3.6 The distribution of cell types among different nuclei

To the best of my knowledge, no single study, systematically investigated the distribution of DCN cell types in the different cerebellar nuclei. However, some studies addressed cell distribution across a specific cerebellar nucleus or specific cell type distribution across the nuclei. One type of the DCN cells, the glycinergic premotor projection cell, was found only in the rostral part of medial nucleus (Bagnall et al. 2009) while other types generally spread to several nuclei.

The medial nucleus was found to accommodate mostly small cells (Beitz and Chan-Palay, 1979a, 1979b; Beitz, 1982) which might be an indication of a smaller population of the principal projection cells. Similarly, cells in the medial part of the anterior interposed nuclei were observed to be smaller compared to the lateral part (Ruigrok et al., 2015). Another observed difference among the nuclei is the density of dendrites, which was found to be higher for the posterior interposed nuclei and the lateral nucleus (Hamodeh et al., 2014). Most of the observations presented in this paragraph are, however, not specific to any DCN cell type.

1.5.4 Functional connectivity of the cerebellar cortex to the DCN

Three different types of input: mossy fiber, climbing fiber and the axons of PC, are all combined in a relatively small volume of the DCN (given as 3 mm^2 bilaterally, Hamodeh et al., 2014). Due to this extensive convergence on a small volume, the DCN become “the bottleneck of the cerebellar information transfer on the output side” as stated by Jaeger (2013). The highest number of afferents to the DCN come from the cerebellar cortex, where axons of ~340000 PCs converge (in rats: Harvey and Napper, 1988). In this chapter, I will describe how projections are mapped in the DCN, and how they affect different DCN cells.

1.5.4.1 Projections of the cerebellar cortex to the DCN

The three mediolateral parts of the cerebellar cortex (vermis, paravermis and hemispheres) were found to project to different but broad regions of the DCN (Jansen and Brodal, 1940). Later, studies that used myelin staining and PC axon tracing clearly defined borders of the zones of cerebellar cortex projecting to each nuclei (for a review see Voogd and Glickstein, 1998). Further studies showed a match with olivocerebellar projections to longitudinal regions in the cerebellar cortex (Groenewegen et al., 1979; Buisseret-Delmas and Angaut, 1993). These longitudinal areas are defined by afferent climbing fibers that are coming from different parts of inferior olive, and are split into A, AX, X, B and A2 in the vermis, C1, CX, C2 and C3 in the paravermis, and D1, D0 and D2 in the hemispheres (Voogd et al., 2003). PCs in these zones project to specific parts of the ipsilateral DCN (Figure 9). These corticonuclear projections take part in the cortico-nucleo-olivary loop and support the modular information processing of the cerebellum.

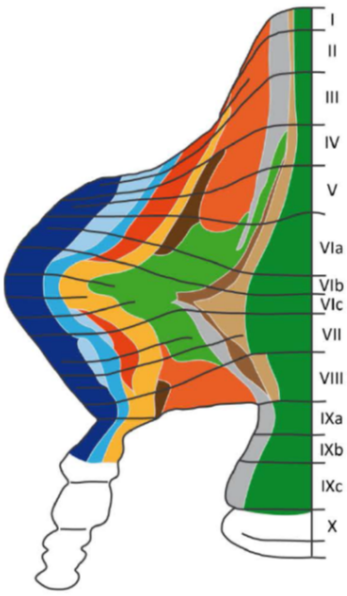

Cortical Area	Targeted by (IO region)	Projects to (DCN region)
A	Medial accessory olive (caudal, subnuc b)	Medial N (lateral), interstitial cell group
A2	Medial accessory olive (caudal, subnuc b1 & c)	Medial N (dorsolateral protuberance)
B	Dorsal accessory olive (dorsal fold)	Vestibular N (lateral)
AX	Medial accessory olive (caudal, subnuc a)	Medial N(lateral), interstitial cell group
X	Medial accessory olive (intermediate, lateral)	Interposed N (posterior), interstitial cell g.
CX	Medial accessory olive (intermediate, medial)	
C2	Medial accessory olive (rostral)	Interposed N (posterior)
C1	Dorsal accessory olive (ventral fold)	Interposed N (anterior)
C3		
D0	Principal olive (subnuc dorsomedial)	Interposed N (anterior- dorsolateral hump)
D1	Principal olive (ventral lamella)	Lateral N (magnocellular part)
D2	Principal olive (dorsal lamella)	Lateral N (parvocellular part)

Figure 9: Afferent and efferent connections of the cerebellar cortex. Specific cortical regions are given with their afferent and efferent connections in the table. Olivo-cortical connections are mediated by climbing fibers and cortico-nuclear connections by PC axons. (adapted from Apps and Hawkes, 2009)

Within the cortico-nucleo-olivary loop described above, corticonuclear projections in the DCN are not as precise as climbing fiber projections to the cortex. Climbing fibers project to highly confined areas in the cerebellar cortex that match with the expression of zebrin II as explained before. However, PCs

converge as overlapping clusters on a smaller volume of the DCN (Apps and Garwicz, 2000; Pijpers et al., 2005). Single PC axons were shown to innervate several nuclei (De Zeeuw et al., 1994a) and their terminals can have different sizes and shapes across different cerebellar nuclei (Sugihara et al., 2009). Anterograde labeling of the projections showed that single DCN cells can receive information from different cerebellar cortical areas (Panto et al., 2001). More specifically, PC projections from mediolateral (Apps and Garwicz, 2000) and rostrocaudal (Sugihara et al., 2009) areas were shown to converge on the same target areas in the DCN. Consequently, the overlapping distribution of cortical inputs suggests that DCN cells can integrate information arriving from different parts of the body rather than from any given single body area.

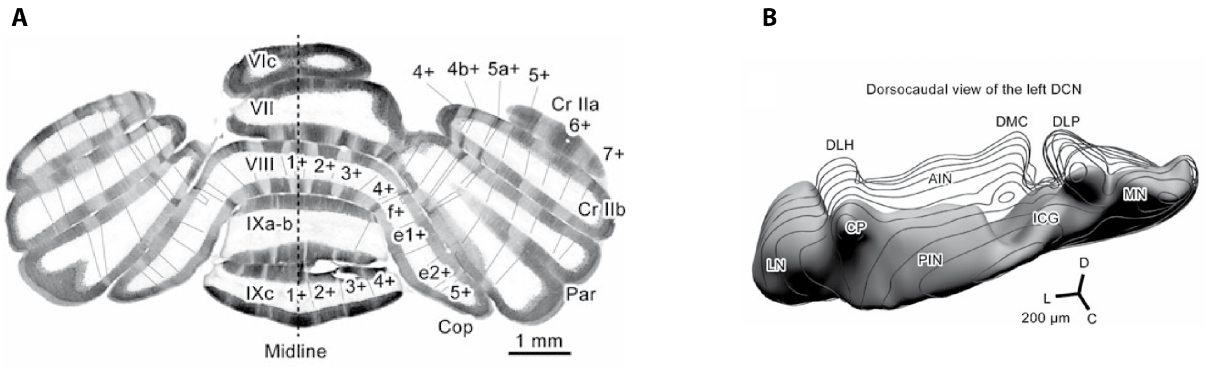

Figure 10: Aldolase C-positive and -negative compartments for the cerebellar cortex and the DCN. (**A**) In the cerebellar cortex, a coronal section shows positive and negative bands (**B**) In the DCN, a caudoventral vs. rostrodorsal division is observed. The medial nucleus (MN), the interstitial cell group (ICG), the posterior interposed nucleus (PIN), the caudal pole (CP) and lateral nucleus (LN) are broadly aldolase C-positive while the other parts, the dorsolateral protuberance (DLP), the dorsomedial crest (DMC), the anterior interposed nucleus (AIN) and the dorsolateral hump (DLH) are aldolase C-negative (adapted from Sugihara, 2011)

A specific study of projections of single PC axons from Sugihara et al. (2009) showed an important pattern in the corticonuclear connections. While single PC axons had overlapping projections, PCs from zebrin II-positive bands (Figure 10 A) projected to caudoventral regions of the DCN and zebrin II-negative PCs projected to rostrodorsal regions of the DCN (Figure 10 B). Interestingly, projections from these two groups did not overlap in the DCN. More specifically in rats, caudoventral part of the medial nucleus was targeted by 1+,2+,3+,a+,c+,4b+,d+ and 5a+ regions of the cortex (all zebrin II-positive) while rostrodorsal part of the medial nucleus was targeted by 1-,2-,a-,2b-,4a-,c-,4b-,d- and 5a- regions (all zebrin II-negative). Caudoventral parts of the interposed nucleus receives projections from 3+,e1+,4+, 5+, 2b+ and 4+ regions while its rostrodorsal part receives projections from 3-,e1-,

3b-, e2-, 4-, 5-, and 6- regions. Finally, lateral nucleus is targeted by 5+, 6+ and 7+ regions of the cortex, and did not receive projections from zebrin II-negative regions. These results illustrate the existence of a cerebellar map to different nuclei with respect to zebrin II expression. Zhou et al. (2014) observed that PCs from zebrin II-positive and zebrin II–negative regions have different spiking frequencies which could have important consequences for the output of the cerebellum, due to non-overlapping projections to caudoventral and rostrodorsal parts of the DCN.

1.5.4.2 Convergence and divergence of Purkinje cells in the DCN

Studying the shape of IPSPs in the DCN cells gives the first idea about the high number of converging inhibitory inputs. Bengtsson et al. (2011), and Uusisaari and De Shutter (2011) observed weak fluctuations in IPSPs instead of single large events which would be explained by the convergence of a high number PCs, each having small contributions. Considering the number of PCs sending projections and the number of cells receiving these projections, a ratio of approximately 7:1 in mouse was obtained, with 200000 PCs (Zanjani et al. 1996) and 30000 DCN cells (Sultan et al. 2002). This ratio was given to be 26:1 in cat and PC synaptic density per nuclear cell was estimated around 11600 (Palkovits et al., 1977). However, it is known that PC axons do not target only one cell in the DCN, and they affect many cells in a conical area. Based on the spread of PC axons, Palkovits et al. recalculated a higher convergence ratio of 860:1 in cat.

The calculation of the convergence using somatic and dendritic areas, gives different results (for details see supplementary information of Person and Raman, 2012). The principal cells have a 300 μm^2 cross-sectional area on average (Uusisaari and Knöpfel, 2007) which makes a spherical somatic surface area of 1257 μm^2. For the same cell, 4 dendrites having 10 µm proximal and 190 µm distal part make 5152 μm^2 cylindrical dendritic surface area. Combining the available information from rat and monkey, an estimation of innervated membrane area can be deduced from the maximal values of the fraction of surface covered by synapses. In lateral nuclei, maximum 63 % of the somatic area (monkey) is covered by synapses, 86 % of which come from PCs (rat) (Chan-Palay, 1977). For proximal dendrites, maximum values are 95 % and 50 % respectively. Given the total membrane area above, it is found that ~3130 μm^2 of a principal projection cell is contacted by PCs. If the area of PC synaptic boutons is taken into account, i.e. 2.5 μm^2 on average (Telgkamp et al., 2004), then the estimate number is of 1250 PC boutons per a principal projection DCN cell. This value was found to be 11600 in an electron microscopy study by Palkovits et al. (1977), however, by evaluating that each Purkinje bouton can give 9 to 10 synaptic densities (Chan-Palay, 1977), a corrected value between 1160 and 1290 was obtained. This result matches with the calculated 1250 PC boutons per DCN cell.

Knowing the number of PC boutons per DCN cell, IPSP conductances can give the number of contributing PCs. The quantal content for PC connections that was calculated using miniature IPSC conductance suggests that unitary events carry 12 vesicles in mice and 18 vesicles in rats. Telgkamp et al. (2004) reported 9 release sites per PC bouton and 0.07 vesicular release probability, which gives 0.63 release probability from at least one site. Using a probability of 0.5, Person and Raman (2011) calculated 24-36 boutons per PC. Finally they suggested that a maximum number of 34-52 PCs converge onto a DCN cell.

Another way of calculating the convergence value of PCs is by obtaining the GABAergic conductance of an isolated DCN cell body through an application of saturating GABA under patch conditions (for details see supplementary information of Person and Raman, 2012). Pugh and Raman (2005) obtained the total conductance as 43 nS (mean) and 71 nS (maximum). Comparing the whole cell surface to the isolated cell body (3130 μm^2 to 681 μm^2), inhibitory synaptic membrane increases by a ratio of ~5 so do conductances (215 nS (mean) and 355 nS (max)). These conductance values are operationally diminished to 75 % due to saturation of synaptic receptors, to 161 nS (mean) and 266 nS (maximum). Finally, the number of converging PCs can be obtained by dividing total conductances to the unitary conductance of ~9 nS as ~18 (mean) and ~ 30 (maximum). These values are in the same range with the previous calculation of 34-52 PCs per DCN cell.

It was also observed that PC axons can diverge to contact 3-5 different DCN cells in mice (Person and Raman, 2012). Despite the low divergence value, single PC projections can affect multiple neurons of different kinds (Teune et al., 1998) and of different nuclei (Sugihara et al., 2009).

1.5.5 Purkinje cell inhibition on different cells of the DCN

In many studies, anatomy, synaptic physiology and plasticity of the PC connections to the DCN were investigated, but this information has been mostly accumulated by studying the large glutamatergic cells, namely the principal cells of the DCN. Until lately, all cells in the DCN were thought to be targeted by PCs with similar properties, but now we know that there are some differences among different cell groups in terms of PC innervation.

The assessment for PC innervation on the DCN cells were done by *in vitro* studies where it is a challenge to keep an entire PC axon intact in a slice. Due to this technical difficulty, the actual effect of a single PC is hard to obtain. However, most of the DCN cell somas and proximal dendrites are intact in the slices and the information compiled below is based on these conditions.

1.5.5.1 Purkinje cell innervation on the principal cells

PCs constitute the majority part of the input that the DCN receives as explained above. PC axons mostly (80 %) synapses on the soma of the principal cells of the DCN (Palkovits et al., 1977; De Zeeuw & Berrebi, 1995, Uusisaari & Knöpfel, 2008). This numerous innervation leads to a strong control of the principal cell activity in the DCN (Lang and Blenkinsop 2011). Without the GABAergic control of PCs, principal cells spike at their maximal rates or they may be subject to depolarization block (Raman et al. 2000). Strong GABAergic input, on the other hand, can inhibit them completely. Consequently, the amount of GABAergic input determines the firing rate of the principal cells.

Simultaneous *in vivo* pair recordings from a single PC and its target cell in the DCN showed that they do not have a strict relation in the firing rates and times: a single PC did not modulate the activity of its target cell in the DCN (McDevitt et al., 1987). For PC-DCN innervation, many different PC axons operate together, and their degree of synchrony determines the inhibitory effect on the principal cells. In slice preparations, a high number of asynchronous GABA releases was observed even if most of the connections coming from the cortex were cut. GABAergic postsynaptic currents were observed at high frequencies up to 70 Hz with amplitudes of up to 300 pA (Uusisaari et al., 2008). Additionally, there is also another source of inhibition that arrives from local cells.

The principal cells receive GABAergic IPSCs from PCs through $GABA_AR$ with α_1 or $\alpha_1/\ \alpha_3$ subunits with a decay time constant of 2.4 ± 0.2 ms (Person and Raman, 2011) at 36 ° C. Such a fast decay in IPSC is among the fastest known for $GABA_AR$ mediated currents (Bartos et al., 2002). This finding explains why the principal cells can maintain their spiking behavior under a high convergence of inhibitory input as summation hardly occurs when inputs are desynchronized. It is indeed found *in vivo* that individual PCs have very small effect on the membrane potential of principal DCN cells. Combined inhibition from converging PC axons introduce only weak fluctuations in postsynaptic principal cell membrane potential when they arrive asynchronously (Bengtsson et al., 2011; Person and Raman; 2011). Such asynchronous events from many PCs keep the principal cells in a dynamic range so that they can decrease or even increase their firing according to slight changes in the inhibitory afferents in a rate coding manner. Consequently, the activity of principal DCN cells can be modified not by individual, but a collective change in the activity of the group of PCs *in vivo*.

1.5.5.2 Effects of synchronized Purkinje cell inputs

In their study, Person and Raman (2011) mimicked IPSPs arriving from 40 different PCs using dynamic clamp on a principal DCN cell that was selected by its soma size. When IPSPs were delivered in an asynchronous way, they provided a tonic inhibition which strongly reduced the firing rate. When IPSPs were delivered in a synchronized way, the total effect of the inhibition was decreased, and the firing rate of the DCN cell was reduced to a lesser extent (Figure 11 A). Most of the target cells received smaller total inhibitory effect as the delivered IPSP synchronization degree was increased from 5% to 50 % (see Person and Raman, 2011, Figure 3c). The reason for this reduced inhibition was the time-locked spiking behavior of the DCN cells following the synchronous IPSPs. Increasing the degree of synchrony reduced the inhibitory effect (Figure 11 B). The same time-locking behavior was observed *in vivo* too, where principal DCN cells recordings were obtained under molecular layer stimulation.

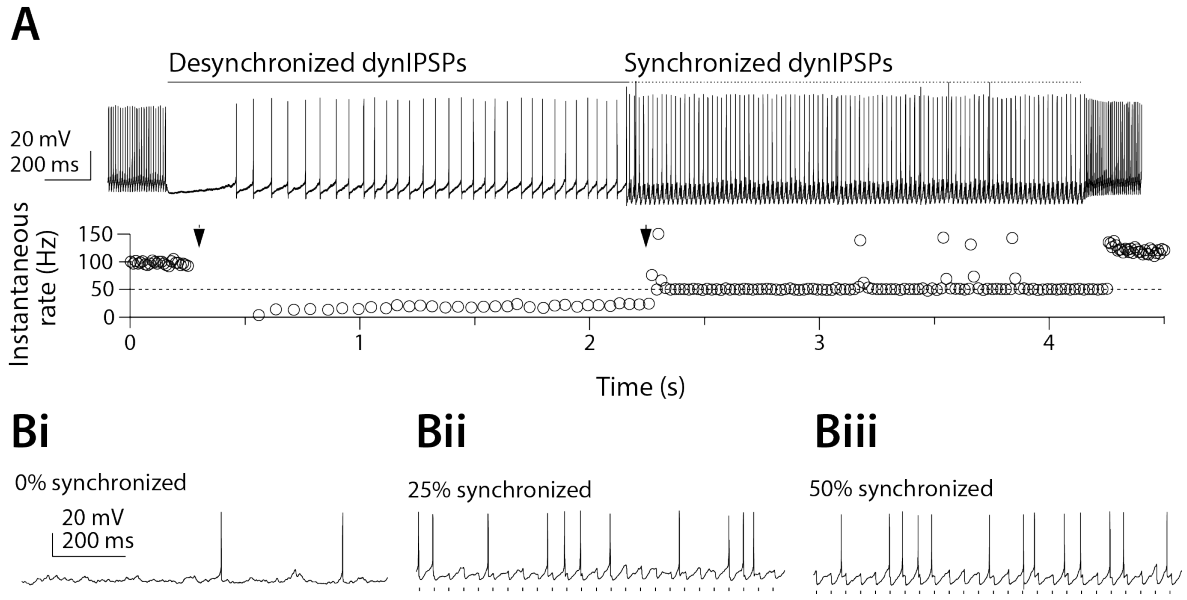

Figure 11: The effect of synchronized PC IPSPs in whole-cell condition. (**A**) Under dynamic clamp *in vitro*, synchronizing IPSPs reduced the net inhibitory effect on a DCN cell (upper graph) and firing rate of the cell was reduced less (**Bi-Bii-Biii**) Degree of synchrony of the IPSPs effected firing rate of the DCN cell gradually (adapted from Person and Raman, 2011)

There are two possible mechanisms that may unexclusively explain this time-locking behavior. First mechanism is the rebound-like single-spike response to the synchronized IPSPs. The principal DCN cells have intrinsic membrane properties that sustain spontaneous activity which is mainly supported by two currents. First one is the tetrodotoxin-insensitive, voltage-independent, cationic currents

(Raman et al., 2000). These cationic currents can depolarize the cell to threshold voltages even under a continuous inhibition of PCs. The second current is a large amplitude low-voltage activated calcium current ($Ca_v3.x$, Molineux et al., 2006). Large diameter DCN cells (putatively principal cells) were observed to fire burst response to current injections *in vitro,* and this response was stronger when current injections were preceded by hyperpolarizations (Molineux et al., 2006). These two conductances, the tonic cationic current and the low-voltage activated calcium current, may take part in the generation of a rebound-like intrinsic responsiveness. Synchronization of IPSCs induces a strong hyperpolarization possibly triggering this mechanism.

The second possible mechanism for the time-locking behavior is based on the temporal gaps in the tonic inhibition of the principal cells. Again, when the IPSCs are synchronized, some short time periods of low inhibition appear during tonic inhibition. These short periods following synchronized events provide a temporal window for the principal DCN cells to spike. Both mechanisms explained triggered by an inhibition from synchronized PCs, and they likely underlie the timed-locked activity of principal DCN cells. Further evidence from *in vivo* patch recordings is needed to deeply investigate this behavior.

1.5.5.3 Purkinje cell innervation on the nucleo-olivary cells

The nucleo-olivary cells of the DCN are also innervated by PC axons at the soma and/or proximal dendrites (Teune et al, 1998) similar to the principal cells. Differences between the principal cells and nucleo-olivary cells have been studied in detail in a recent *in vitro* study (Najac and Raman, 2015). One-third of the nucleo-olivary cells are found to have no functional input from the PCs while the actual ratio could be lower since the dendritic inputs of PCs might have been cut during slicing. Under electrical or optogenetic stimulation of PCs, GABAergic IPSCs that were evoked in the nucleo-olivary cells were much slower than the ones recorded in the principal cells (decay time constant ~25 ms compared to ~2 ms). Expression of both slowly-gating (α_3) and fast-gating (α_1) units at different ratios in GABAergic neurons of the DCN were observed by Uusisaari and Knöpfel (2008) and such a mixed expression seems to underlie long decay time constants.

This long decay time constant leads to a stronger inhibition of nucleo-olivary cells as PC stimulation can suppress their activity. The time-locked spiking behavior observed in the principal DCN cells was not present in the nucleo-olivary cells: their spiking activity did not follow IPSCs from PCs and appeared to be random (Najac and Raman, 2015). This shows that nucleo-olivary cells transmit PC activity in a rate coding manner *in vitro* by decreasing firing rate under increased PC activity, without coding for any information about PC spike timing.

1.5.5.4 Purkinje cell innervation on the inhibitory nucleo-cortical cells

The inhibitory nucleo-cortical cells have similar properties with nucleo-olivary cells (both are GABAergic) and they were found to receive smaller currents from PCs at lower rates with long decay time constants (up to 100 pA at 3 Hz) compared to the non-GABAergic principal cells. Another difference was the location of the PCs contacts on these cells. Results of recordings from Uusisaari and Knöpfel (2008) suggested that non-GABAergic cells receive IPSCs around soma and proximal dendrites while GABAergic cells receive IPSCs at the distal dendrites.

A recent study challenged the previous findings by specifically targeting nucleo-cortical cells *in vitro* thanks to their mixed GABA/Glycinergic phenotype (Ankri et al., 2015), and they were found to receive large inhibitory currents from PCs (mean amplitude of 416.5 ± 332.1 pA). Decay time constant of IPSCs (3.28 ± 0.72 ms) was also found to be similar to that of principal cells. Ankri et al. suggest that inhibition from PCs have a stronger control of nucleo-cortical cells compared nucleo-olivary cells.

1.5.5.5 Purkinje cell innervation on other cells in the DCN

With the latest classification of the DCN cells, two more cells - non-inhibitory interneurons and glycinergic premotor projection cells - remain to be discussed in terms of PC innervation. The validity of a separate class of non-inhibitory interneurons is questioned in the previous chapter and they do not appear to differ from the principal cells in terms of PC innervation.

The glycinergic premotor projection cells of the medial nuclei, as the last group, also have similar properties of PC innervation with principal cells of the DCN (Bagnall et al., 2009). Their soma was found to be extensively targeted by many PC terminals and they have the same fundamental circuit structure compared to the principal cells.

1.5.5.6 Plasticity of PC connections in the DCN

Only few studies to date have demonstrated long-term plasticity at the PC to the DCN connections, and they are restricted to the principal cell only. When PC inputs are not strong enough to generate rebound depolarization, low frequency stimulation resulted in LTD of PC-originating IPSPs (Morishita and Sastry, 1996). However, under strong PC stimulation, burst of inputs and rebound depolarization of the DCN cells was observed and the connection was potentiated (Aizenman et al., 1998). This connection also exhibit short term depression (STD) characteristics. High frequency input from PCs was filtered by a considerable STD (Telgkamp and Raman 2002; Pedroarena and Schwarz 2003) (Figure 12) and this feature decreased the effect of complex spikes of PC on the DCN cells.

Some factors restrict the effect of this depression: PCs have around 10 active zones with low release probability and spillover mediated transmission properties (Telgkamp and Raman 2002; Pedroarena and Schwarz 2003). Finally, the roles of STD mechanisms in behavioral context are yet to be demonstrated (Jaeger, 2013).

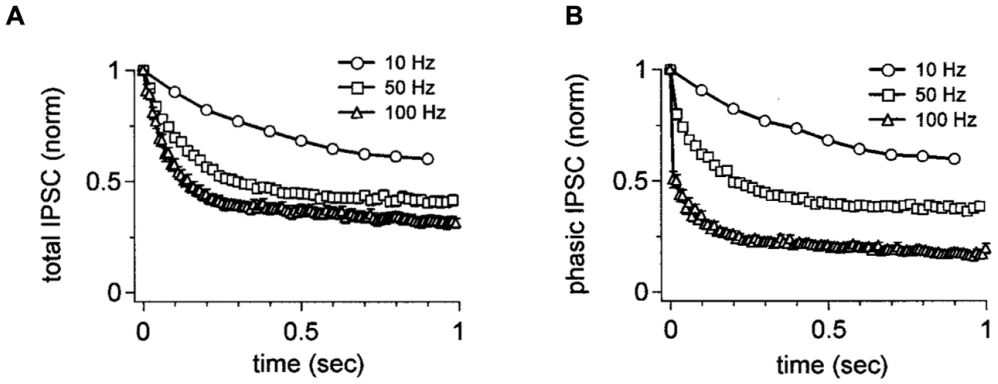

Figure 12: Short-term depression characteristics of PC to the DCN cell connection. (**A**) Total IPSC was reduced in fixed frequency inputs and (**B**) for 100 Hz input phasic component was strongly depressed very quickly (adapted from Telgkamp and Raman, 2002)

1.5.6 Information processing in the DCN

Until late 1990s**,** the DCN used to be considered as a relay station which transfers the information processed in the cerebellar cortex. In recent studies, the details of the different DCN cell types and plasticity mechanisms in the DCN have been discovered, and now we have a complex picture of the DCN. This picture is not complete but it reveals some important points about information processing in the DCN.

Inputs from 3 different pathways: cerebellar cortex, mossy fiber and climbing fiber, converge onto the DCN, and lead to a challenging question: how can these input pathways cooperate in the modulation of spiking activity? This cooperation was only studied during a few specific behavioral tasks such as eyeblink conditioning, and both the cerebellar cortex and the DCN were shown to develop associated neural responses (McCormick and Thompson, 1984) during learning. It was later discovered that learning in the DCN was triggered by learning in the cortex (Garcia et al. 1999), however, eyeblink conditioning was learned and stored in the DCN circuitry even when simple spikes of PCs were suppressed (Wada et al., 2007) which shows the importance of PCs' complex spikes for learning. It was also discovered that eyeblink response could be acquired or sustained even if the DCN was lesioned in mice (Koekkoek et al., 2003; Sakamoto and Endo, 2010). However, an intact DCN was

required for stimulus discrimination in the delay eyeblink conditioning task (Sakamoto and Endo, 2013). Consequently, intact inputs from the cerebellar cortex are needed for learning in the DCN, and after that the DCN can store motor memories to carry out the task without the cerebellar cortex. After the training, inactivating the cortex does not totally stop the conditioned response, but disrupts its timing (Perrett et al. 1993; Holdefer et al. 2005, for a review see Mauk, 1997).

Below I will first summarize the effects of mossy and climbing fiber input and their plasticity in the DCN. Then, I will elaborate on information integration in the two important cell types that contribute to the generation of cerebellar output: the inhibitory nucleo-cortical cells that provide local inhibition and the principal cells that make the final output of the DCN. Possible interactions between the input pathways and intrinsic networks within the DCN will be the main focus.

1.5.6.1 Mossy fiber innervation and plasticity in the DCN

Together with the large amount of inhibitory inputs arriving from PCs, excitatory inputs from mossy and climbing fibers also project to the DCN cells. Mossy fibers have high ramification in the DCN and can contact different areas (Shinoda et al. 2000). In the cerebellar cortex, multiple patches that receive mossy fiber inputs represent specific body areas (Shambes et al., 1978; Ekerot and Jörntell, 2001), but such a precise localization in the DCN does not exist. The DCN cells were shown to respond to multiple areas of the body upon air-puff stimulation *in vivo,* and they had large bilateral mossy fiber receptive fields in all three nuclei (Rowland and Jaeger, 2005). In basal conditions, activity of mossy fibers is low but during cerebellar behaviors their firing rate can increase up to 100 Hz (van Kan et al., 1993). This increased activity excites the DCN cells through a direct synaptic connection. Bengsston and Jorntell (2014) made *in vivo* whole cell recordings of the DCN cells under cutaneous stimulation of mossy fiber receptive fields which evoked synaptic excitation in the membrane potentials (Figure 13 A). This direct excitation from mossy fibers seemed to linearly modulate the DCN cell activity (Lang et al., 2016).

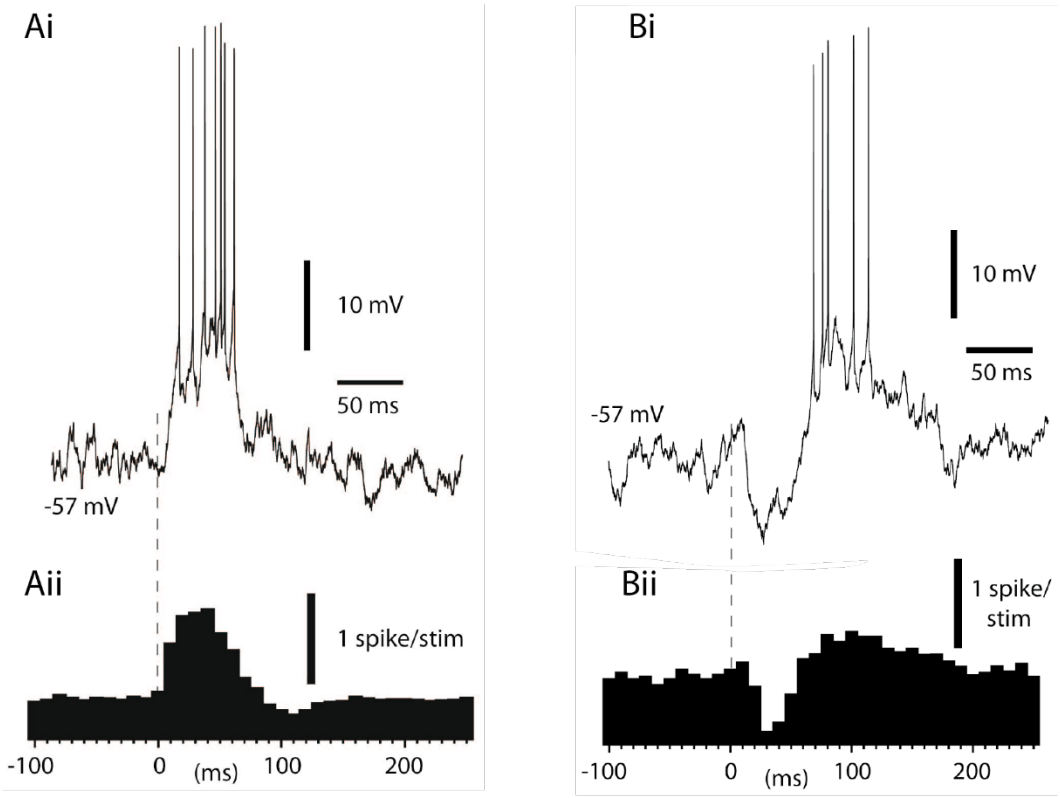

Figure 13: Integration of inputs in a DCN cell *in vivo.* (**A**) Stimulation of mossy fiber receptive field resulted in high frequency spiking. (**B**) Stimulation of climbing fiber and mossy fiber receptive fields together added a short-latency inhibition to the response and a smooth long latency excitation was observed. Further details are given in the text (adapted from Bengtsson and Jörntell, 2014).

Mossy fibers also evoke indirect responses in the DCN cells through the cerebellar cortex which depend on the functional connectivity between granule cells and PCs. Cutaneous stimulation of parallel fiber receptive fields leads to excitation of PCs (Figure 14 Ai) and inhibition in the DCN cells (Figure 14 Aii). The same pathway can also lead to the opposite response (Figure 14 Bi and Bii). After the acquisition of the eye blink conditioning, the conditioned response delivered through mossy fibers inhibits PCs and excites the DCN cells (for a review, see Mauk, 1997). Consequently, the functional connectivity in the cortex determines the indirect effect of the mossy fibers in the DCN cells, which can be inhibitory or excitatory.

This indirect pathway is also important for the plasticity of the direct mossy fiber connections in the DCN (Pugh and Raman, 2006). Previously, these connections were found to be potentiated by strong burst of stimulations *in vitro* (Racine et al. 1986) which might have led to the activation of multiple pathways. Later with more physiological stimulations, Pugh and Raman (2006) showed that the

plasticity of this connection did not occur without the cooperation of the cerebellar cortex such that mossy fiber connections in the DCN were not potentiated when PC inhibition was blocked. They demonstrated that a sequential collaboration of synaptic excitation and inhibition was needed for potentiation: the excitation coming from mossy fibers should be followed by the inhibition coming from the PCs with a delay of 250 ms. Changes in the relative timing of excitation and inhibition changed the plasticity and a depression was observed if the timing did not matched (Figure 15 A-B).

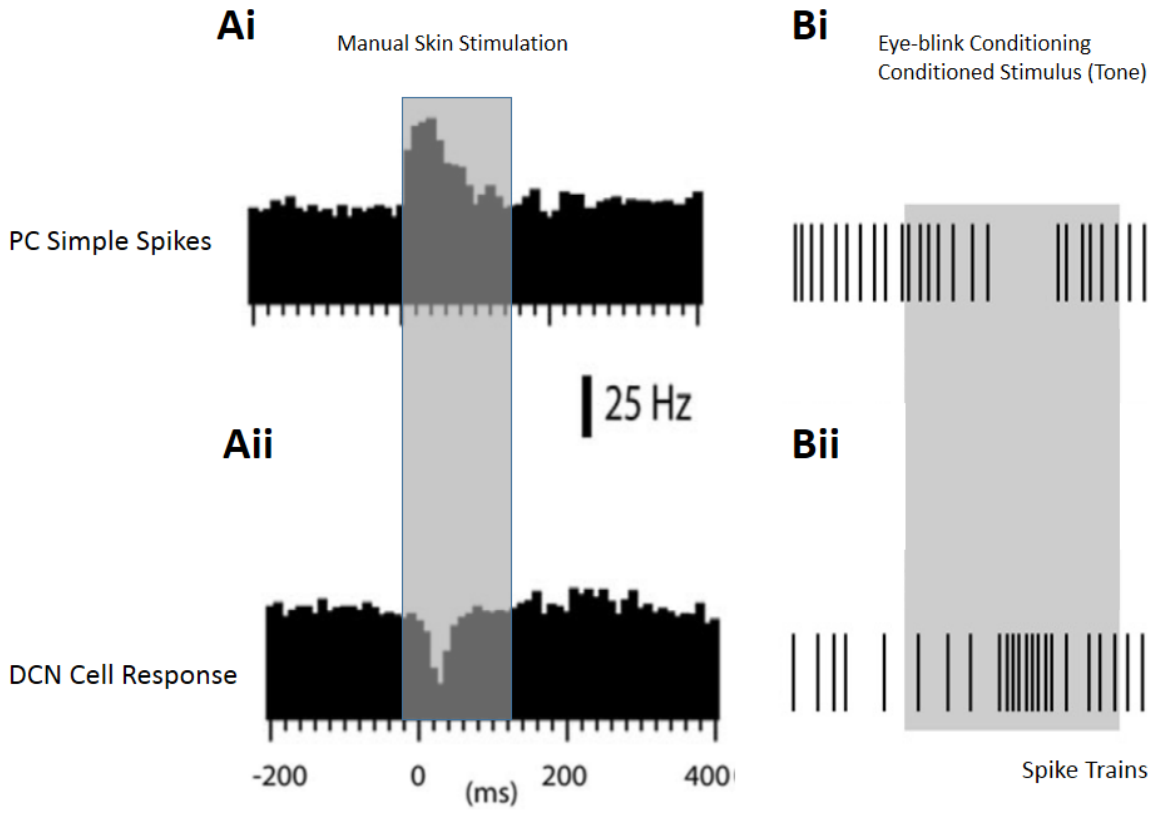

Figure 14: Different responses evoked by mossy fiber in PCs and in DCN cells. (**A**) Manual skin stimulation excited PCs (**Ai**) and inhibited the DCN cells (**Aii**) however same pathway can lead to opposite responses (**B**) after eye-blink conditioning where PCs were inhibited (**Bi**) and the DCN cells were excited (**Bii**) (adapted from Bengtsson et al., 2011 and Mauk, 1997)

In the DCN cells, the sequential excitation and inhibition triggers a multistep signaling pathways which uses Calcium-dependent enzymes (α-CaMKII) and controls specific Ca channels (L-type) that governs this complex LTP mechanism (Person and Raman, 2010).

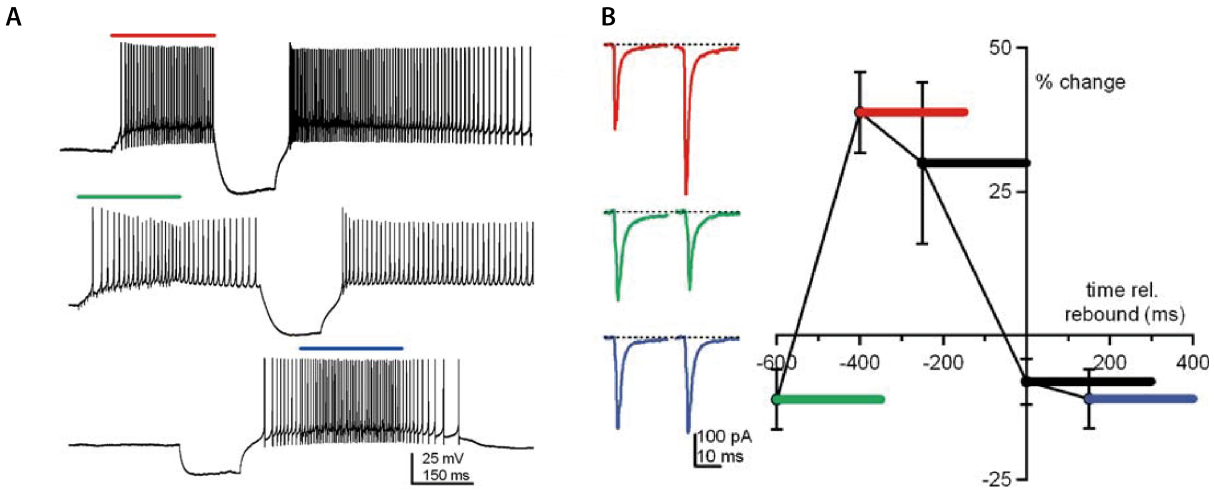

Figure 15: Long term potentiation of mossy fiber EPSCs in the DCN. (**A**) DCN cell responses following three induction protocols. EPSP trains at 133 Hz of 250 ms duration (colored bars) and hyperpolarizations of 150 ms duration were applied with different timings (**B**) Relative timings of the EPSP train and the hyperpolarization period resulted in different long term potentiation profiles. Further details are given in the text (adapted from Pugh and Raman, 2008).

1.5.6.2 Climbing fiber innervation in the DCN

The other excitatory efferent connection to the DCN is projected from the inferior olive with the climbing fibers. Compared to mossy fibers, climbing fibers make connections that preserve the olivo-cortico-nuclear loop (Apps and Garwicz, 2000; Pijpers et al., 2005). They had been reported to target the distal dendrites of different types of the DCN cells (van der Want and Voogd, 1987; De Zeeuw et al., 1997), however, somatic and proximal connections were also shown later (Shinoda et al., 2000). Optogenetic stimulation of the inferior olive resulted in only small excitatory effect on the DCN cells *in vitro* and *in vivo* (Lu et al., 2016). During spontaneous activity, this small excitatory effect (~1 mV) was followed by bigger inhibitory effect (~ 7 mV) which was introduced by the indirect pathway through the PCs (Figure 16). Same response was observed as short latency inhibition in Figure 13 B.

Given specific feature of the climbing fiber inputs leading to a small direct excitatory effect and an indirect inhibitory effect might be important for controlling the plasticity of PC and/or mossy fiber inputs. Also, climbing fiber collaterals were found to target the small cells in the DCN (Shinoda et al., 2000), but unfortunately we don't have further information about the cell types or plasticity mechanisms.

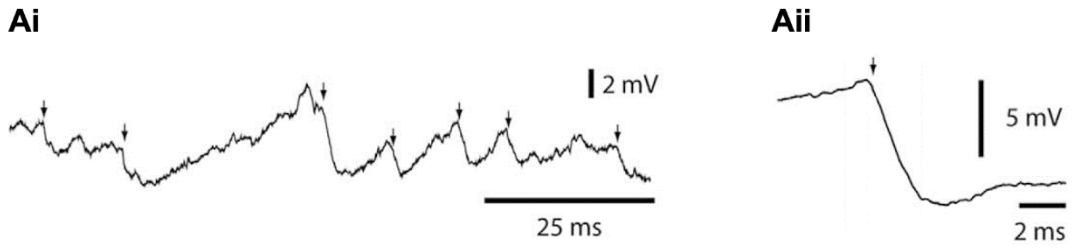

Figure 16: Climbing fiber induced IPSPs in a DCN cell recorded *in vivo.* (**Ai**) Spontaneous effect of hyperpolarizations in the membrane potential and (**Aii**) zoom into one of the events. (adapted from Bengtsson et al., 2011)

1.5.6.3 Integration in the inhibitory nucleo-cortical cells

To summarize the information given above, the nucleo-cortico cells in the DCN were shown to receive strong PC inhibition (Ankri et al., 2015). They spike at low frequencies *in vivo*, relying on the excitatory inputs to the DCN, however properties of their potential climbing and mossy fiber connections have not been specified, to the best of my knowledge. Their predicted function in the intrinsic DCN circuitry is to provide local inhibition proportional to the incoming excitation and inhibition whose relative effects are not known.

1.5.6.4 Integration in the principal cells

The principal cells spike around 60 Hz *in vivo* (Rowland and Jaeger 2005) and can be excited up to 200 Hz with low frequency adaptation (Uusisaari and Knöpfel, 2011). Their spiking behavior under sensory stimulation *in vivo* displays a complicated modulation, combining direct and indirect effects. Rowland and Jaeger (2005) recorded 3 different phases of modulation in response to a brief touch stimulation to the face of an anesthetized rats which was an air puff lasting around 2.5 ms with ~10 ms effects on the skin (Figure 17).

First a fast excitatory response (Figure 17- red) was recorded within 15 ms after the stimulation onset. This excitation is likely to be induced by the direct connections of the mossy or climbing fibers. It was followed by a strong inhibition (Figure 17- blue) lasting ~250 ms where the DCN cell was shut down for a small period of ~100 ms, and then its firing rate increased slowly. This period corresponds to the indirect effect though PCs. After the inhibition period, the increase in the firing rate continued and a long-latency excitation (Figure 17- yellow) period was observed. This last phase might be caused by the disinhibition through the nucleo-olivary pathway and/or by the intrinsic excitability of the principal cells.

Interestingly, Rowland and Jaeger observed similar three-phase responses in all three nuclei however, some of the recorded cells did not show the three phases. When the stimulation strength was changed, the number of responding cells changed differently among the nuclei. The authors suggested that the observed common response contradicts the idea of specific receptive fields in the DCN. However, this observation might be caused by the stimulation method used: the air puff skin stimulation was relatively long (2.5 ms) and probably affected other sensory modalities. Also, some reflex mechanisms could have been triggered since it resulted in a big vibration of the skin (~2 cm diameter) lasting for ~10 ms. Consequently, the stimulation used is questionable for its unimodular effect since similar *in vivo* studies prefer much shorter (0.2 ms) low intensity electrical skin stimulation (Bengtsson et al., 2011).

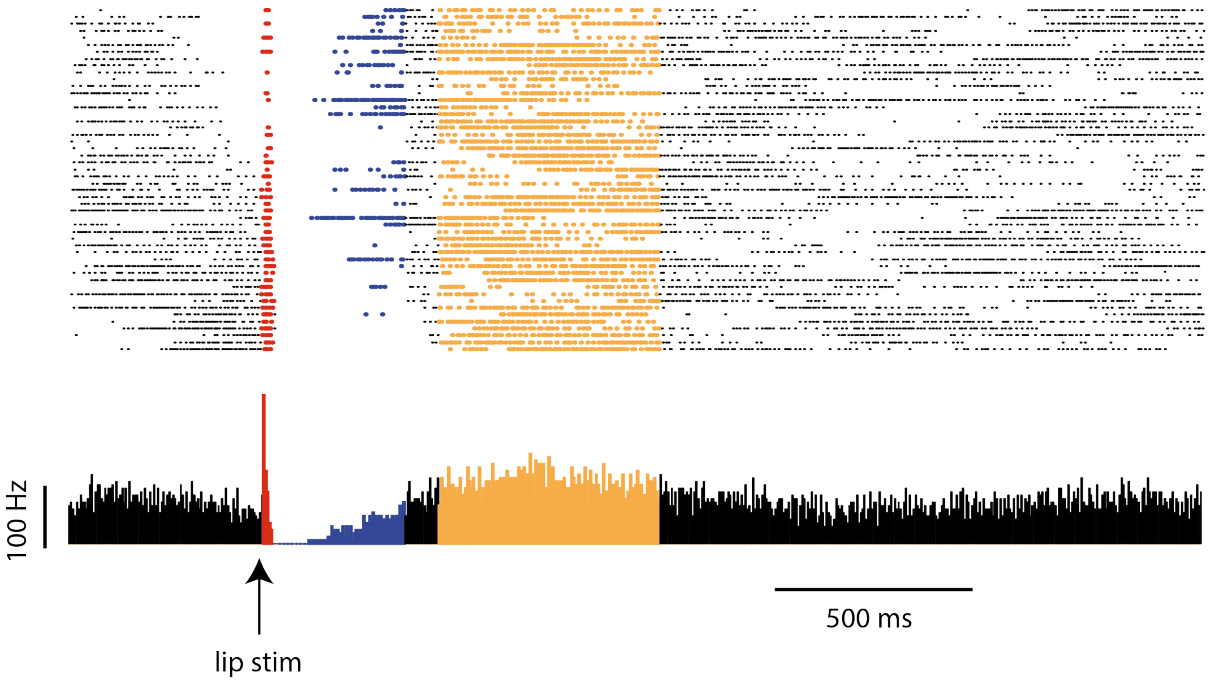

Figure 17: Sensory modulation of a DCN cell in an anesthetized rat. Spike events as dots during the trails (top) and resulting instantaneous firing frequency profile (bottom) given. A fast excitation response (red), a strong inhibition period (blue), and a long latency excitation period (yellow) were observed. Details are given in the text. (adapted from Rowland and Jaeger, 2005)

1.5.6.5 Receptive fields in the DCN

As an update on Rowland and Jaeger (2005) study, physiological skin stimulations to specific areas showed that receptive fields in the DCN do exist and different responses can be evoked in the same

cell. Bengtsson and Jörntell (2014) showed *in vivo* that a DCN cell can respond very differently according to climbing fiber receptive field of its afferent PCs (color coded, Figure 18).

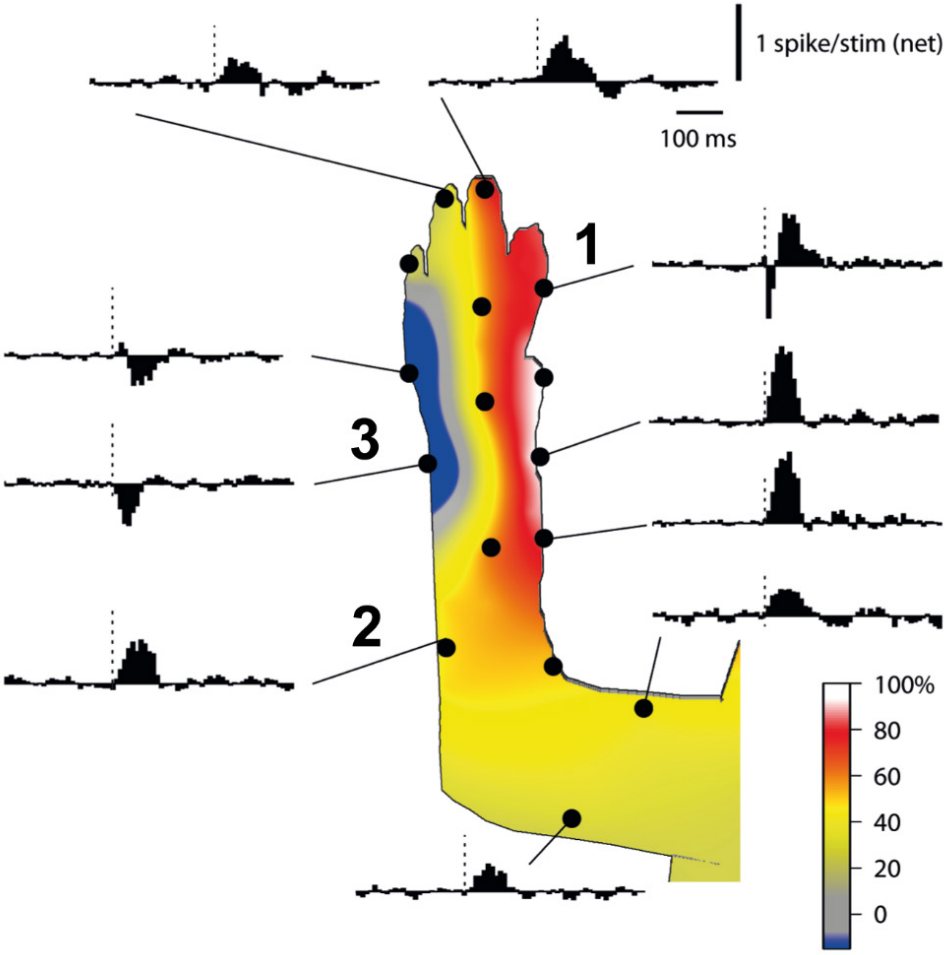

Figure 18: Stimulation of skin areas evoke very different responses in a DCN cell *in vivo*. (**1**) Strong short latency inhibition observed by stimulation of climbing fiber receptive field only and (**2**) mostly only excitation response was observed. In some regions **(3)** only inhibition was effective. Color bar represents relative climbing fiber receptive field for the recorded cell. Further details are given in the text (adapted from Bengtsson and Jorntell, 2014).

The first area with strong climbing fiber effect showed a three phase response (Figure 18 -1) as discussed earlier. The second stimulation area was outside the receptive field and only a long-lasting excitation was observed without the indirect inhibition from PCs (Figure 18 -2). This effect was probably caused by direct mossy fibers connections. Another possibility is that (a group of) afferent PCs were inhibited in this case and they disinhibited the DCN cell (similar to Figure 14 B) which depends on the synaptic connectivity in the cerebellar cortex. The third stimulation area, close to the

second one, showed a totally different response profile where only inhibition was recorded (Figure 18 -3). There are at least two possible non-exclusive sources for this inhibition: (a group of) afferent PCs could be excited in the cerebellar cortex which inhibit the DCN cell and/or the nucleo-cortical cells could inhibit neighboring cells locally. All of these responses show the complex integration possibilities in the DCN cells.

1.5.6.6 PC inhibition vs local inhibition in the DCN

As mentioned before, the principal cells receive inhibition from the local collaterals of the nucleo-cortical cells and also from PCs. This local inhibition has significant effect on the activity of the principal cells, being smaller but comparable to that of PCs. Optogenetic stimulation of nucleo-cortical cells was observed to result in IPSCs for 48.3% of the principal cells with the IPSC amplitude of 145 ± 152 pA (Husson et al., 2014). Inhibitory currents evoked by PC stimulations were much larger due to the convergence of many PCs, ranging from ~250 pA to 3nA. However, spontaneous IPSC amplitudes recorded from the principal cells were small (71 ± 31 pA: Telgkamp and Raman, 2002). Consequently, the relative effect of the local inhibition depends on the synchronicity of converging PCs connections which may override the local inhibition completely. When PC and local inhibitory synapses were compared, temporal properties of the synaptic events (paired-pulse ratio and decay time constants) were not different (Husson et al., 2014) which supports the similar effect of the inhibition from these connections.

Another recent study focusing on information processing in the DCN drew attention to the possible functional effects of local inhibition (Baumel et al., 2009). In this study, harmaline was injected into the inferior olive in freely moving animals and the climbing fiber firing rate increased up to 10 Hz. Consequently, frequent quiescence periods were observed in the DCN cells which were previously firing in a stochastic manner. DCN cells were totally inhibited in these periods. Authors suggest that these quiescence periods may be introduced by local inhibition in the DCN, considering the functional efficiency of local inhibition in DCN circuitry.

2 OBJECTIVES OF THE STUDY

Background

DCN cells integrate information from different sources and the biggest number of inputs come from PCs. Some of the functional properties of these connections seems to be resulted from high number of converging PCs and intrinsic properties of different cell types in the DCN. For the functional operation between PCs and DCN cells, both rate and temporal coding properties have been previously observed *in vivo* and how these coding mechanisms are preferred remains as an open question.

Given this background as a summary of properties mentioned in the introduction part of my thesis, we aimed to investigate the temporal properties of connections of PCs in DCN. In order to achieve this aim, we focused on our region of interest as Lobule IV/V of the cerebellar cortex and the medial DCN and recorded from these connected regions simultaneously.

Specific research questions of the PhD project:

- How do PCs and DCN cells from connected regions behave under stimulation *in vivo*?
- Is it possible to distinguish different cell types in DCN using extracellular recordings?
- How are PC inputs coded by different cell types in DCN *in vivo*?

3 RESULTS

3.1 Multiple cells from connected regions in the cerebellar cortex and in the DCN are simultaneously recorded under optogenetic stimulation *in vivo*

In this study, PCs in the cerebellar cortex and the medial DCN cells were recorded simultaneously. Previous studies with the CD1 L7-ChR2 mouse strain demonstrated that PCs are reliably excited with blue light illumination while DCN cells were inhibited with the same stimulation (Chaumont et al., 2013). However previously these two effects were not observed simultaneously.

3.1.1 Tracing PC projections with virus and dye injections

In order to trace connections between PCs and DCN cells, virus and tracer injections were done to the Lobule IV – V in the vermis of the cerebellar cortex. Projections of PCs to DCN were reconstructed using confocal imaging microscopy. Firstly, AAV 2/1 (adeno-associated virus) with green fluorescent protein (GFP) was injected (Figure 19 A). Projections were observed from the vermis to the medial and the interposed nuclei (Figure 19 A). Targeted DCN cells in the medial DCN were found 2.2-2.6 mm ventral and 600 μm posterior to the injected PCs in the cortex (see methods for details of the injections)

Similar projection results were also obtained with DiI (lipophilic cationic indocarbocyanine dye) injections (Figure 19 B). Projections of PC from vermis of lobule IV-V were traced down to the medial DCN. These tracing experiments identified the organization of the connectivity between our recording locations in our CD1 mice strain and provided coordinates to target these locations during *in vivo* experiments.

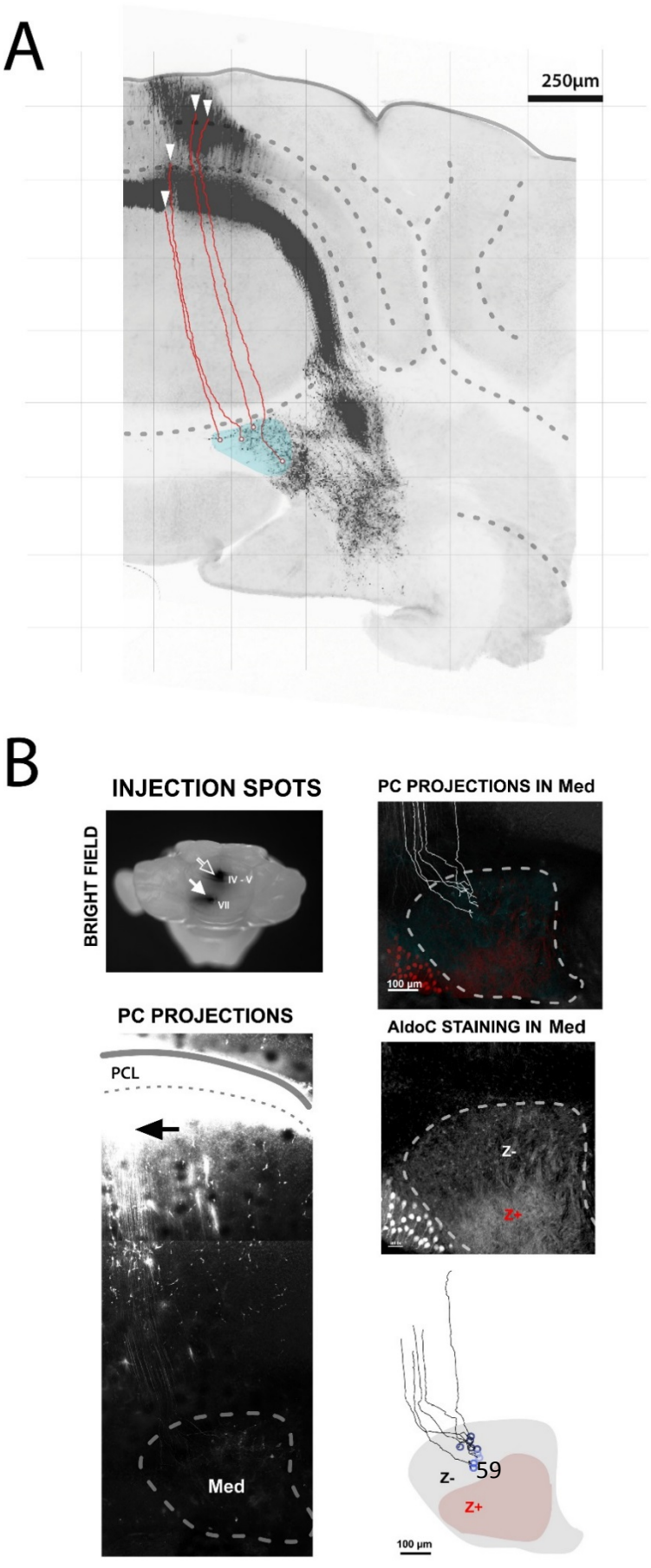

Figure 19: PC projections to the medial DCN obtained with two different injection methods. (**A**) Virus injection into Lobule IV/V infecting PCs and their projections (in red) were traced through a stack of slices (z-projection) to the medial DCN (blue shaded area) (**B**) DiI injection in the cerebellar cortex labelled PCs and their projections to the medial DCN. Tracing single PC axons showed that they project only into zebrin negative part of the DCN (Aldolase C staining in Med).

3.1.2 Determining recording areas after the experiments

During *in vivo* experiments, multielectrodes were painted with DiI tracer in order to mark the recording locations. After the recordings, cerebella were fixed in paraformaldehyde and histologically analyzed after slicing. We only analyzed the experiments in which the recording electrodes were situated in the vermis of Lobule IV/V and in the medial DCN (Figure 20).

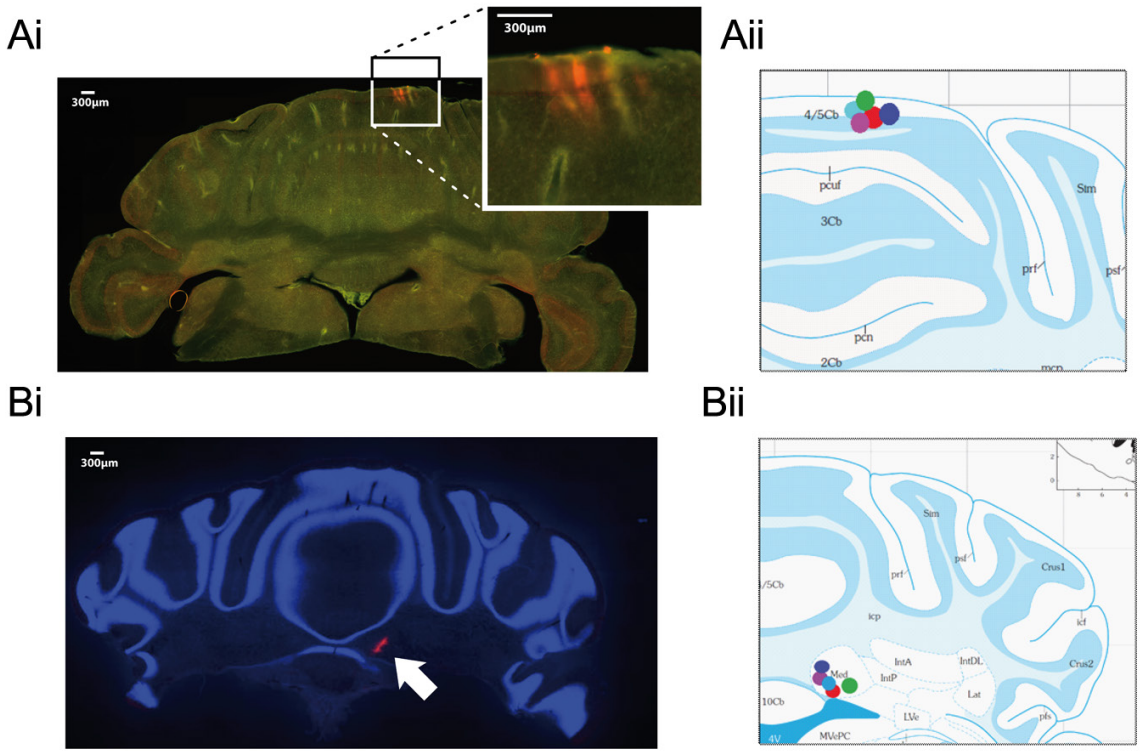

Figure 20: Recording locations obtained after histological analysis. (**Ai**) An example of coronal cerebellar slice with electrode marks in the cerebellar cortex was obtained after an experiment (**Bi**) Similar electrode mark with one shank (white arrow) was observed in the medial DCN (**Aii**) Recording locations in the cortex and (**Bii**) in the medial DCN from five experiments are shown on the coronal maps with different colors

3.1.3 Simultaneous multielectrode recordings from the two areas

In the experiments, we used a Multichannel Systems acquisition amplifier that allowed us to record simultaneously 32 channels from two different recording areas: the cerebellar cortex and the medial DCN. In each recording area, 16 channels were used in 4 tetrodes each having 4 recording sites, designed to align in a diamond shape (see methods for the electrode structure). This specific alignment of recording sites receive signals from close but different areas.

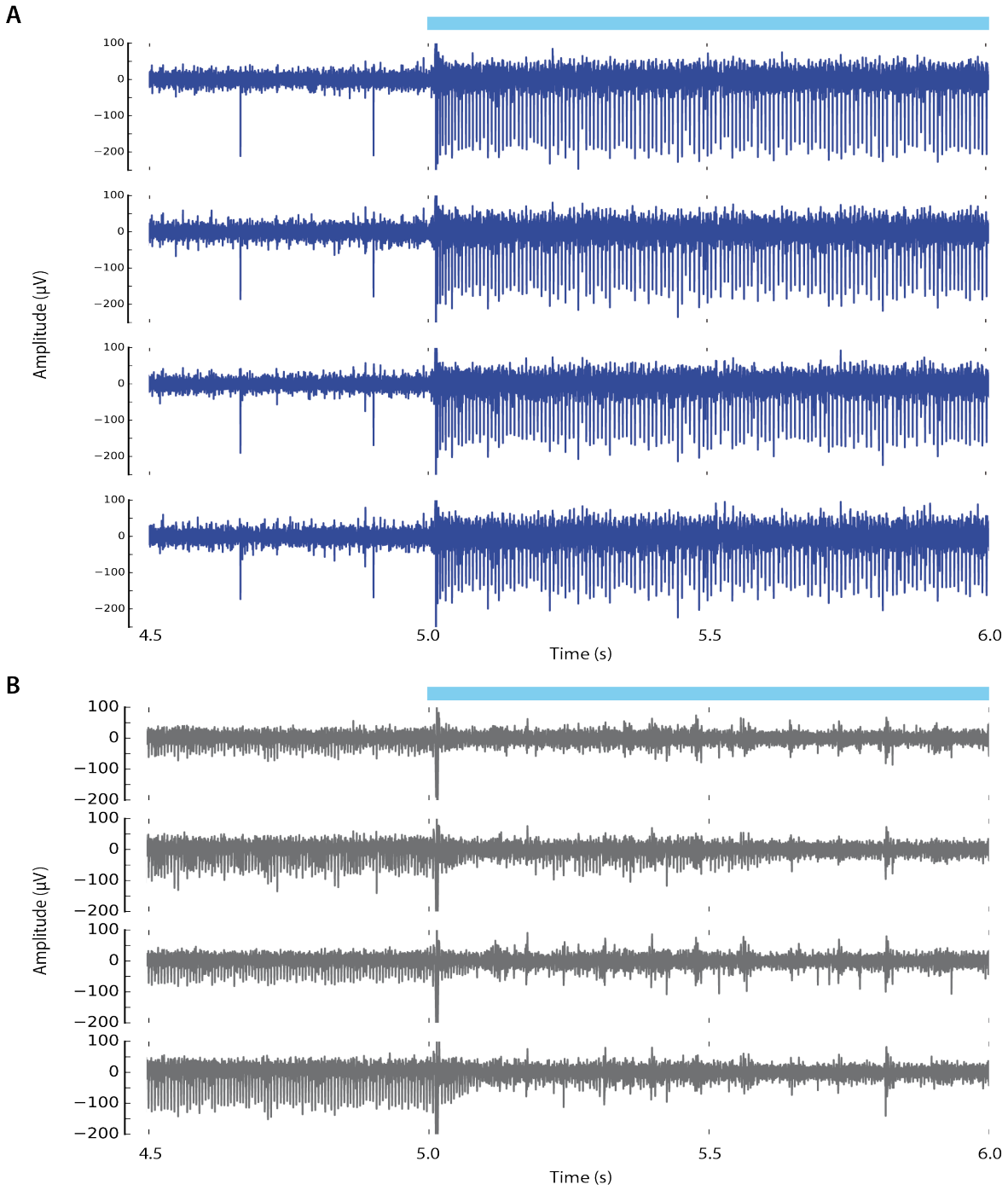

Figure 21: Four channels tetrode recordings *in vivo.* (A) Extracellular spikes of a PC, excitation elicited with optogenetic stimulation (onset t= 5 s), raw signals were filtered for low frequencies below 200 Hz (B) Extracellular spikes of a DCN cell inhibited under same conditions

The two groups of cells, PCs and DCN cells were targeted using the coordinates obtained with injection experiments. Expected responses triggered by ChR2 activation in PCs were excitation in PCs and a resulting inhibition in DCN cells. These two effects were observed simultaneously under steady blue light illumination of the cerebellar cortex. Spiking activities were observed through 4 different channels of the recording tetrodes with slight differences in each channel (Figure 21). These differences helped to identify and isolate simultaneous spike spiking activity of multiple cells. Finally, spike times and waveforms of multiple cells were sorted. Details of spike sorting in given in methods.

In 13 animals (25 recording sites) activities of 39 DCN cells were isolated (5 cases of single, 14 cases of double and 2 cases of triple simultaneous DCN cell recording). In 18 recording sites from the same experiments, spikes from single cells could not be isolated because the waveforms of multiple cells were similar to each other and they were excluded from the rest of the analysis.

These results confirm the recordings done in Chaumont et al. (2013) study in which excited PCs and inhibited DCN cells were recorded separately with ChR2 activation. In the present study, these responses were recorded simultaneously (Figure 22).

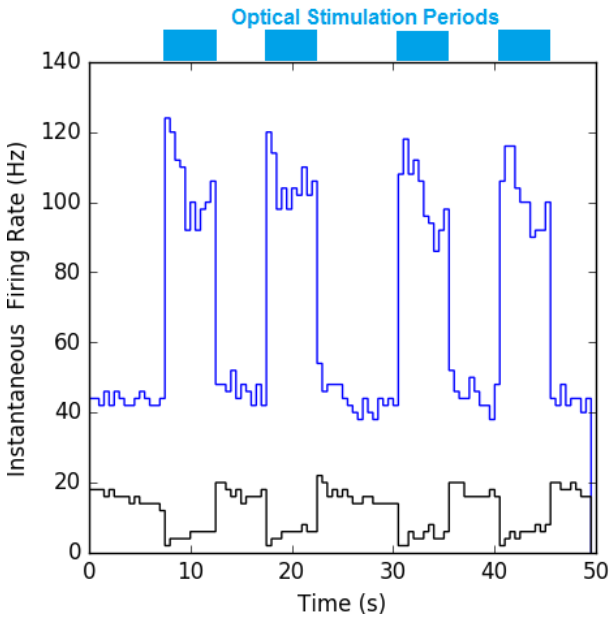

Figure 22: Simultaneous Recording of a PC and a DCN *in vivo.* During optical illumination periods PC activity was reliably excited (blue trace) and DCN cell activity was inhibited (black trace).

3.2 Two groups of DCN cells are identified using their waveforms

The DCN are known to include more than one type of neurons. However, *in vivo* extracellular techniques used do not allow to selectively record cells from this region. Previous studies selected only a portion of recorded DCN cells by grouping them according to baseline firing rates and spike-widths *in vivo* (Bengtsson et al., 2011) or soma size and fluorescent properties *in vitro* (Person and Raman, 2011, Ankri et al., 2015). In the current study, inhibition response in DCN cells induced by the optogenetic activation of PCs was used as the recording criteria and no further selection was done. During multiunit recordings, together with the inhibited cell, other cells were also simultaneously obtained from the same area. This allowed us to investigate several cells at one recording site. Such an approach where cells are not selected but classified permitted to check different responses of the cells and their interactions inside the neuronal network of DCN *in vivo*.

Waveforms from different cells had different shapes. We therefore decided to classify the recorded cells according to the shape of their waveforms by using 10 waveform parameters: 1) positive peak onset time, 2) positive peak rise slope, 3) positive peak half-width, 4) positive decay time, 5) negative peak value, 6) negative peak time, 7) negative onset time, 8) negative rise slope, 9) negative half-width and 10) negative decay time. Details of obtaining waveform parameters are given in the methods.

3.2.1 Discrimination of cells based on waveform parameters

DCN cells were classified according to their waveform parameters using Hierarchical Clustering on Principal Components (Husson et al., 2010) in R statistical software (R Core Development Team., 2015). We first determined how many clusters can be obtained. Initially the variance within the merged clusters had smaller values at the lower branches of the dendrogram (Figure 23). At further steps, clusters with bigger differences were merged so the variance within the clusters grew. This change in the variance was represented in the length of the vertical connection lines in the dendrogram (Figure 23). Consequently acceptable levels of variance within the clusters were determined. In this way, hierarchical tree structure suggested 2 groups of cells with respect to their waveform parameters.

The same information about the change in the variance within the merged clusters was given in the inset bar chart as well (Figure 23). This bar chart showed that there was a big increase in the variance

when the last two clusters are joined. Such a big change was not observed in the previous steps, meaning that this dataset can be divided into 2 groups.

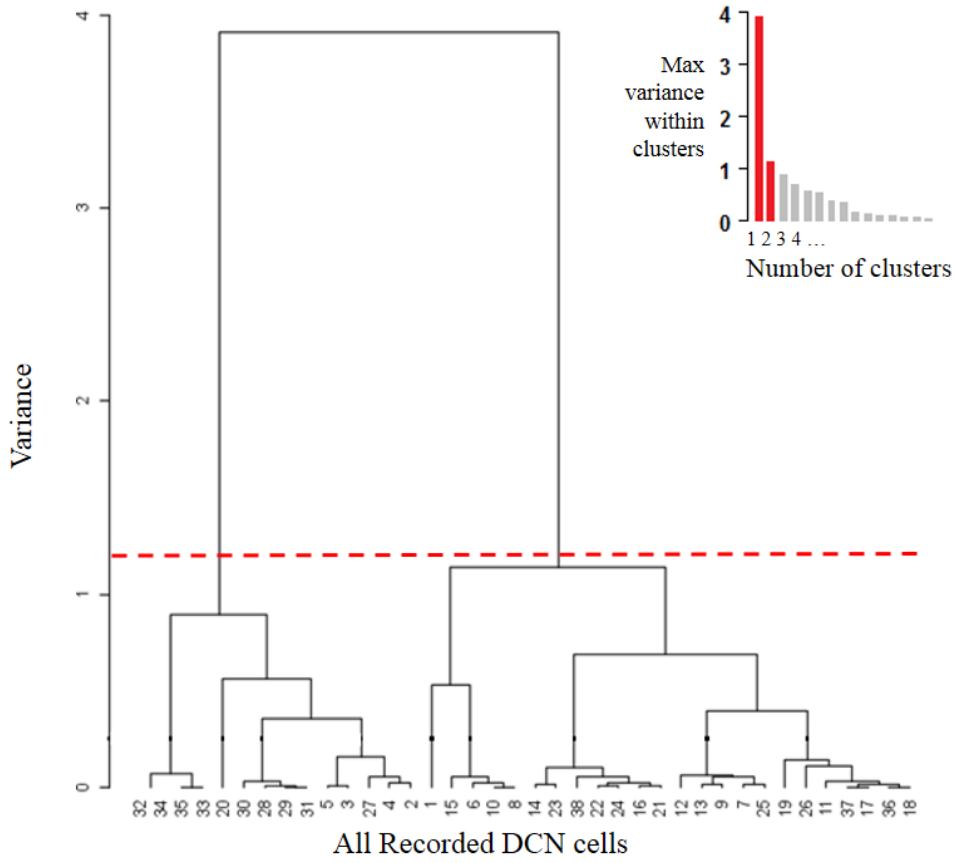

Figure 23: Hierarchical clustering tree. Cells with similar parameters were joined initially and clusters were formed. Variance within the clusters increased as they include more cells and change in variance was represented by the vertical lines. Same data given in the bar chart (upper right corner) showed that having more than 2 clusters did not decrease the variance within the clusters notably.

After the determination of the optimal number of clusters, the contributions of the principal components were assessed. The first principal component was found to explain 41.98% of the total variance in the dataset while the second explained 18.45%. We then plotted cells with respect to first and second principal components illustrating 2 clusters in the factor map (Figure 24). Group 1 cells were located on the negative part for the first principal component while Group 2 were located on the positive part. This distinction also showed a clear separation between the two groups.

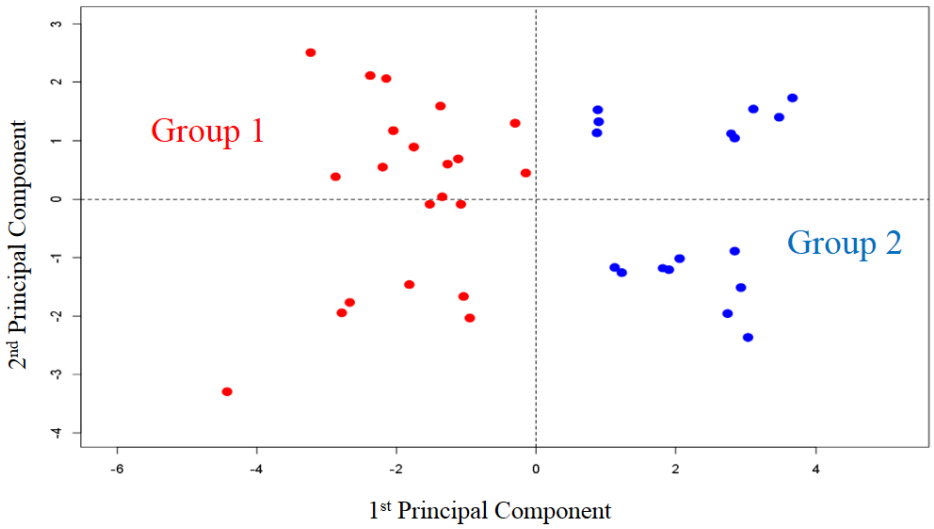

Figure 24: Distribution of cells with respect to 1st and 2nd principal components. Two groups were separated with having positive and negative values for the 1st principal component.

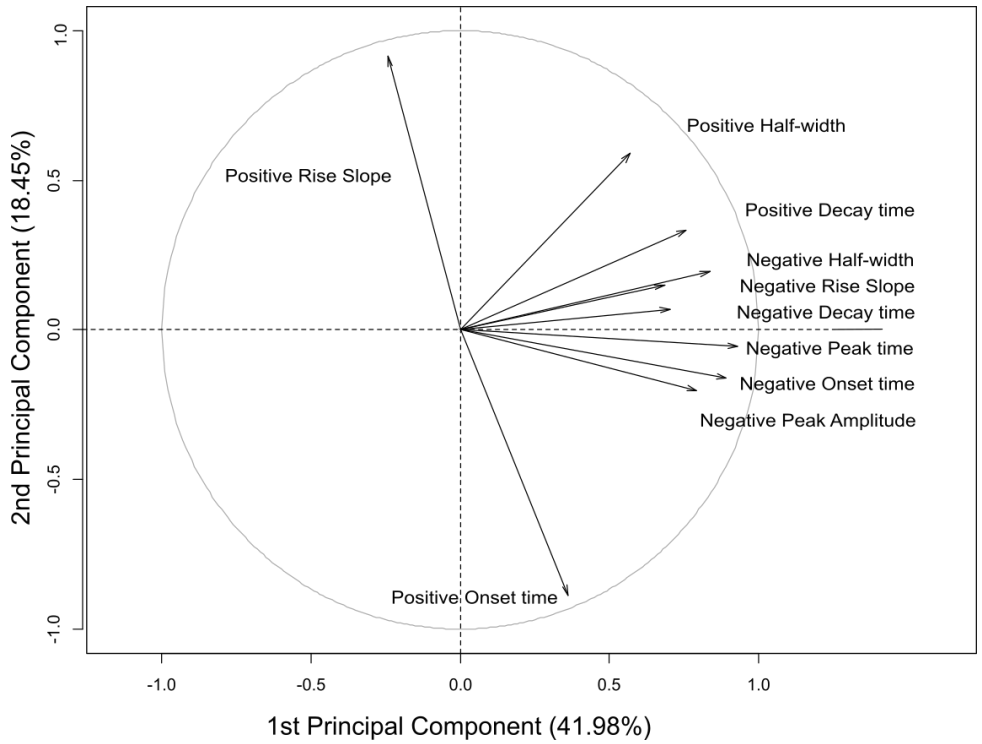

Figure 25: Contribution of waveform parameters to principal components. Parameters related with the falling phase of the spike waveforms were found to explain 41.98% of the total variance.

We noted that 8 out of 10 waveform parameters contribute to the 1st principal component which deal with the falling phase of the waveforms (Figure 25). This phase of the waveforms was therefore the key factor in the clustering. Indeed the average waveforms obtained from the two groups show significant difference in the falling phase (Figure 26). The second principal component can explain only a smaller portion of variability with contributions of positive onset time and positive rise time parameters since these were not very different between the two groups. Consequently, 39 DCN cells were grouped in two: Group 1 had 22 cells (from N=9 animals) and Group 2 had 17 cells (from N=6 animals).

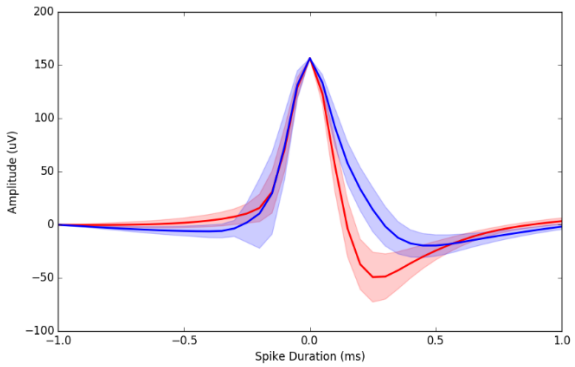

Figure 26: Average waveforms of the two groups with standard deviations. Clear differences obtained with hierarchical clustering and principal component analysis (shaded area standard deviation)

3.2.2 Properties of the two groups of cells

As described in the introduction part, several *in vitro* studies have focused on the classification of DCN cells so far. The difference in the average waveforms obtained (Figure 27 Ai) strikingly matched with the waveforms recorded from GABAergic and non-GABAergic cells *in vitro* by Uusisaari et al. (2007). GABAergic cells have broader action potentials compared to non-GABAergic cells and the difference is significant in the falling phase of the action potentials (Figure 27 Bi).

Interestingly, the two groups of recorded cells were found to have significant difference in their firing rates (Two sample t-test, $p < 0.000005$, Figure 27 Aii). Group 1 cells had higher baseline firing rates with an average of 63.9 ±5.0 Hz while Group 2 cells were spiking at lower rates (23.2 ±4.7 Hz). GABAergic DCN cells also had a slower firing rate than others in cell-attached *in vitro* condition (Figure 27 Bii). This difference in firing rates is also in the same direction with the firing rates obtained for the two groups *in vivo* (Figure 27 Aii). Such a match between the two groups suggest that Group 1 cells obtained *in vivo* may represent the non-GABAergic populations in DCN, principal cells

(glutamatergic premotor projection cells) –and possibly glycinergic premotor projection cells of the medial nuclei. Accordingly, Group 2 cells may represent the GABAergic populations: mixed-type inhibitory nucleo-cortico cells with local collaterals and nucleo-olivary cells. These groups, to the best of our knowledge, represent the first demonstration of simultaneous recording and discrimination of different DCN cells *in vivo*.

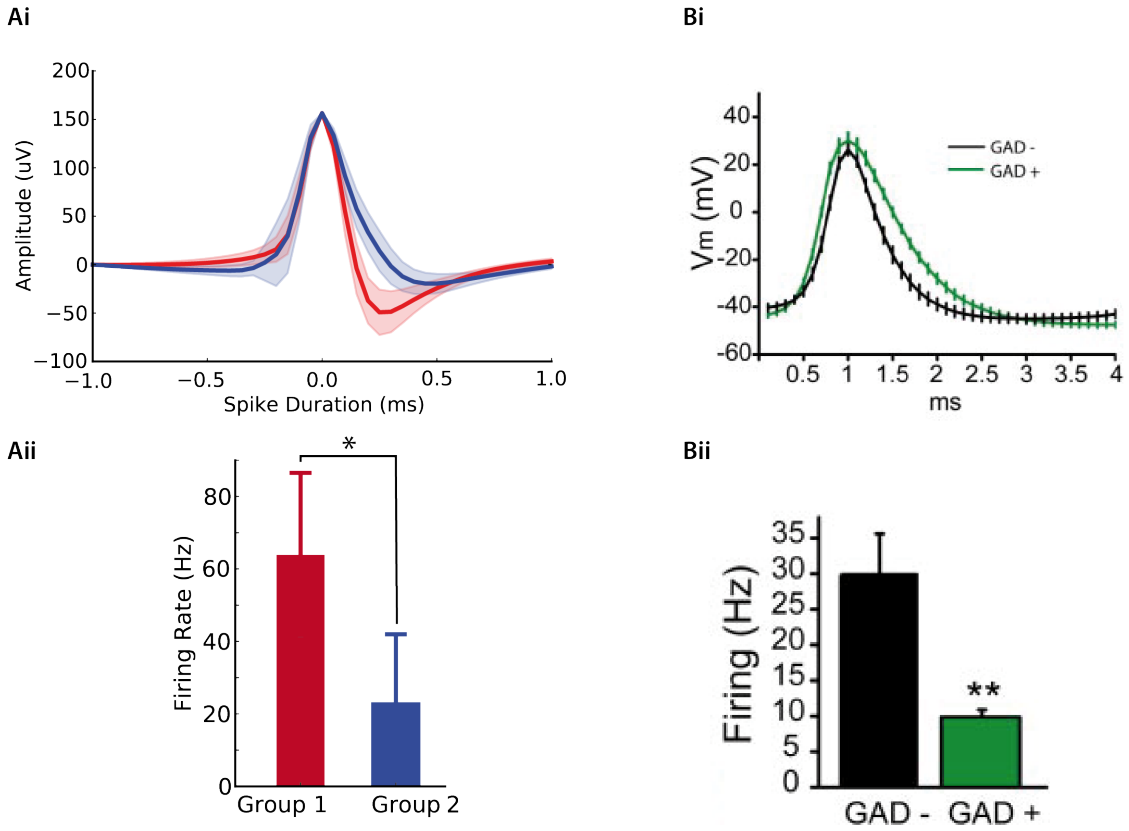

Figure 27. Comparison of Group1 / Group 2 DCN cells *in vivo* (present study) and non-GABAergic (GAD-) / GABAergic (GAD+) DCN cells (Uusisaari et al., 2007) *in vitro*. (Ai) Group 1 (red) and Group 2 (blue) had difference in average waveforms during falling phase **(Bi)** Similar difference in waveforms was observed in GAD- and GAD+ cells **(Aii)** Group 1 and Group 2 cells had significant difference in firing rates (*p< 0.000005) again similar to obtained **(Bii)** *in vitro* between GAD- and GAD+ cells (**p < 0.005).

3.3 Low and high frequency oscillations in the DCN have different durations and phase locking ratios

In this chapter, we studied the local field potentials (LFP) and their relation to spiking activity (phase locking) in DCN recordings. For this analysis, the baseline periods of recordings were used. Before each episode of stimulation, five seconds of baseline were recorded. Five baseline periods from five successive episodes were concatenated to obtain 25 seconds of analysis interval. For each experiment, 10 intervals for a total length to 250 seconds were analyzed.

3.3.1 Detection of LFP in the DCN

We detected LFPs in 1-200 Hz frequency range and grouped them in frequency bands: delta (1 Hz to 4 Hz), theta (4 Hz to 10 Hz), beta (10 Hz to 30 Hz), gamma (30 Hz to 80 Hz) and high frequencies (80 Hz to 200 Hz) based on De Zeeuw (2008). In Figure 28 A, an example of recording illustrates prominent oscillations around 4 Hz, observed by low-pass filtering frequencies above 20 Hz. For further analysis, the time frequency analysis package in the OpenElectrophy (Garcia and Fourcaud-Trocmé, 2009) framework was used.

In the analysis, Morlet scalograms were obtained, then significant oscillations detected (Figure 28 Bi-Bii) above the threshold of three standard deviations from the mean power (Chapuis et al., 2009). Further details of the analysis are given in the Methods chapter. In Figure 28 Bi, oscillations around 4 Hz were detected as a thin line lasting for the whole interval (10 seconds) together with shorter oscillations around 30 Hz. For the next detection band 55-200 Hz (Figure 28 Bii), shorter oscillations were detected more frequently around 100 Hz.

For the same experiment in Figure 28 A&B, 250 seconds of total recording time was analyzed and oscillations around 4 Hz were observed for long durations (around 170 seconds in total) while oscillations at higher frequencies had shorter durations (Figure 28 C).

Detected oscillations were grouped in frequency bands, averaged for all cells (n= 39) and compared with the whole recording duration of 250 seconds (given as percentage, Figure 28 D). Interestingly, the longest duration of oscillations were observed in the delta and theta bands, including low frequencies up to 10 Hz. Higher frequencies were detected for much shorter durations, up to maximum 5% of the recording time. The durations of oscillations were all significantly different from each other based on Mann–Whitney U tests (p values < 0.05) expect for beta and gamma bands (Figure 28 D). The median percentage of oscillation durations in beta and gamma bands were 1.73%

and 1.18% and the distributions in the two groups didn't differed significantly (Mann–Whitney U = 404.0, n1 = n2 = 29, P = 0.40).

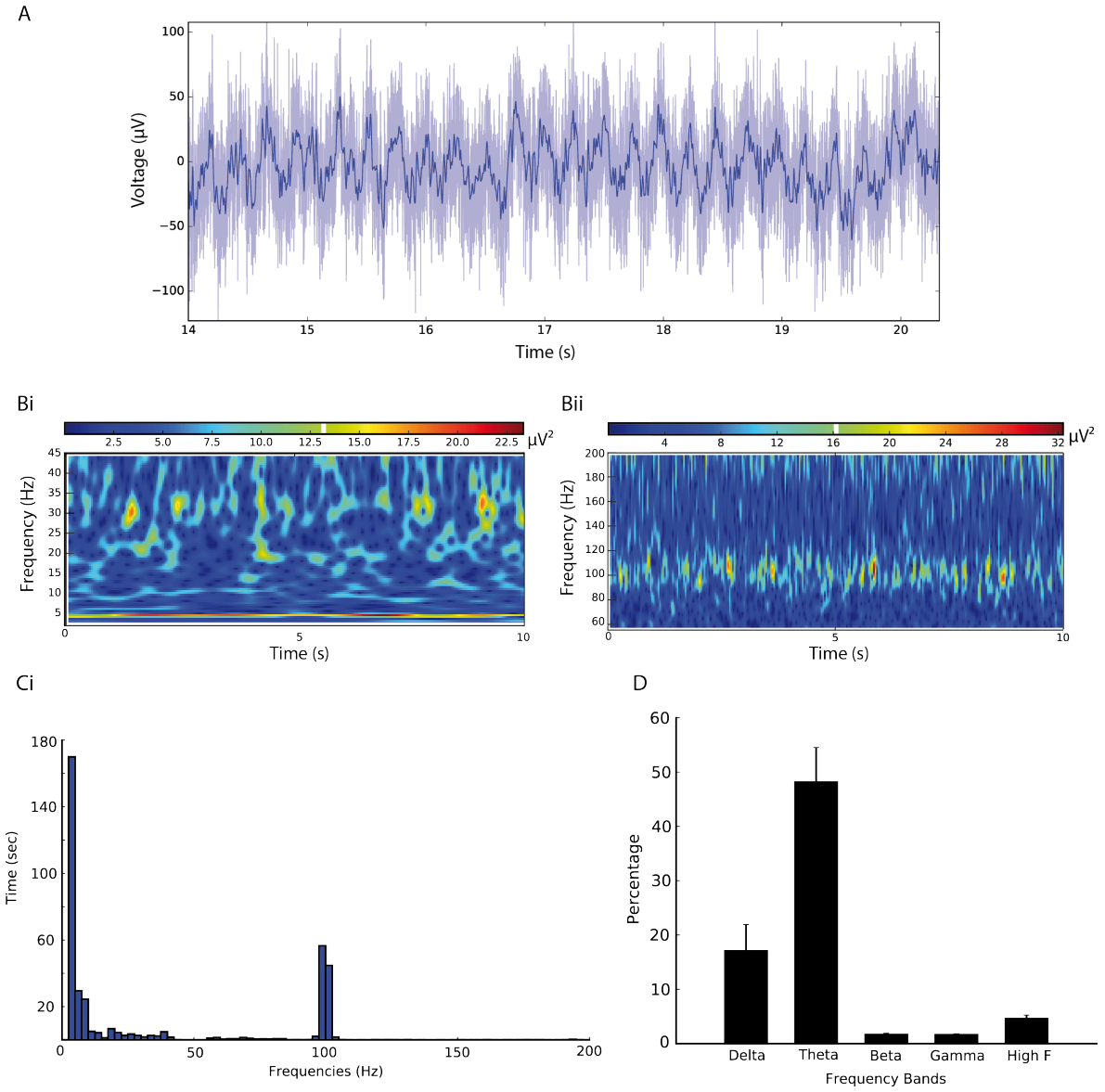

Figure 28: Detection of oscillations in DCN. (**A**) Raw signal (light blue) and filtered signal below 20 Hz (dark blue) were given. Prominent oscillation at 4 Hz was observed. (**Bi**) The same recording was analysed as a block of 10 seconds for 1-45 Hz range. Long duration oscillations around 4 Hz (thin band) were detected together with simultaneous shorter oscillations around 30 Hz using the time frequency map (**Bii**) For 55-200 Hz range, frequency oscillations around 100 Hz with shorter durations were detected. (**C**) Total durations of oscillations in the given experiment during total recording time (250 seconds). (A, B and C obtained from the same experiment) (**D**) Average duration of detected oscillations for 29 recordings, given as percentage of total recording time.

3.3.2 Phase locking to detected oscillations in the DCN

We investigated the relation between oscillations recorded in the DCN and the discharge of individual cells, particularly how they relate to the phase of a given oscillation. In order to prevent the contamination of the LFP by the recorded cell discharge, the phase locking was determined on a different shank of the multielectrode than the cell recording site. Therefore the two recording sites were separated at least by 150 μm. Due to this reason, this analysis was restricted to the experiments having minimum two shanks in the DCN which was the case for 17 cells in Group 1 and 12 cells in Group 2. For this analysis, detected oscillations were grouped by frequency (bins of 1±5 Hz) between 1 to 200 Hz. For each frequency, phases of spikes of a recorded cell were calculated with respect to the detected oscillations.

Since some of the detected oscillations had short durations, we analyzed phase locking activity only when a cell had minimum 10 spikes in a frequency bin. Phase values of the spikes were plotted as histograms within - π and + π range and these histograms were fitted with Von Mises distribution to find the phase concentration degree (κ) and preferential phase (Figure 29 Ai and Aii). When the cell did not discharge at a specific time of the detected oscillations, phase histogram showed a flat distribution and Von Mises distribution had a low phase concentration degree (κ = 0.286, Figure 29 Ai). However, when the cell discharged at a preferred time during the oscillation, phase values showed a peak in the distribution with a preferred phase and a high phase concentration degree (κ = 1.622, Figure 29 Aii). We set the significance level for phase locking at a threshold of Kappa > 0.5 as in Villette et al. (2010).

For each frequency, a single kappa value was calculated based on the oscillations in ±5 Hz range. Calculated kappa values were displayed in Figure 29 B with the threshold at 0.5. A cell was considered phase locked in a band if kappa values crossed the threshold value of 0.5 in that band. Following that, percentages of phase locked cells in frequency bands were obtained for the two groups of DCN cells (Figure 31 C). No phase locked activity was observed for delta and theta bands. For Group 1 (n = 17) 2, 11 and 15 cells were phase locked to oscillations in beta, gamma and high frequency bands, respectively. For Group 2 (n=12), there were 3, 10 and 8 cells fired phase locked spikes to the oscillations in the same bands. The two groups did not show clear differences based on percentage of phase locked cell.

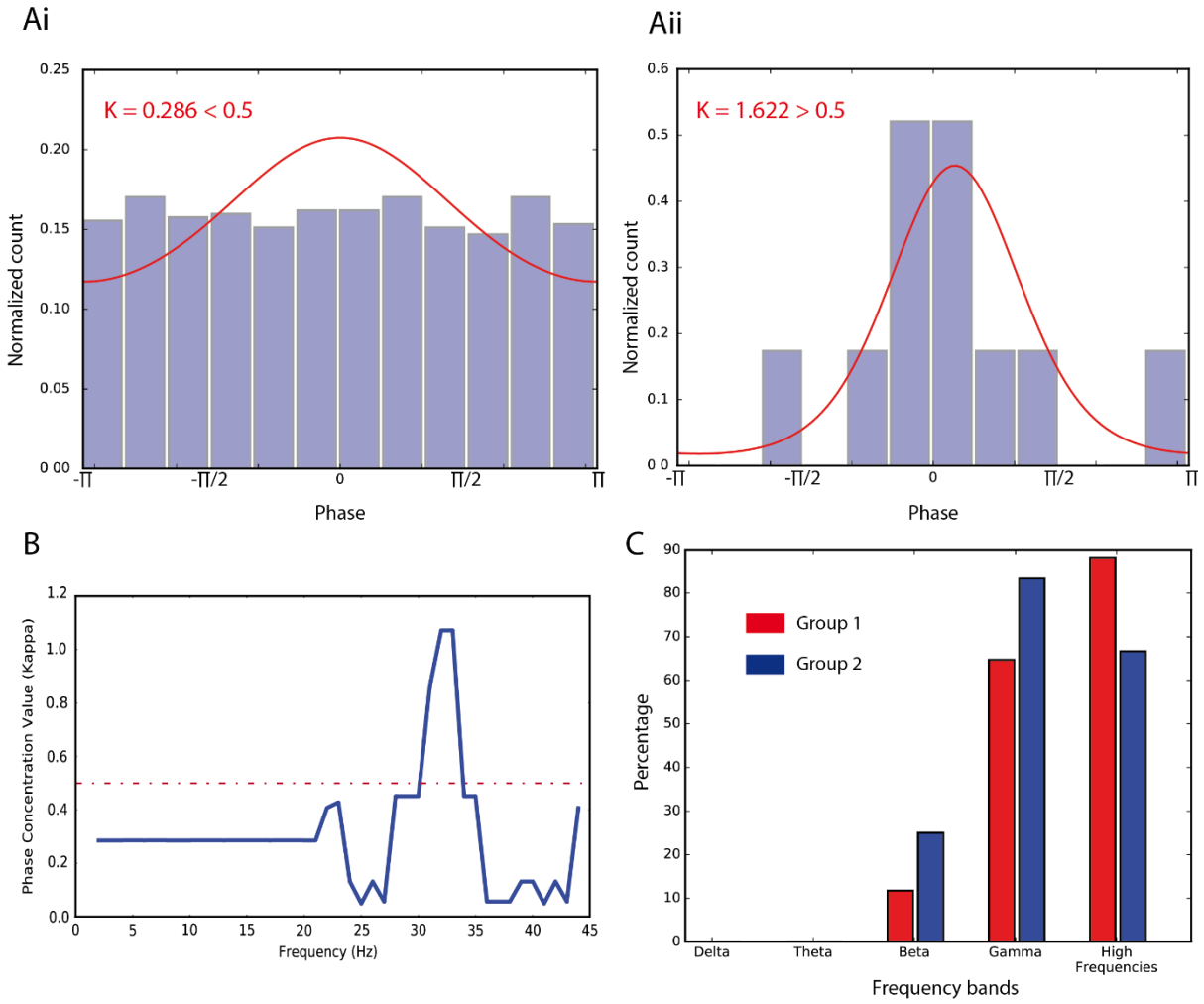

Figure 29: Phase locking to detected oscillations in DCN. (**Ai**) and (**Aii**) showing normalized phase distributions of spikes from a not phase-locked and a phase-locked cell, separated by a threshold of 0.5 for phase concentration value (κ) (**B**) For an example cell, kappa values cross the threshold at 32 Hz and this cell was considered as phase-locked in the gamma band. (**C**) Percentages of phase-locked cells in Group 1 (n=17) and Group 2 (n=12).

3.4 Specific responses of the two groups of DCN cells to optogenetic PC activation

In the current study, responses of the DCN cells to different PC stimulation protocols were recorded and temporal characteristics of these responses were investigated. Stimulation protocols were blue light illumination of PCs with 6 temporal properties: a steady illumination, three fixed frequency illuminations at 40 Hz, 65 Hz and 115 Hz with pulses of 5 ms, a Poisson distributed random illumination with pulses of 5 ms with and finally a ramp of increasing frequency illumination from 10 Hz to 80 Hz (Figure 30).

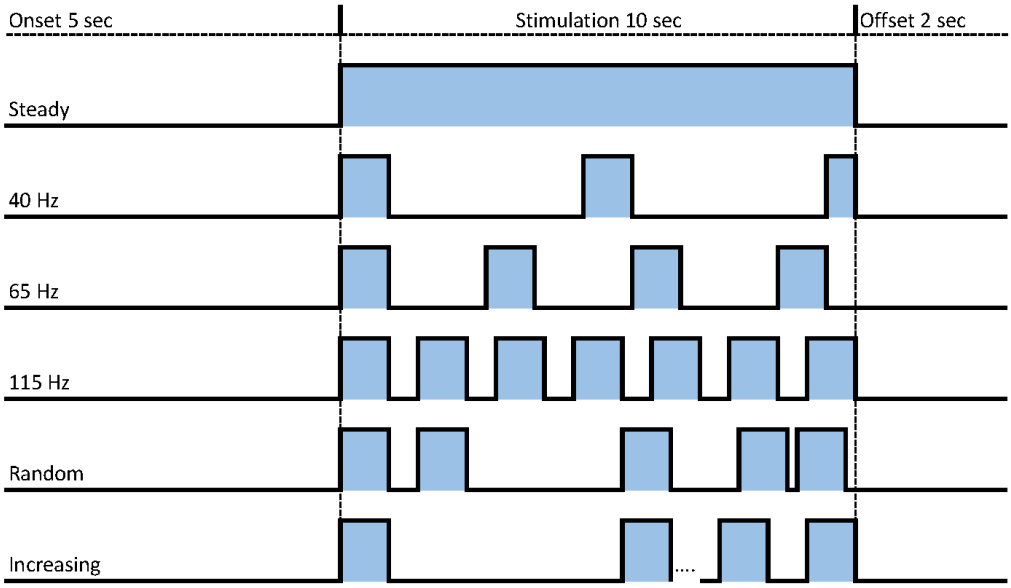

Figure 30: Protocols applied for optogenetic stimulation of PCs. Protocols lasted 17 s at each trial with a 5 s baseline, 10 s stimulation and 2 s post stimulation period.

3.4.1 Functional connectivity of PCs to DCN cell groups

Steady illumination mostly resulted in strong inhibition of DCN cells. Although this inhibition was the recording criteria in the experiments (see Methods), tetrode recordings allowed multiunit recordings simultaneously and other cells were also recorded together with the clearly inhibited cells. However, almost all of the recorded cells were inhibited (n= 37) except 2 cells that were unexpectedly excited (Figure 31 A). Importantly, the inhibition did not depend on baseline firing rate of the DCN cells. (No correlation was observed for Group 1: r= -0.18, n= 39, p =0.40 and for Group 2: r= -0.06, n= 39, p= 0.83). Both intrinsically fast (Group 1: 63.9 ±5.0 Hz) and slow cells (Group 2: 23.2 ±4.7 Hz) were inhibited at different levels.

To further investigate the inhibitory effect of PC stimulation, distributions of the inter spike intervals (ISI) during baseline vs. stimulation conditions were compared for each DCN cell and they all showed significant difference (n= 39, for all t-tests $p < 0.05$). These results showed that PCs are functionally connected both to GABAergic and non-GABAergic cells in the DCN and can modulate their firing rates. The principal cells of DCN, putatively represented by Group 1 cells, were previously reported to be inhibited by PC stimulations (Lang and Blenkinsop 2011). Inhibitory effect of PCs was shown also for nucleo-olivary cells of DCN (Najac and Raman, 2015) *in vitro* and my results *in vivo* confirm these findings. When higher frequencies of stimulation were used (65 Hz and 115 Hz), DCN cells were gradually inhibited more. Increased activity in PCs lead to a graded inhibition of DCN cells showing that PCs can control the firing rate of DCN cells in a rate coding manner (Figure 31 B).

In my experiments, we also investigated the influence of the power of illumination. Increased light intensity stimulates PCs in a bigger area in the L7-ChR2 mice (Chaumont et al., 2013). Accordingly, DCN cells receiving converging projections from PCs were expected to be more inhibited. Firing rates were compared for 2X vs. 1X illumination power as shown in the Figure 31 C and almost half of the DCN cells were more inhibited with increasing illumination power but, unexpectedly, the other half was less inhibited. Group 1 cells had a correlation between the firing rate ratio and baseline firing rate ($r = -0.44$, n= 39, $p = 0.04$) however Group 2 cells didn't have ($r = -0.19$, n= 39, $p = 0.48$). Consequently, we couldn't increase the number of stimulated PCs or their firing rates systematically. As demonstrated in Chaumont et al (2013), PCs increase their firing rates with increasing illumination power however, depending on their baseline firing rates, they are also subject to a depolarization block when illumination is too strong. This issue is revisited in the discussion.

Figure 31: Effect of PC stimulation on firing rate in DCN cells (Group1: red, Group 2: blue). (**A**) Firing rate ratio of DCN cells under 40 Hz stimulation vs. baseline, x-axis: baseline firing rate. Most of the DCN cells were inhibited (except for 2 cells) without any relation to baseline firing rates in both of the groups. (**B**) Gradual effect of increasing stimulation frequency (Baseline-40 Hz-65 Hz-115 Hz) on inhibition of DCN cells (**C**) Effect on illumination power on the inhibition of DCN cells, ratios of firing rates under 2X and 1X illumination power given with the results of correlations to baseline firing rate

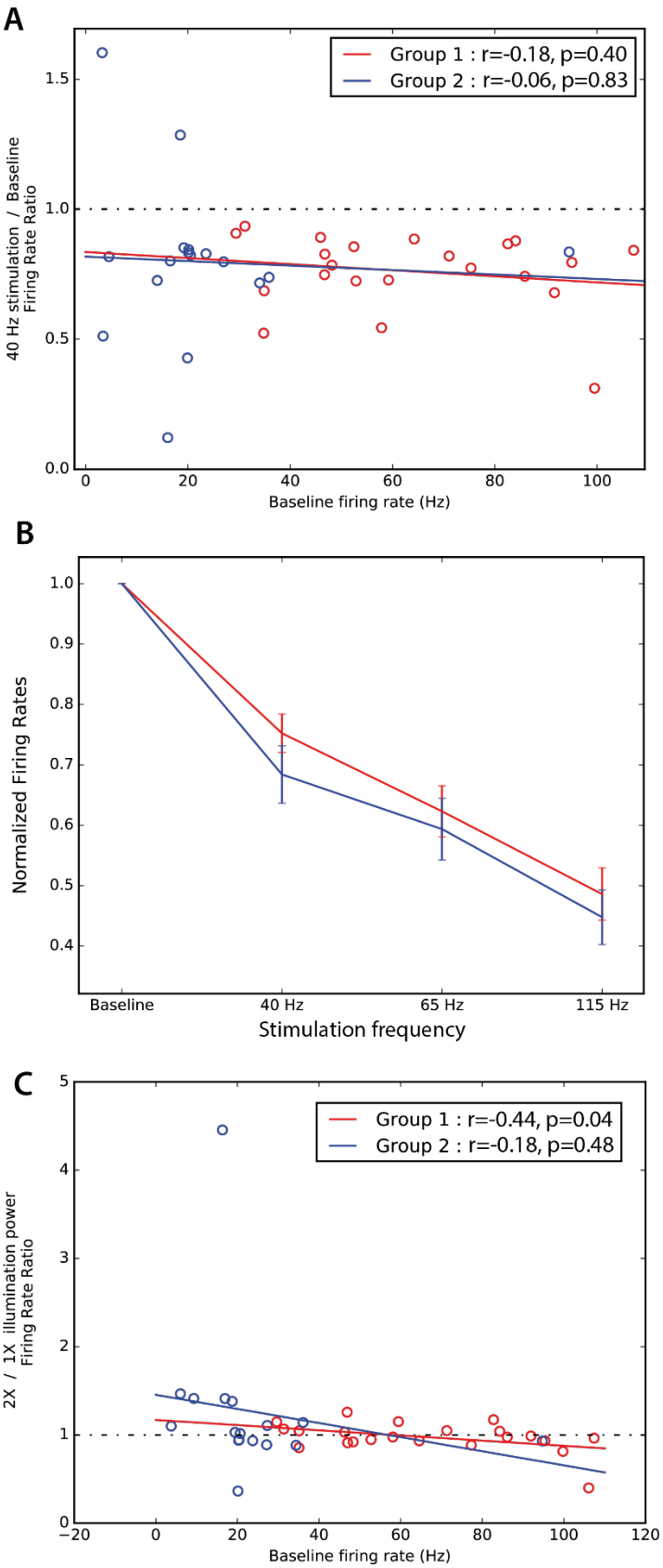
A
Group 1 : r=-0.18, p=0.40
Group 2 : r=-0.06, p=0.83
40 Hz stimulation / Baseline
Firing Rate Ratio
Baseline firing rate (Hz)
B
Normalized Firing Rates
Baseline
40 Hz
65 Hz
115 Hz
Stimulation frequency
C
Group 1 : r=-0.44, p=0.04
Group 2 : r=-0.18, p=0.48
2X / 1X illumination power
Firing Rate Ratio
Baseline firing rate (Hz)

3.4.2 DCN cells from group 1 are time-locked to PC stimulation

PCs have a strong control on the activity of the principal DCN cells as described in the introduction and confirmed in my results. This control is enabled by GABAergic inhibitory connections from tens of converging PCs. Consequently, the principal DCN cells can be gradually inhibited as show above. Another property of this connection is that synchronized PC inputs can evoke time-locked spiking in the principal cells of DCN (Person and Raman, 2011).

In the current study, we analyzed whether a DCN cell discharges time-locked to PC stimulation by comparing baseline with three stimulation frequencies 40 Hz, 65 Hz and 115 Hz (Figure 32). We determined ISI distributions of DCN cells (Figure 34 Ai-Bi, Cell A-B), auto correlograms to reveal the periodic spiking (Figure 32 Aii-Bii) and power spectrum density analysis to assess the strength of any specific frequency in the discharge (Figure 32 Aiii-Biii). Consequently, time-locked spiking was quantified as the power density value at the stimulation frequency.

Analysis demonstrated that for both types of cells (Figure 32 Ai-Bi) ISIs were longer which indicated the inhibitory effect of PCs stimulation. For Cell A, ISIs were matching with inter stimulus intervals (25 ms, 15.4 ms and 8.6 ms) for 40 Hz, 65 Hz and 115 Hz stimulations. This periodic spiking behavior was easily observed in autocorrelograms (Figure 32 Aii) however it was not observed for Cell B (Figure 32 Aii). Accordingly, Cell A had peaks at the stimulation frequencies in the power spectrum density (Figure 32 Aiii) while Cell B didn't have dominant peaks (Figure 32 Aiii). Power density values obtained at the stimulation frequencies were used to represent the strength of the time-locked spiking. These values were obtained from the 2 groups and compared (Figure 33). For stimulation frequencies of 40 Hz, 65 Hz and 115 Hz, power density values of Group 1 were 8.52 ± 2.86, 2.72 ± 0.95, 0.83 ± 0.48 $spikes^2/s^2Hz$, respectively and of Group 2 were 1.60 ± 1.23, 0.70 ± 0.62, 0.12 ± 0.11 $spikes^2/s^2Hz$, respectively and they didn't have normal distributions. Median power density values for Group 1 (n=22) and Group 2 (n=17) were 2.97 and 0.01 $spikes^2/s^2Hz$ at 40 Hz, 1.17 and 0.01 $spikes^2/s^2Hz$ at 65 Hz, 0.08 and 0.01 $spikes^2/s^2Hz$ at 115 Hz. Using Mann-Whitney tests, significant differences between the two groups were found for all 3 stimulation frequencies (Figure 33, $U= 33.0$, $p < 0.00005$, $U= 50.0$, $p < 0.0005$, $U= 72.0$, $p < 0.005$).

Figure 32: Time-locked spiking of DCN cells to fixed frequency stimulation of PCs (Cell A-B). Two cells are given to compare ISI distributions (**Ai-Bi**), autocorrelograms (**Aii-Bii**), and power spectra (**Aiii-Biii**) under baseline and three fixed frequency stimulation conditions: 40 Hz, 65 Hz and 115 Hz. Time-locked activity was quantified as power spectrum density values of the autocorrelograms at stimulation frequencies.

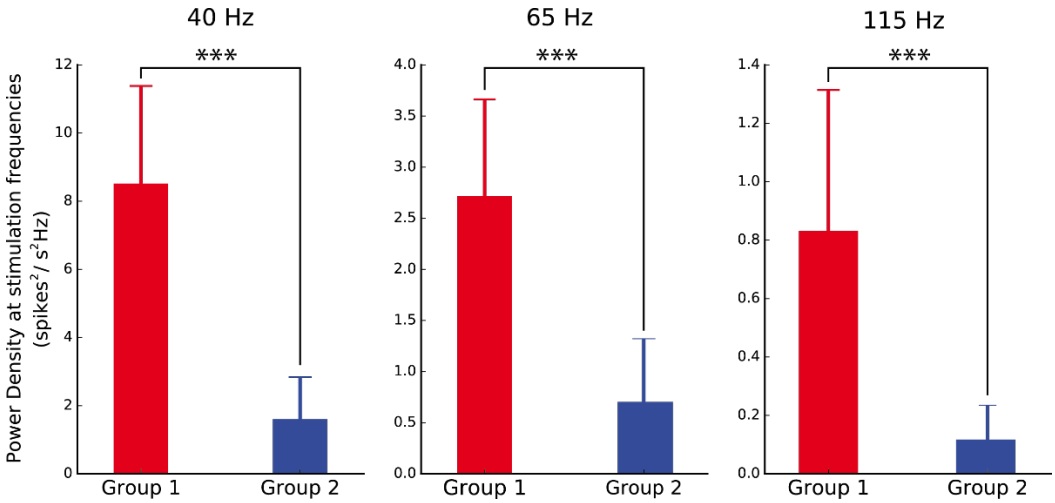

Figure 33: Average power density at stimulation frequencies for Group 1 (n=22) and Group 2 (n=17). For each stimulation frequency of PCs, Group 1 DCN cells had higher power density of autocorrelograms compared to Group 2 DCN cells. Distributions were significantly different in the three cases (Mann–Whitney tests: ***p < 0.005, *U= 33.0* at 40 Hz, *U= 50.0* at 65 Hz, *U= 72.0* at 115 Hz).

Another method to assess for the time-locked spiking in DCN cells is to analyze the distribution of spikes between stimulation pulses. Time-locked activity results in regular spiking following each stimulation with a fixed delay so that distribution of the spikes between the stimulation periods is not uniform. This method was used by Najac & Raman (2015) and they demonstrated *in vitro* that the principal cells of DCN are time-locked to PC activity. On the contrary, nucleo-olivary cells were shown to keep a uniform spiking activity between stimulation pulses and do not fire time-locked spikes. We applied the same analysis to the DCN cell groups obtained in this study.

Using this method, results obtained in power spectral density analysis were confirmed and clear differences were observed between DCN cell groups (Figure 34). Almost all Group 1 cells were found to reject uniform distribution (Rayleigh test, $p< 0.01$) except for 3 out 22 cells for 65 Hz stimulation and 5 out of 22 cells for 115 Hz stimulation (Figure 34). Group 2 cells, on the other hand, mostly did not reject uniform distribution (Rayleigh test, $p< 0.01$). During 40 Hz, 65 Hz and 115 Hz stimulations respectively: 13, 10 and 14 cells out of 17 cells kept spiking uniformly and did not fire time-locked spikes.

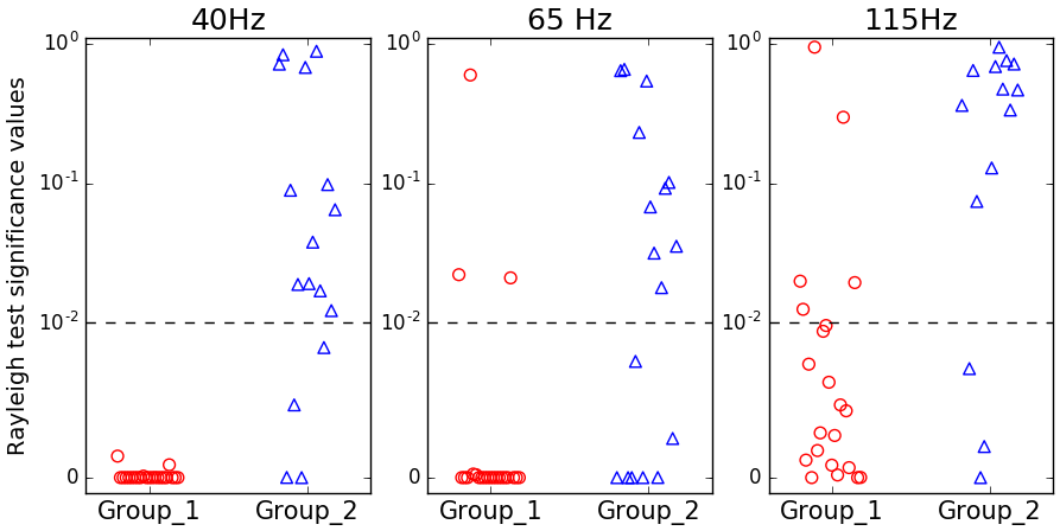

Figure 34. Rayleigh test for uniform distribution was rejected for time-locked cells. Distributions of spikes between the stimulation pulses were non-uniform for time-locked spiking cells.

3.4.3 Distinct Dynamic Ranges in DCN cell groups

Another distinction between the GABAergic and non-GABAergic cells *in vitro* is their ability to spike at a wide range of frequencies. Non-GABAergic cells were found to fire up to 200 Hz with injected current while GABAergic cells can discharge at 50 Hz maximum (Uusisaari and Knöpfel, 2008). We tested this behavior *in vivo* by Poisson distributed random stimulation. This protocol included stimulation pulses between 5 Hz and 210 Hz and capacities of DCN cells to respond in these frequencies were tested.

In Figure 35 A-B, normalized instantaneous firing frequency (IFF) histograms for 2 example cells are shown (Cell A and Cell B, in red and in blue), overlaid with the histogram of PC stimulation frequencies in gray. Cell A can discharge over a wide range of frequencies up to 200 Hz (Figure 35 A, red) while Cell B discharged only in a narrow band up to 50 Hz (Figure 35 B, blue). Same results were observed in the cumulative distribution graph (Figure 35 C) given below where instantaneous firing frequencies of Cell A (red) were similar to the stimulation frequencies (black) and Cell B had only low frequencies. In the next step, normalized instantaneous firing frequency histograms of cells were compared with the histogram from the stimulation using a Kolmogorov-Smirnov goodness-of-fit test. Cell A did not have a significantly different IFF distribution compared to stimulation as expected ($p= 0.14$) while Cell B had a significant difference ($p < 0.01$). Similar to Cell A, most of the Group 1

cells (16 out of 22) did spike at similar frequencies with stimulation frequency (Figure 35 D). Most of the Group 2 cells, as observed for Cell B, on the other hand, did not spike at these frequencies and Kolmogorov-Smirnov test was rejected ($p < 0.01$), (Figure 35 D).

Considering this findings together with the time-locked spiking results given above, Group 1 cells mostly can follow PC synchronization up to 200 Hz while Group 2 cells cannot spike follow PC activity. Interestingly, such a high frequency stimulation of PCs can still evoke time-locked spiking in their efferent DCN cells, mostly the principal projection cells represented in Group 1.

Figure 35: Different dynamic ranges in DCN cell groups. (**A**&**B**) Normalized histograms of instantaneous firing frequency for Cell A & B (in red & blue), normalized histogram of stimulation frequencies (in gray) (**C**) Cumulative distributions of IFF for Cell A, Cell B and stimulation together (**D**) Comparison of cumulative distributions of stimulation frequencies and DCN cells' firing frequencies, Kolmogorov-Smirnov test for different distributions was significant for most of the Group 2 cells.

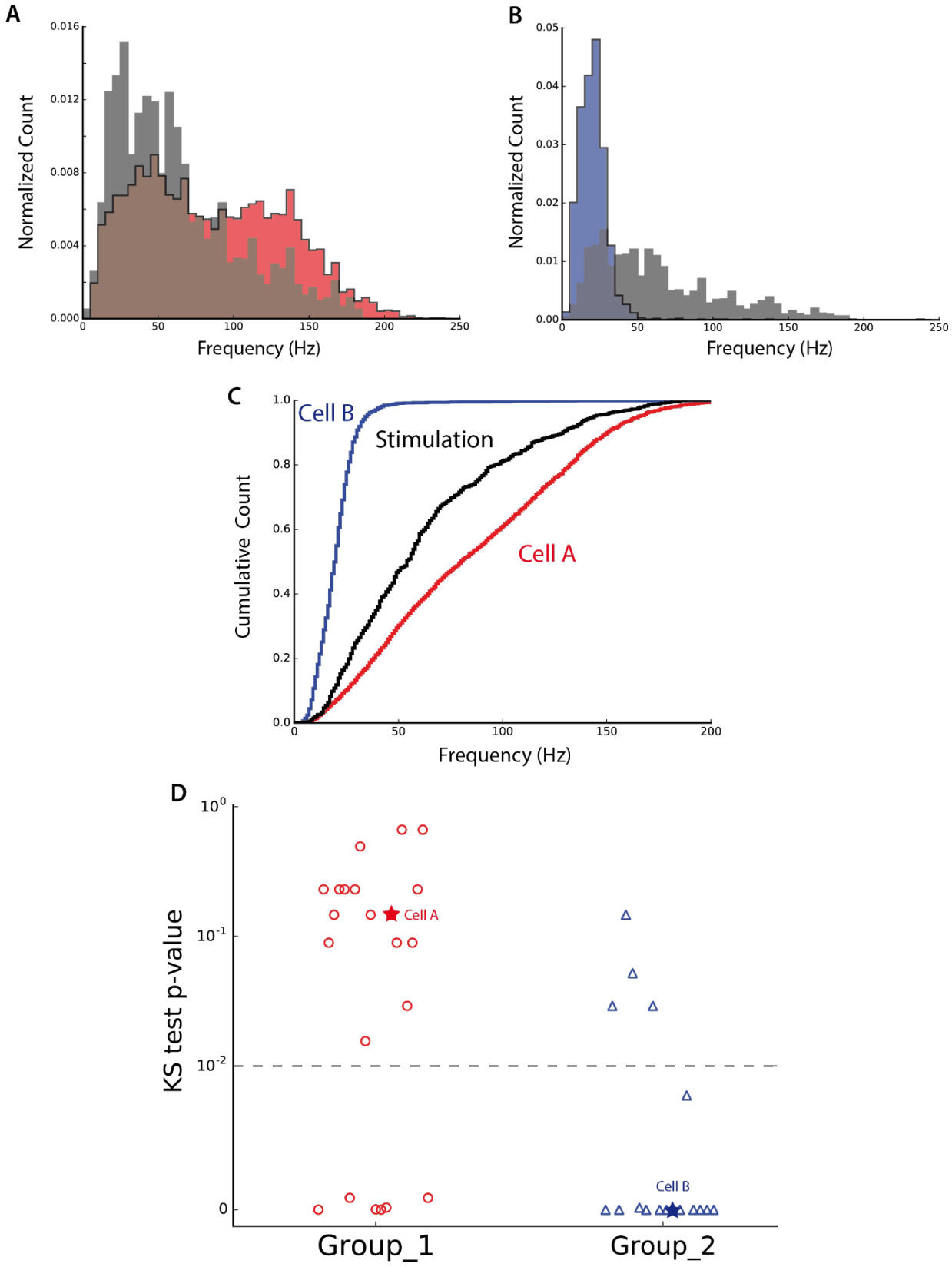
A
Normalized Count
Frequency (Hz)
B
Normalized Count
Frequency (Hz)
C
Cell B
Stimulation
Cell A
Cumulative Count
Frequency (Hz)
D
KS test p-value
Cell A
Cell B
Group_1
Group_2

3.4.4 Spiking relation between simultaneously recorded cell pairs from the two groups

In my experiments, 22 cell pairs were obtained with simultaneous recordings and unfortunately only three of them were with cells from different groups (one cell from Group 1 and one cell from Group2). Two pairs had cells from the same tetrodes and one pair had cells from adjacent tetrodes (with 150 µm distance). We investigated possible relations within the pairs using cross-correlations between the spiking activities of the cells. Especially local inhibitory connection to the principal DCN cells (of Group 1) from the nucleo-cortical cells (of Group 2) was expected to be observed.

Unfortunately, no clear relations were observed in the cross-correlations during baseline or any of the stimulation conditions (one pair given in Figure 36). Simultaneously recorded cells didn't seem to have any correlated activity. Lack of related activity in the pairs will be examined in discussion.

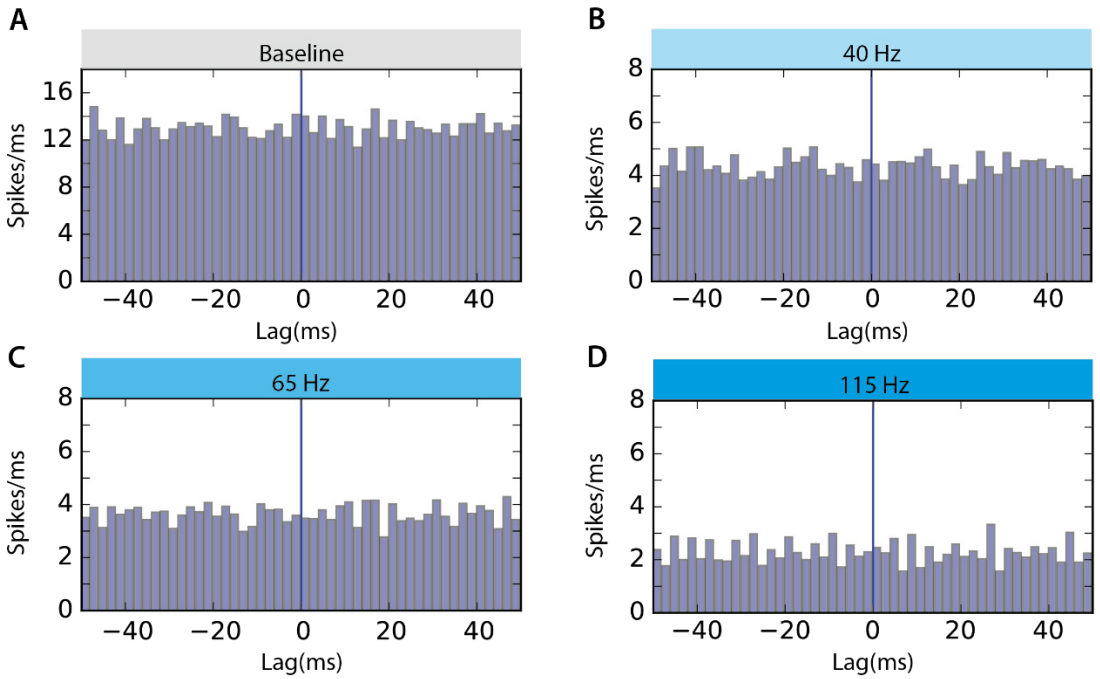

Figure 36: Cross-correlation graphs for a Group1 cell - Group2 cell pair. Baseline and three stimulation frequency conditions showed that there was no clear relation in the spiking activity of the cells.

4 DISCUSSION

4.1 Revisiting research questions and outlook

In my study, optogenetic stimulation of PCs was administered *in vivo* and excitatory responses in PCs were recorded together with the resulting inhibitory responses in DCN cells. The medial part of Lobule IV-V of the cerebellar cortex was targeted to record PCs which mostly send projections to the medial nucleus in which the DCN cells were simultaneously recorded. Inhibitory responses in the DCN cells were investigated while PCs were stimulated with different protocols.

At the end of our experiments and analysis, we couldn't find a correlational behaviour between spike times of individual PCs and DCN cells simultaneously recorded connected regions (data not shown). This result was in accordance with McDevitt et al. (1987) study. However we observed excited spiking activity in PCs and resulting inhibited spiking activity in DCN cells. Both excitation and resulting inhibition occurred gradually with increasing stimulation frequencies. Given this finding, we propose that the inhibitory connections between PCs and DCN cells functions in a rate coding manner. Limits of rate coding in this connections should be checked with different stimulation frequencies from 5 Hz to 250 Hz.

Using the extracellular action potential waveforms *in vivo*, we could isolate two groups of cells with significant differences. Since these differences matched with *in vitro* distinction of GABAergic and non-GABAergic cells, we proposed our *in vivo* groups as candidate GABAergic and non-GABAergic cells. However it is known that there are also distinction between DCN cells in terms of their glutamatergic and glycinergic properties. In this respect, our study could only have answered a portion of the question about distinguishing DCN cells *in vivo*, only for their GABAergic properties. Further techniques to record the DCN cells selectively in vivo is needed to answer the remaining part of this question.

We found that only the candidate non-GABAergic DCN cells discharged time locked to fixed frequency stimulation while the candidate GABAergic cells did not react to PC inhibition in a temporal manner. Consequently we proposed that temporal coding is only functional for the non-

GABAergic DCN cells. Further improvements to distinguish DCN cells will help to extend our understanding about the coding mechanisms in DCN.

4.2 Discrimination of DCN cells *in vivo*

Principal component analysis on DCN cells' spike waveforms isolated two groups which had clear differences in their waveform parameters: especially in terms of half-width and falling phase. These two groups were also significantly different for their baseline firing rates. Interestingly, these properties (waveform shape and firing rate) matched with *in vitro* properties for GABAergic and non-GABAergic cells (Uusisaari at al., 2007). Consequently, we proposed to define our two groups of cells recorded *in vivo* as follows (see Table 1). Group 1 cells with narrow spikes and high firing rate may represent the non-GABAergic cells; Group 2 cells with larger spikes and low firing rates may represent the GABAergic cells including the mixed-type inhibitory nucleo-cortico cells with local collaterals and nucleo-olivary cells.

		Group 1 (non-GABAergic)	Group 2 (GABAergic)
Firing rate	*In vivo* *extracellular	63.9 ±5.0 Hz	23.2 ±4.7 Hz
	In vitro *experiment at 24 °C	29.9 ±5.8 Hz	9.8 ±1.0 Hz
Action potential width	*In vivo* *(positive + negative) peak	0.47 ± 0.08 ms	0.65 ± 0.11 ms
	In vitro *whole-cell current clamp	0.70 ±0.05 ms	0.99 ±0.05 ms

Table 1: Comparison of DCN cell groups obtained *in vivo* (present study) and *in vitro* (Uusisaari at al., 2007). Parameters obtained with extracellular recordings *in vivo* are compared with whole-cell current clamp recordings *in vitro.*

The differences of firing rates recorded *in vivo* and *in vitro* may result from differences in experimental temperatures and/or disconnected afferents due to slicing. Action potential widths *in vivo* were estimated as sum of half-widths from positive and negative peaks of the extracellular waveforms which were lower but proportional to those obtained *in vitro*.

Previous *in vitro* studies have defined five different types on DCN cells which fell into two main groups mentioned above. The first main group was the non-GABAergic cells, mostly composed of the principal cells, projecting to premotor areas. Other non-GABAergic cells were the glycinergic premotor projection cells found in medial nuclei (Bagnall et al. 2009) and the non-inhibitory

interneurons (Uusisaari at al., 2007), however they were not extensively studied yet and their properties were given only in a few studies. The second main group, the GABAergic DCN cells were the nucleo-cortical cells with local collaterals and the nucleo-olivary cells (see Introduction, section 1.5.3). Our extracellular recordings allowed discrimination of the DCN cells in those two main groups.

4.2.1 Comparison of extracellular and whole-cell recording techniques

The silicon probes used in my experiments allowed to record extracellular activities from the cerebellar cortex and the DCN. Under optogenetic stimulation of PCs, spiking activities of 57 DCN cells were recorded. We followed a conservative approach during spike sorting and 18 recordings were omitted because spikes were not isolated clearly and finally 39 DCN cells were used for further analyses. Extracellular recordings did not give a direct measure of the membrane potentials but the voltage fluctuations represent the electrical signature of action potentials. Extracellular signatures were found to predict intercellular properties of the cells in similar recordings (Henze et al., 2000).

An advantage of the extracellular recording is that the measurement does not interfere with the cell. Using the isolated spike waveforms, I could obtain significant differences in the waveforms of two groups of DCN cells. A recent study, which was published after I wrote the introduction chapters, also found the same differences in DCN cells with *in vivo* whole cell recordings (Canto et al., 2016) where DCN cells were clustered in two groups with large-small soma size, short-long spike widths and fast-slow firing frequencies. Expectedly, the differences in spike-widths and firing frequencies between the groups were similar to my findings and these cell groups were also suggested to be non-GABAergic and GABAergic DCN cells as proposed in my study.

However, in Canto et al. (2016) whole-cell recordings did not allow the discrimination of cell groups with their intrinsic physiological properties using k-means clustering. Groups were obtained after the addition of morphological properties (for example soma size). Authors noted that physiological properties were distributed over a wide range across cells as a continuum which represented the rich repertoire of DCN cells. They were recorded from three different nuclei, the anterior interposed, posterior interposed and medial nuclei which have different functions. Therefore, the authors suggested that functional differences among the nuclei (De Zeeuw and Ten Brinke, 2015) might underlie the large variability in the cell properties. In fact, the cerebellum takes part in very different tasks from basic balance to cognitive functions as I mentioned in the introduction, however there is no evidence whether the functional differences are related with the physiology of the DCN cells, to the best of my knowledge. Still, there might be some regional differences in DCN. One of the afferent

connections come from PCs that take part in different functions and they were found to have regional differences in their simple spike firing frequency related with zebrin band patterns in the cerebellar cortex (Zhou et al., 2014). A zebrin band pattern was also found in the DCN (Sugihara, 2011) and this pattern may underlie possible differences in DCN cells. Hence, the variability of DCN cells between zebrin bands remains to be explored to understand the variability in the physiology of DCN cells.

In Canto et al. (2016) study, another reason for the wide range of recorded physiological properties of DCN cells was the variability in the recording status of whole-cell recordings. Notably, membrane resistances were spread between 9.63 and 3352.1 MΩ with two orders of magnitude difference. In a previous *in vitro* study of DCN cells, Czubayko et al. (2001) applied a recording criterion of minimum 150 MΩ input resistance (access + membrane resistance) and excluded cells with low membrane resistances which might be an indicator of unhealthy cells. Another study of *in vivo* whole cell recording of DCN cells (Bengtsson et al., 2011) obtained much smaller ranges in spike-widths in cats although a direct comparison is not possible. Still, it is important to note that in this study access resistance was 7-15 MΩ which was smaller than the threshold used by Canto et al. (2016) study and small access resistance might have ensured to obtain relevant biophysical properties. Overall, different recording criteria used in the studies above probably affected selection of cells in better conditions and change the variability of the physiological properties.

Finally, when my results were compared with Canto et al. (2016) study, the ratio of silent cells observed was smaller (3 in 39 cells vs. 3 in 18 cells). This difference may come from the type of anesthesia used since ketamine used in Canto et al. (2016) study is known to inhibit the activity of NMDA receptors (Hirota and Lambert, 1996). Consequently, DCN cells were likely to be less excited resulting in lower firing frequencies and higher ratio of silent DCN cells.

In conclusion, despite some discrepancies between extracellular and whole-cell recording techniques the same discrimination of cells into two groups were obtained in Canto et al. (2016) and in the present study. We think there is enough evidence that these groups represent the non-GABAergic (Group 1) and GABAergic (Group 2) cells of the DCN.

4.3 Changes in oscillations and phase locking under anesthesia

In the cerebellar cortex, under urethane anaesthesia, prominent oscillations were recorded around 1 Hz and transient oscillations in the theta band around 4 Hz (Frederick et al., 2014). Recorded slow wave oscillations were related to granule and Golgi cell activities in the cerebellar cortex (Ros et al.,

2009). In my recordings from the DCN, delta and theta band oscillations were found around 17% and 48% of the total time, respectively, however there was no phase locked activity of DCN cells at these bands. These oscillations were reported to be related with the communication of the cerebellum to distinct brain areas like neocortex (Ros et al., 2009, Courtemanche et al., 2013). Therefore, the absence of phase-locked activity within the DCN for the slow oscillations is not surprising. Multielectrode technique used in this study allowed us to measure the oscillations and spiking activity from two different tetrodes in DCN with maximum 300 μm distance which finally provide information about medium scale interactions within the DCN.

The beta band oscillations (around 5-40 Hz) were suggested to entrain granule and Golgi cells in the cerebellar cortex through afferent connections from the mossy fibers (Courtemanche et al., 2009). During a grip task in monkeys, DCN cell activities were coherent with primary cortex oscillations in the beta band (Soteropoulos and Baker, 2006). Similarly, in my recordings, some DCN cells were phase locked to the beta band oscillations. Group 2 cells had a higher percentage of phase locking (25% compared to 12% in Group 1) which might come from sensory inputs of excitatory mossy fiber terminals. Group 2 (proposed GABAergic) cells have low firing frequencies and excitatory afferents are more likely to trigger spikes in this group compared to spontaneously active cells of Group 1. These predictions need to be examined by further experiments in awake behaving mice to observe the contributions of muscle contractions (Holdefer et al., 2000) to LFPs and phase locking.

A higher percentage of cells were phase locked to the oscillations in the gamma and high frequencies bands in both groups (Group 1: 65% and 88%, Group 2: 83% and 67%, respectively). Compared to the low frequencies, these oscillations were expected to represent transient local interactions (Buzsáki and Silva, 2012) which is in agreement with my recording conditions where the oscillations were detected within 300 μm distance from the spiking activity. As expected, recorded oscillations in the gamma and high frequencies bands had short durations (around 2% and 5% of the time, respectively) occurring transiently. Further analysis are planned to obtain the interactions between the two groups of cells under phase locking conditions at fast oscillations.

4.4 Manipulation of optogenetic stimulation intensity *in vivo*

During my experiments, we observed responses of one or more cells in the cerebellar cortex and the DCN. In these settings, it was possible to evaluate the expected response to the optogenetic stimulation as excitation in PCs and inhibition in DCN cells. In the experimental procedures, I used two levels of illumination power and I tried to avoid depolarization block in PCs caused by high level

of optogenetic stimulations in L7-ChR2 mice (Chaumont, 2013). After the experiments, I have found that half of the DCN cells were inhibited less with increased illumination power, which showed that some of the PCs were in depolarization block. As described in the introduction, each DCN cell receives inputs from approximately 40 PCs and it was not possible experimentally to observe whether all of these PCs were in depolarization block. Consequently, we could not observe possible effects of increased activity of converging PCs on DCN cells systematically.

In order to reduce the effect of PC depolarization block in the future experiments, it might be suggested to use an automated control for the illumination power so that it can be adjusted in small steps systematically and transition into depolarization blocks for PCs can be delayed. Such a manipulation procedure would probably allow to increase activities of PCs gradually and to observe small changes in the inhibition that DCN cells receive.

4.5 Rate and temporal coding in DCN

In my study, optogenetic stimulation of PCs at 40 Hz inhibited DCN cells from both groups which confirmed the functional connectivity of PCs to all DCN cells. With increasing frequency of PC stimulation, inhibitory effect gradually increased and showed that this connection can drive DCN cells in a rate coding manner (Figure 37 A). Change in the level of activity of PCs was sufficient to modulate the firing rates of the DCN cells and this gradual modulation was reliably observed in both of the DCN cell groups. However, proposed GABAergic cells were slightly more inhibited, as shown in the results.

Interestingly, beside the rate coding, PC inhibition resulted in temporal coding in a group of DCN cells. Group 1, the non-GABAergic cells, discharged time-locked spikes to fixed frequency inhibitory inputs of PCs. For optogenetic stimulation of PCs at 40 Hz, 65 Hz and 115 Hz, Group 1 cells had synchronous spiking activity at stimulation frequencies as determined from autocorrelograms. Groups 2 cells didn't show synchronized spiking activity and the difference between the groups was statistically significant as explained in the results. This difference was confirmed by a second analysis on the latency of spikes following each stimulation period. Synchronized spiking activity in PCs entrained spiking in non-GABAergic DCN cells which lead to a temporal control that modulated timings of spikes.

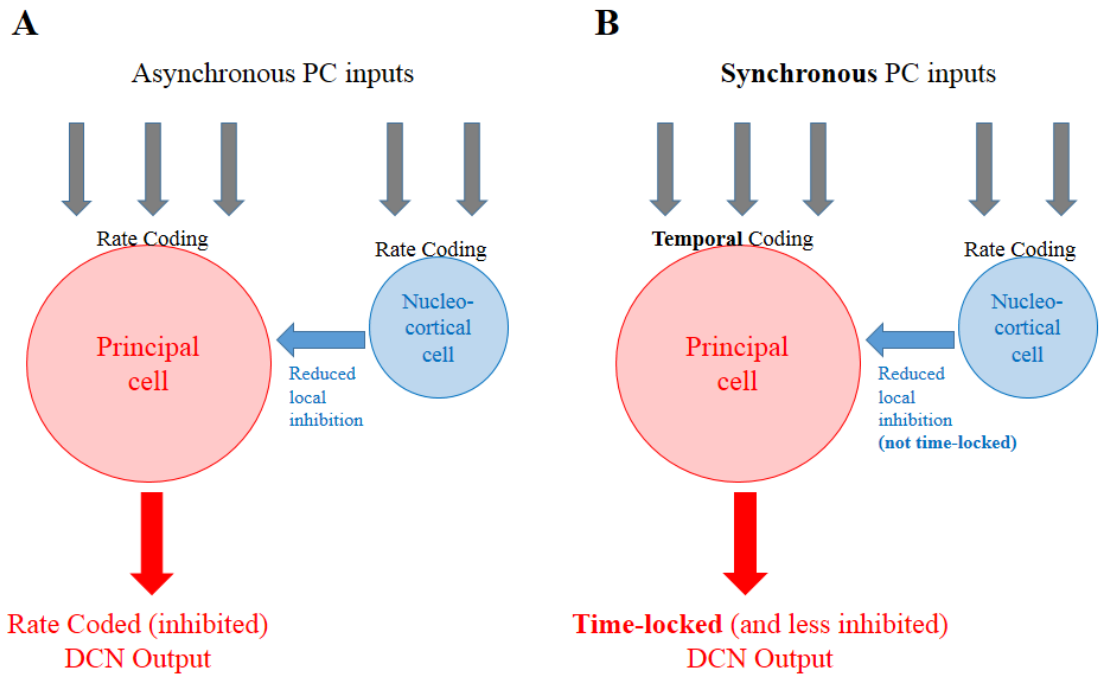

Figure 37: Effects of asynchronous and synchronous PC inputs in DCN. (**A**) Asynchronous PC inputs inhibit both principal and nucleo-cortical cells. Local inhibition is likely to decrease together with nucleo-cortical cell discharge (**B**) Synchronous PC inputs lead to a rebound-like time-locked responses in the principal cells that can drive DCN output. Local inhibition is still reduced and not time-locked so that it doesn't decrease time-locked DCN output.

Since we postulate that Group 1 cells represent the non-GABAergic projecting cells with big soma size, these results confirmed the time-locked spiking of "large neurons" of DCN from Person and Raman (2011) study. Similarly, proposed GABAergic cells (Group 2) demonstrated the absence of such property in line with the *in vitro* results for the GABAergic nucleo-olivary cells of the DCN from Najac and Raman (2015) study. Moreover, the other GABAergic cells of the DCN belonging to Group 2, the nucleo-cortical cells were also found to lack time-locked spiking after PC stimulations *in vivo*. Consequently, PC inhibition controlled not only firing rates of the principal projection cells but also their spike timing while it controlled only firing rates of the GABAergic cells (Figure 37 B).

In conclusion, fixed frequency optogenetic stimulations induced synchronized activity in a group of PCs and their inhibitory projections then control the timing of the principal DCN cells. With increasing frequencies of illumination, the principal DCN cells were inhibited more however their spikes were still time locked to the synchronized PC inputs. Considering the given results, inhibitory inputs of PCs can control both rate and timing of spiking of non-GABAergic DCN cells. It is known that PCs can go through regular spiking periods (Shin et al., 2007) with a common synchrony during specific movements (Heck et al., 2007). Such synchronized durations may introduce a transition from

rate coding to temporal coding for the downstream DCN cells (Person and Raman, 2012). Consequently, activity patterns in PCs determines the coding scheme to control the non-GABAergic principal DCN cells.

The GABAergic cells of the DCN, on the other hand, were not temporally affected by the synchronized PC inputs and did not fire time-locked spikes (Figure 37 B) probably because they lack some specific types of currents found in non-GABAergic cells. These are voltage independent tonic cationic currents and low-voltage activated (T-type) calcium currents (Raman et al., 2000; Molineux et al., 2006) which induce a rebound-like intrinsic responsiveness in the non-GABAergic (principal) DCN cells (Group 1). These channels support depolarization after hyperpolarization periods introduced by synchronized PC inputs. The nucleo-cortical cells of Group 2 have less potassium channels compared to the principal DCN cells (see introduction) which leads to less depolarizing currents and weaker afterhyperpolarizations (Raman et al., 2000; Alonso-Espinaco et al., 2008). Similarly, the other GABAergic cells, nucleo-olivary cells did not show any postinhibitory rebound responses in previous *in vitro* studies (Zheng and Raman, 2011; Najac and Raman, 2015). Consequently, GABAergic cells of the DCN did not have channels responsible for postinhibitory responses and cannot respond to hyperpolarizations by time-locked spiking.

The lack of temporal control of the GABAergic cells of DCN may have an important consequence that reinforces time-locked spiking of the non-GABAergic DCN cells. Since the nucleo-cortical cells (GABAergic) are not temporally controlled then the local inhibition they provided by them is not temporally controlled too (Figure 37 B). Consequently, the principal cells (non-GABAergic) will not receive a temporally controlled inhibition which would otherwise diminish time-locked output of DCN. Local inhibition is probably reduced by PC inputs thus it will further enhance the time-locked spiking of the principal cells.

4.6 Integration of excitatory and inhibitory afferents in the DCN

Since the afferents from different sources converge on the DCN cells, the control of PC inhibitory inputs might be limited (Figure 38). Assuming that mossy fiber direct inputs (excitatory) and indirect inputs through the cerebellar cortex (inhibitory) project to same DCN cells, Person and Raman (2012) suggested that overlapping inputs may disrupt the temporal coding of PCs. This conditions depends on the time course of the excitatory/inhibitory inputs and their decay time constants. In DCN cells, $GABA_A$ and AMPA receptors act with fast kinetics while NMDA has a longer decay time constant

(Figure 39). Excitation from mossy and climbing fibers introduced a potent NMDA input with a slow decay which constraints the temporal integration of excitation *in vitro* (Gauck and Jaeger, 2003). Spontaneous EPSCs had a long time course with decay time constant of 13.6 ± 3.2 ms (Anchisi et al., 2001) while IPSCs had shorter decay time constant around 3 ms (Husson et al., 2014, Person and Raman, 2012). Consequently, inhibitory connections are expected to have a more precise control on spike timing while excitatory connections would modulate spike rate in a longer time course. Still, effective fluctuations in AMPA excitatory currents were suggested to override PC inputs, while NMDA currents didn't have such an effect (Jaeger, 2011).

Another possible factor determining the efficiency of inputs is the distribution of the local inhibition in DCN which is not yet studied, to the best of my knowledge. Bengtsson and Jorntell (2014) showed that a DCN cell responded very differently to the stimulation of various areas of the arm in a decerebrated animal. Purely excitatory or inhibitory responses were observed, showing that they can override each other. These findings suggested that mappings of climbing fiber and mossy fiber receptive fields, and their indirect effects through PCs determine the integrated output of the DCN cell. The spread of local inhibition within these mappings add another factor for integration. Canto et al. (2016) found two DCN cells with small soma size and wide neurites, noting that they might be nucleo-cortical cells. Thus, local inhibition might be well spread in DCN. Rowland and Jaeger (2005) recorded only inhibitory responses to air puff stimulation in ~40% of DCN cells *in vivo* that may demonstrate an effective spread of local inhibition. Inhibition from PCs were followed by a long-latency excitation in general (Rowland and Jaeger, 2005; Bengtsson et al., 2011) which was missing for these cells. Consequently, the prevalence of inhibitory responses supports the idea that local inhibition is distributed in a non-specific volume which goes beyond the borders of the receptive fields in DCN. Further properties of local DCN circuitry should be investigated, especially to check for effects on the time-locked spiking responses.

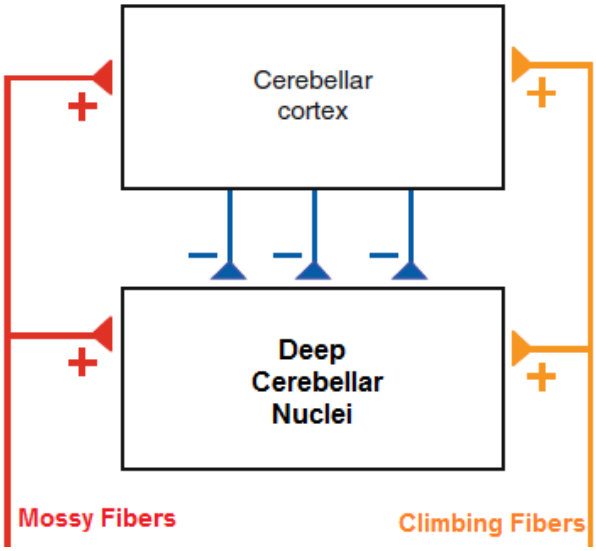

Figure 38: Converging of several input in cerebellar nuclei. Two excitatory afferents, mossy fibers and climbing fibers project to DCN directly. They also indirectly affect DCN with inhibitory connections of PCs from the cerebellar cortex.

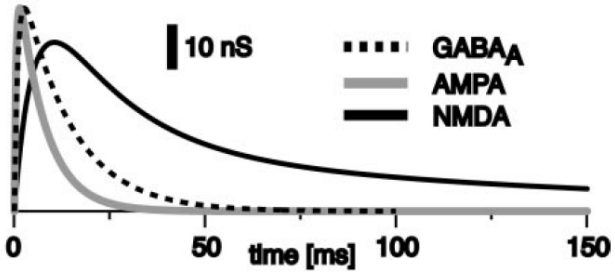

Figure 39: Unitary conductances for AMPA, NMDA and $GABA_A$ inputs. Compiled from several other studies (Audinat et al., 1992; Cull-Candy et al., 1998; Anchisi et al., 2001) ($GABA_A$ scaled to 0.56 of actual value for visualization). Inhibitory and excitatory conductances have different kinetics that determine their influence (adapted from Gauck and Jaeger, 2003)

4.6.1 Efficacy of local inhibition *in vivo*

In my experiments, multiple DCN cells were recorded and classified using their waveform parameters. Simultaneous activities of cells from different groups (proposed non-GABAergic and GABAergic cells) were obtained in three cases, however cross-correlograms of the spiking activities of these three pairs showed no clear relation. It was shown *in vitro* that the non-GABAergic cells

receive local inhibition from a portion of GABAergic cells (Husson et al., 2014) but this effect wasn't observed in my study, suggesting that functional connectivity of the local inhibition was weak *in vivo* compared to other afferents from the PCs, mossy fibers and climbing fibers.

One reason for the lack of a relation in the cross-correlograms might be the low frequency discharge of the nucleo-cortical cells (Ankri et al., 2015) that generate local inhibition. Their activity is expected to depend on the excitatory inputs of DCN, mostly given by mossy fibers and these inputs may be low in our experimental conditions. In a previous *in vivo* study, air puff stimulation have evoked long durations of inhibition in DCN cells (up to hundreds of milliseconds) and these durations were linearly increased by air puff intensity (Rowland and Jaeger, 2005). The source of this inhibition may be local such that sensory information carried by mossy fibers may directly excite the nucleo-cortical cells to provide local inhibition (Figure 40, Ai and Bi). These inputs may not strongly excite spontaneously active principal cells if they are not precisely targeted however same afferents may have a stronger net excitatory effect for the intrinsically slow firing nucleo-cortical cells. Consequently, mossy fiber afferents may be important for the efficacy of the local inhibition.

The nucleo-cortical cells have big dendritic structures (Uusisaari and Knöpfel, 2013; Canto et al., 2016) which may provide off-module inhibition to distal principal DCN cells (Figure 40, Aii and Bii). We can consider the nucleo-cortical cell in Module A (NC-A) that projects to Module B and inhibits the principal cell B (Figure 40 Aii). This case would require long axonal projections of the nucleo-cortical cells which were not studied yet, to the best of my knowledge. Another case of off-module inhibition may result from excitation of the nucleo-cortical cell (NC-B) through its dendrites crossing to Module A. It would again result in inhibition of the principal cell B (Figure 40 Bii). High ratio of inhibitory responses in DCN (Rowland and Jaeger, 2005) support these possibilities which need to be investigated starting from the excitatory effect of mossy fibers on the nucleo-cortical cells in the DCN.

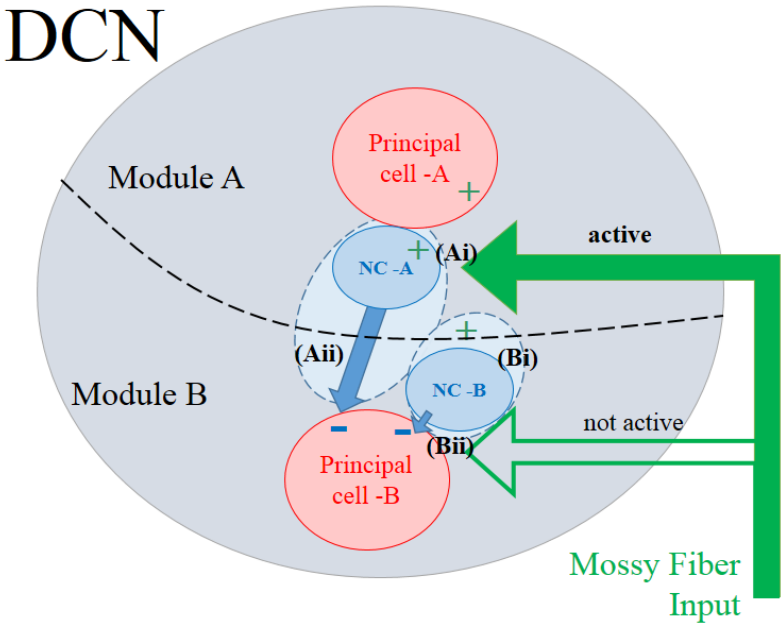

Figure 40: A speculative off-module inhibition pathway in DCN. Mossy fiber afferents are expected to selectively project to different modules of the DCN, given as Module A and Module B. An active mossy fiber afferent may excite nucleo-cortical cells in the same module directly (**Ai**, NC-A) or in a neighboring module through dendritic extensions (**Bi**, NC-B). The principal cell in Module B may be inhibited by these nucleo-cortical cells through axonal extensions (**Aii)** or directly **(Bii**). Spread of local inhibition in DCN may serve as an off-module inhibitory pathway.

Mixed inhibitory outputs of the nucleo-cortical cells (GABAergic and glycinergic) to the principal DCN might be responsible for another pathway than just local inhibition. Husson (2014) pointed that glycinergic transmission in DCN may potentiate NMDA currents which was observed in cultured neurons (Johnson and Ascher, 1987). This pathway may support the smooth excitatory drive in the principal DCN cells by NMDA currents and indirectly enhance time-locked spiking in response to synchronized PC inputs.

Another reason for the lack of a clear relations in the pairs can be that the recorded GABAergic cells were the nucleo-olivary cells, which do not project to the non-GABAergic cells within the DCN, to the best of my knowledge. The number of pairs observed in my study was very low and possibly the nucleo-cortical cells that provide the local inhibition was not sampled adequately. Further experiments should be done to increase the number of pairs where two cells belonging to different groups were simultaneously recorded.

5 MATERIALS AND METHODS

5.1 Virus / Dye injections and tracing experiments

For DiI (1,1-dioctadecyl-3,3,3,3 tetramethylindocarbocyanine perchlorate, ThermoFisher, US) injections, P20-P30 CD1 mice were anesthetized by 4% isoflurane for induction followed by continuously administration at 2% with O_2-medical air. An incision was made in the scalp to expose the skull over the cerebellum and the skull over the desired injection areas was drilled using a handheld picospritzer II (Parker Instrumentation, US). After that, pulled glass needles were used to inject a small amount of DiI diluted at 10% in N,N-dimethylformamide. The injections completed in our laboratory with Elise Savier and Kevin Dorgans.

For virus injections, recombinant adeno-associated viral particles (rAAV2/1, 2.8X1012 GU/ml) carrying cDNA for GFP expression under the CMV promoter were used. Mice were anesthetized by an intraperitoneal injection of a mixture of ketamine (100 mg/kg), medetomidine (1 mg/kg) and acepromazine (3 mg/kg). The virus was loaded into a graduated pipette equipped with a piston for manual injections (Wiretrol II, Drummond Scientific Company, US). By applying gentle pressure, final volume of 0. 5 µl was delivered into the tissue at an approximate speed of 250nl/min. The pipette was left in place for at least ten minutes after injection for virus diffusion. After two weeks of recovery, injected mice were sacrificed by transcardiac perfusion of paraformaldehyde 4% and cerebellar slices (50µm) were prepared for subsequent analysis. Virus injections completed in our laboratory with Francesca Binda.

Serial confocal acquisitions (1 µm Z-stack resolution) were performed (Leica, SP5, II, Germany) onto sequential sections of cerebellar slices. Some Purkinje cells were individually traced with ImageJ (NIH, US) plugin “Simple neurite tracer”.

5.2 In-vivo experimentation

5.2.1 Mouse model and optogenetic stimulation

In our experiments, genetically modified mouse strain CD1 L7-ChR2 (1.5-4 months old) was used. Mice were kept and bred in the Chronobiotron (UMS 3415, CNRS, Strasbourg) animal facility. To prevent the impact of ovarian hormones female mice were not included in the experiments. L7-ChR2 strain was developed in our laboratory and used in several studies like Chaumont et al. (2013), Proville et al. (2014) and Ankri et al. (2015). It expresses channelrhodopsin (ChR2) fused to green fluorescent protein (GFP) specifically in PCs. Blue light illumination around 460 nm evoked inward currents in PCs through the ChR2 channels. These channels were extensively found in the dendrites so that inward currents sum up to reliably generate action potentials in PCs (Chaumont et al., 2013). Blue light at 460 nm wavelength was produced by LED (Prizmatix; UHP-T-LED 460, IL). Optical fiber was placed over the Lobule IV/V above the surface of the tissue.

For optical stimulation, six different protocols were used: one with steady illumination of 10 seconds and others with 5 ms illumination pulses at different frequencies. Three of them had fixed frequencies (40Hz, 65 Hz and 115 Hz) of illumination. Random stimulation protocol had Poisson distributed frequencies up to 200 Hz.

5.2.2 Surgery

Mice were anesthetized using urethane (1.9 g/kg i.p.) and pain reflexes were followed to disappear then a tracheotomy was performed. After that, mice were placed in a stereotaxic frame (Narashige, JPN). The body temperature was maintained using a heating blanket (CWE Inc, TC-1000, US) and monitored through a rectal probe. An incision was made in the scalp over the skull covering the cerebellum and a craniotomy was done to uncover the dorsal vermis and paravermis of the cerebellar cortex and these surfaces were constantly moisturized with a saline solution (NaCl 9 g/L).

5.2.2.1 Effects of anesthetic agent urethane

Urethane influences a wide array of receptors without blocking any specific one (Hara and Harris, 2002). These moderate changes on several receptors, NMDA, AMPA, GABA and glycine, were suggested to induce the anesthetic effect of urethane altogether. Since none of the receptors were severely blocked, urethane was proposed for electrophysiological studies (Hara and Harris, 2002).

Urethane was reported to induce sleep like cycles in different brain regions (Clement et al., 2008). It did not blocked oscillatory activity such as low frequency oscillations including theta band. Indeed,

these oscillations were similar to those in awake animals (Courtemanche et al., 2013). However, high frequency oscillations were slowed down in hippocampus under the urethane effect (Ylonen et al., 1995).

5.2.3 *In vivo* multielectrode recordings

In order to record PCs and DCN cells, we performed multiunit extracellular recordings in the cerebellar cortex and in the medial DCN, simultaneously. Custom design silicon probes (Figure 41, 2*16 channels, Atlas Neuroengineering, BE) were lowered into Lobule IV-V in the vermis to record PCs and through the Lobule VI in the paravermis to record the DCN cells using motorized micromanipulators (Luigs and Neumann, DE). We started data acquisition when the expected responses to optical illumination were obtained in both regions. For this purpose, a portable 32 channels acquisition amplifier (ME32-FAI-µPA, MultiChannel Systems, DE) was used at 20 kHz sampling rate and 5kHz low pass filtering. Illumination protocols were executed using a Raspberry Pi (UK) single board computer.

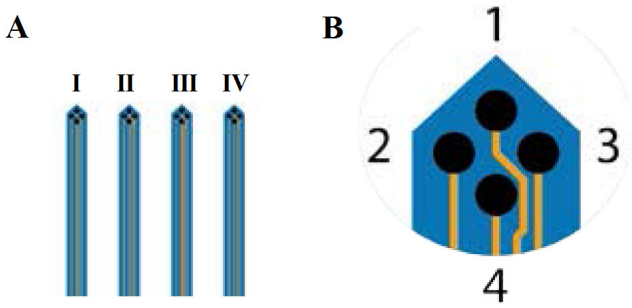

Figure 41: Silicon probe structure with 16 channels. (**A**) Four parallel shanks of the probe (I-II-III-IV) were used to record activities from a large area with 150 µm spacing between each shank (**B**) Four recording sites (1,2,3,and 4; each having 15 µm diameter) were positioned in a diamond shape separated with ~20 µm distance in our custom design, which gave different voltage recordings that helped spike sorting (see Figure 21 and 22).

5.3 Data Analysis

5.3.1 Detection of local field potentials

Extracellular recording signal from one channel of the tetrodes was used for the time-frequency analysis to detect LFPs. The method used was described by Roux et al. (2007) where spectral components of the signal are detected by applying continuous wavelet transform. For this process, a series of Morlet wavelets (Kronland-Martinet et al., 1987) were chosen and this method enabled

detection of simultaneous oscillations at different frequency bands. Detected transient oscillations were represented in a heat map where the power of oscillations was given for all frequencies and instants of recording time. Maxima points in the heat map above the defined threshold (3 standard deviations from the mean power) were detected and joined by ridge extraction method described by Roux et al. (2007). A threshold of minimum of 5 cycles were used in the detection of oscillations. Finally the total duration and frequency shifts of the oscillation were obtained.

5.3.2 Spike sorting

In order to isolate the activities of cells recorded by the same tetrodes, different spike sorting techniques can be used. A straight forward method is to measure the amplitudes of the spikes in each recording site of the tetrodes, where the cells can be distinguished according to their distances to different recording sites (Gao et al., 2012). Another method is to apply principal component analysis to the spikes obtained in the 4 channels and then to group them according to their similarities. We used the principal component analysis method on an open source software, OpenElectrophy (Garcia and Fourcaud-Trocmé, 2009). Steps of the spike sorting process is shown in Figure 42 A: after applying a high-pass filter of 200 Hz, a manual threshold was determined and spike peaks were obtained in the 4 channels. Before spike sorting, stimulation artifacts which led to high voltage deflections in the recordings were cleaned by home-made scripts, similar to the study Rowland and Jaeger (2008).

Waveforms of each spike from the 4 channels were obtained for ± 1 ms from the spike peak. Consequently, we obtained 41*4 data points sampled at 20 kHz (for each of 4 channels: 20 data points before the spike peak, 1 for the spike peak and 20 after the spike peak) for each spike waveform. These data points were used for the principal component analysis to cluster the spikes coming from different cells (Figure 42 B). The isolated spikes shown in Figure 42 A were assigned to two cells (Figure 42 C).

Figure 42: Spike Sorting with OpenElectrophy software. (**A**) Raw signals in four channels were high-pass filtered and a manual threshold was applied to detect spike peaks. (**B**) Graphical user interface of the OpenElectrophy software allowed principal components analysis and clustering. The scattering of the two first principal components of spikes showed two clusters meaning two different spike waveforms from two different cells (**C**) As the result, spikes with different shapes were separated.

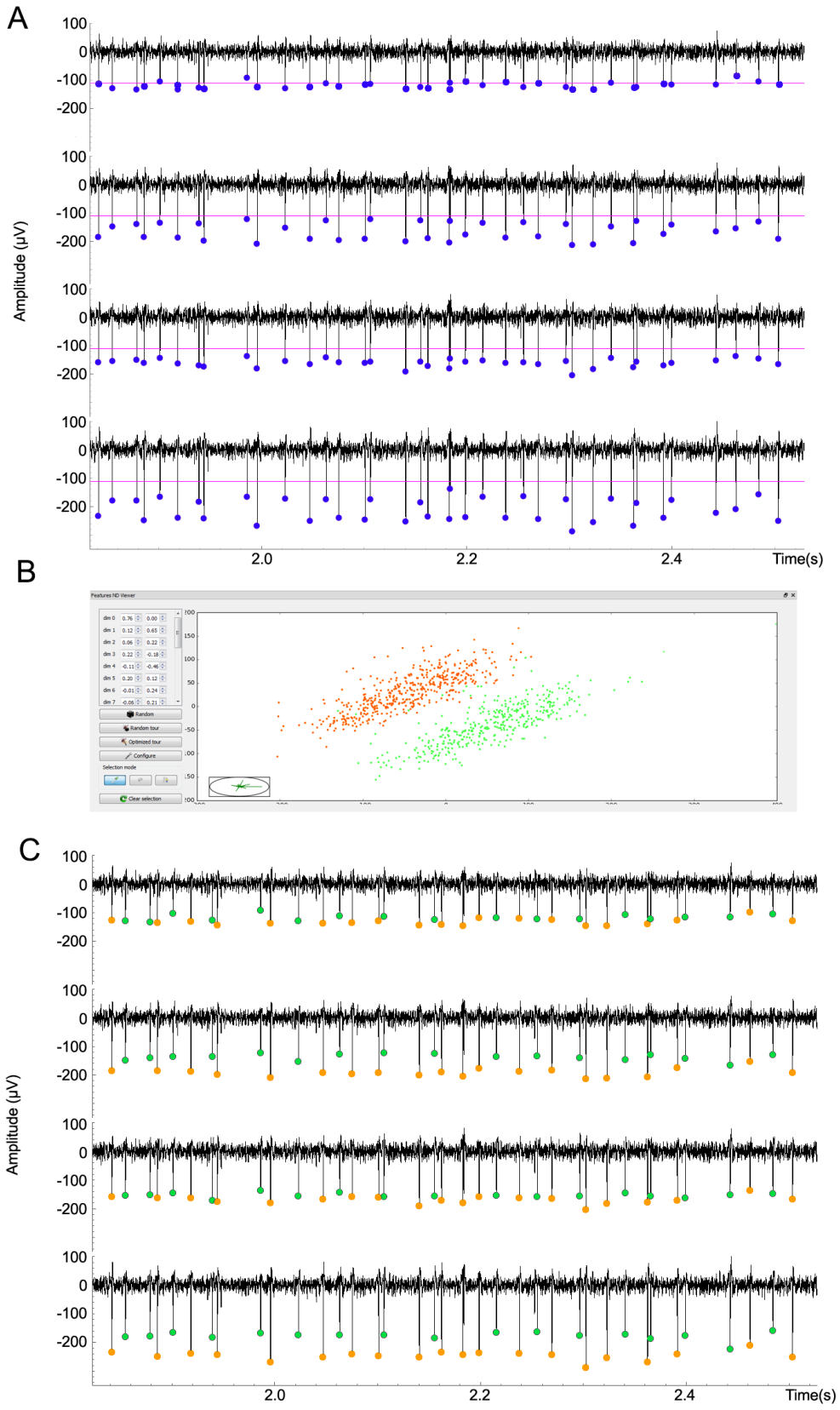
A
100
0
-100
-200
Amplitude (µV)
2.0
2.2
2.4
Time(s)
B
C
Amplitude (µV)
2.0
2.2
2.4
Time(s)

5.3.3 Obtaining waveform parameters

Spike waveforms of the isolated DCN cells from all experiments were used for the classification (n= 39, N=13). Average spike waveform of each cell was calculated from baseline firing periods. In the next step, waveforms were normalized to positive spike peaks to take care of possible differences in extracellular recording distances between the cells and the electrodes. Waveform parameters obtained are given below (Figure 43).

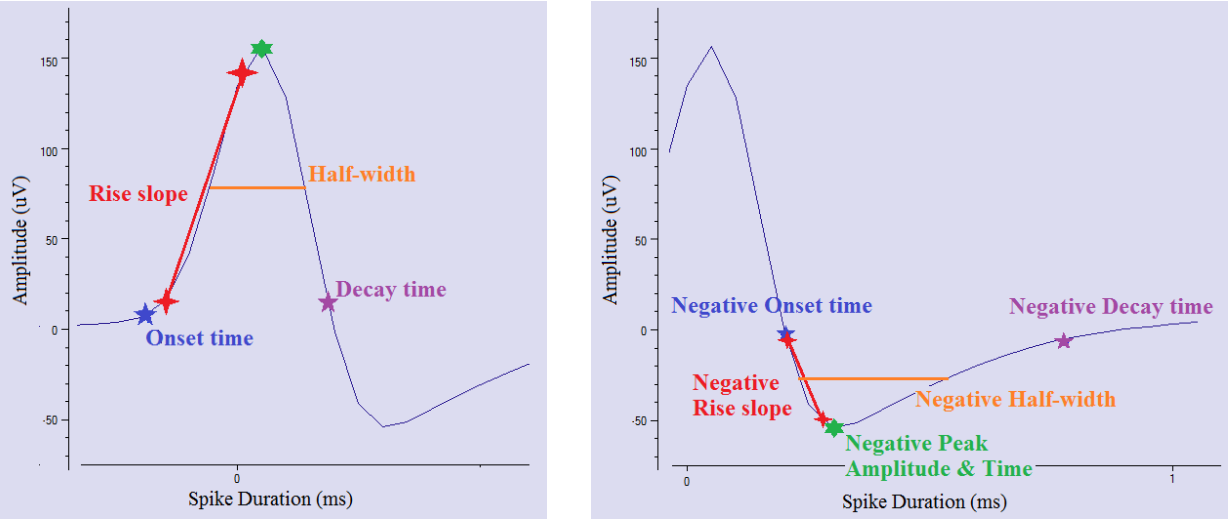

- Positive Onset time (Time point where spike waveform reaches 5% of its peak)

- Positive Rise slope (Slope of the spike between 10% and 90% of its peak)

- Positive Half-width (Time duration for the spike between 50% of its peak in the rising phase to 50% of its peak in the falling phase)

- Positive Decay time (Time duration for the spike to fall from 100% to 10% of its peak)

- Negative Peak amplitude (value of the negative peak in the falling phase)

- Negative Peak time (Time point where spike reaches its negative peak in the falling phase)

- Negative Onset time (Time point where spike waveform reaches 5% of its negative peak in the falling phase)

- Negative Rise slope (Slope of the spike from10% to 90% of its negative peak in the falling phase)

- Negative Half-width (Time duration for the spike between 50% of its negative peak in the falling phase to 50% of its negative peak in the refractory phase)

- Negative Decay time (Time duration for the spike to rise from 100% to 10% of its negative peak in the refractory phase)

Figure 43: Parameters extracted from the average waveform in an example cell.

5.3.4 Hierarchical clustering on principal components

Principal components are obtained by orthogonal transformations of the ten waveform parameters obtained above. The first principal component represented the highest variance in the data and following principal components were chosen as orthogonal to previous ones representing the maximum possible variance. Hierarchical clustering is then applied using the principal components.

The unsupervised process of selecting clusters to merge based on the Euclidian criteria allows the construction of a hierarchy. In a dataset, total (multidimensional) variance is constant. When clusters are formed, total variance is shared by variance within the clusters and between the clusters. In the algorithm, Ward criterion minimizes the increase of the variance within the clusters at each step. It starts with taking each cell as a cluster and calculates the Euclidean distance between all the clusters in the 10 dimensional space of the waveform parameters. The two closest clusters with respect to the Ward's criterion are then merged in each step. Ward's criterion is given as:

$$\text{Ward's } (A, B) = (I_A I_B / I_A + I_B) \, d^2(\mu_A, \mu_B)$$

where d the Euclidean distance, μ_A and μ_B centers of the clusters A and B, I_A and I_B the cardinality (number of elements) of clusters A and B.

When there is a big increase in the variance at a specific step compared to previous steps, the new cluster presented a higher level of variance than the merged ones. Theoretically, the merged clusters may belong to different populations due to the big increase in the variance. Consequently, hierarchical clustering is used to define the optimal number of clusters in a dataset.

5.3.5 Statistical analyses

Statistical analyses were performed using python packages (scipy functions). Normality of data was assessed with scipy.stats.normaltest function checking skewness and kurtosis of the distributions. Normal distributions were given as mean and standard error of mean, unless otherwise stated.

In Figure 27 Aii, firing frequency difference between Group 1 and Group 2 was determined with two sample t-test ($t= -5.822$, $p< 0.000005$).

In Figure 28 D, the duration of detected oscillations didn't have normal distributions among recordings, parametric Mann Whitney U tests were used to compare them and groups with significant difference was determined with $p < 0.05$.

In Figure 31 A&C, we used Pearson's R correlation tests to assess the predictive value of baseline firing rates for the inhibitory responses. Linear correlation inside a cloud of points was tested with the correlation index r and related p value.

In Figure 32, time-locked activity of DCN cells was determined by the power spectral density of their autocorrelograms at stimulation frequency. First, corrected autocorrelograms were obtained with subtraction of shifted autocorrelograms. Then, power spectral density was calculated using matplotlib.mlab.psd function that applies Welch's average periodogram method.

In Figure 33, the two group of cells didn't have normal distributions in power density values thus Mann–Whitney U tests were used to compare them.

In Figure 34, latencies of spikes following stimulation pulses were tested for uniform distribution. For this analysis, latency distributions were compared with Rayleigh distributions using Kolmogorov-Smirnov goodness-of-fit test. Nonuniform distributions were detected by rejection of Rayleigh distribution fit with $p < 0.01$.

In Figure 35 D, Distribution of firing frequencies were compared with the distribution of stimulation frequencies using Kolmogorov-Smirnov goodness-of-fit test and matched between the distributions were rejected by $p < 0.01$.

6 REFERENCES

Ahn, A. H., Dziennis, S., Hawkes, R., & Herrup, K. (1994). The cloning of zebrin II reveals its identity with aldolase C. *Development (Cambridge, England)*, *120*(8), 2081–90. Retrieved from http://www.ncbi.nlm.nih.gov/pubmed/7925012

Aizenman, C. D., Manis, P. B., & Linden, D. J. (1998). Polarity of Long-Term Synaptic Gain Change Is Related to Postsynaptic Spike Firing at a Cerebellar Inhibitory Synapse. *Neuron*, *21*(4), 827–835. http://doi.org/10.1016/S0896-6273(00)80598-X

Albus, J. S. (1971). A theory of cerebellar function. *Mathematical Biosciences*, *10*(1–2), 25–61. http://doi.org/10.1016/0025-5564(71)90051-4

Alonso-Espinaco, V., Elezgarai, I., Díez-García, J., Puente, N., Knöpfel, T., & Grandes, P. (2008). Subcellular localization of the voltage-gated potassium channels Kv3.1b and Kv3.3 in the cerebellar dentate nucleus of glutamic acid decarboxylase 67-green fluorescent protein transgenic mice. *Neuroscience*, *155*(4), 1059–69. http://doi.org/10.1016/j.neuroscience.2008.07.014

Altman, J., & Bayer, S. A. (1977). Time of origin and distribution of a new cell type in the rat cerebellar cortex. *Experimental Brain Research*, *29*(2), 265–74. Retrieved from http://www.ncbi.nlm.nih.gov/pubmed/913518

Anchisi, D., Scelfo, B., & Tempia, F. (2001). Postsynaptic Currents in Deep Cerebellar Nuclei. *Journal of Neurophysiology*, *85*(1), 323–331. Retrieved from http://jn.physiology.org/content/85/1/323.abstract

Andersen, B. B., Korbo, L., & Pakkenberg, B. (1992). A quantitative study of the human cerebellum with unbiased stereological techniques. *The Journal of Comparative Neurology*, *326*(4), 549–60. http://doi.org/10.1002/cne.903260405

Angaut, P., & Sotelo, C. (1973). The fine structure of the cerebellar central nuclei in the cat II. Synaptic organization. *Experimental Brain Research*, *16*(4), 410–30. http://doi.org/10.1007/BF00233433

Angaut, P., & Sotelo, C. (1989). Synaptology of the cerebello-olivary pathway. Double labelling with anterograde axonal tracing and GABA immunocytochemistry in the rat. *Brain Research*, *479*(2), 361–5. http://doi.org/10.1016/0006-8993(89)91641-7

Ankri, L., Husson, Z., Pietrajtis, K., Proville, R., Léna, C., Yarom, Y., … Uusisaari, M. Y. (2015). A novel inhibitory nucleo-cortical circuit controls cerebellar Golgi cell activity. *eLife*, *4*(MAY), 1–26. http://doi.org/10.7554/eLife.06262

Apps, R., & Garwicz, M. (2000). Precise matching of olivo-cortical divergence and cortico-nuclear convergence between somatotopically corresponding areas in the medial C1 and medial C3 zones of the paravermal cerebellum. *The European Journal of Neuroscience*, *12*(1), 205–14. Retrieved from http://www.ncbi.nlm.nih.gov/pubmed/10651875

Apps, R., & Garwicz, M. (2005). Anatomical and physiological foundations of cerebellar information processing. *Nature Reviews Neuroscience*, *6*(4), 297–311. http://doi.org/10.1038/nrn1646

Apps, R., & Hawkes, R. (2009). Cerebellar cortical organization: a one-map hypothesis. *Nature Reviews. Neuroscience*, *10*(9), 670–81. http://doi.org/10.1038/nrn2698

Armstrong, D. M., & Edgley, S. a. (1984). Discharges of nucleus interpositus neurones during locomotion in the cat. *The Journal of Physiology*, *351*, 411–32. Retrieved from http://www.ncbi.nlm.nih.gov/pubmed/6747870

Asanuma, C., Thach, W. T., & Jones, E. G. (1980). Nucleus interpositus projection to spinal interneurons in monkeys. *Brain Research*, *191*(1), 245–8. http://doi.org/10.1016/0006-8993(80)90327-3

Audinat, E., Gähwiler, B. H., & Knöpfel, T. (1992). Excitatory synaptic potentials in neurons of the deep nuclei in olivo-cerebellar slice cultures. *Neuroscience*, *49*(4), 903–11. http://doi.org/10.1016/0306-4522(92)90366-A

Bagnall, M. W., Zingg, B., Sakatos, A., Moghadam, S. H., Zeilhofer, H. U., & du Lac, S. (2009). Glycinergic projection neurons of the cerebellum. *The Journal of Neuroscience : The Official Journal of the Society for Neuroscience*, *29*(32), 10104–10. http://doi.org/10.1523/JNEUROSCI.2087-09.2009

Bartos, M., Vida, I., Frotscher, M., Meyer, A., Monyer, H., Geiger, J. R. P., & Jonas, P. (2002). Fast synaptic inhibition promotes synchronized gamma oscillations in hippocampal interneuron networks. *Proceedings of the National Academy of Sciences*, *99*(20), 13222–13227. http://doi.org/10.1073/pnas.192233099

Bastian, A. J. (2006). Learning to predict the future: the cerebellum adapts feedforward movement control. *Current Opinion in Neurobiology*, *16*(6), 645–649. http://doi.org/10.1016/j.conb.2006.08.016

Baumel, Y., Jacobson, G. A., & Cohen, D. (2009). Implications of functional anatomy on information processing in the deep cerebellar nuclei. *Frontiers in Cellular Neuroscience*, *3*(November), 14. http://doi.org/10.3389/neuro.03.014.2009

Beitz, A. J. (1982). Structural organization of the fastigial nucleus. *Experimental Brain Research*, *47*(Suppl. 6), 233–249.

Beitz, A. J., & Chan-Palay, V. (1979). The medial cerebellar nucleus in the rat: nuclear volume, cell number, density and orientation. *Neuroscience*, *4*(1), 31–45. Retrieved from http://www.ncbi.nlm.nih.gov/pubmed/759985

Beitz, A. J., & Chan-Palay, V. (1979). A Golgi analysis of neuronal organization in the medial cerebellar nucleus of the rat. *Neuroscience*, *4*(1), 47–63. Retrieved from http://www.ncbi.nlm.nih.gov/pubmed/104189

Bengtsson, F., Ekerot, C.-F., & Jörntell, H. (2011). In vivo analysis of inhibitory synaptic inputs and rebounds in deep cerebellar nuclear neurons. *PloS One*, *6*(4), e18822. http://doi.org/10.1371/journal.pone.0018822

Bengtsson, F., & Jörntell, H. (2014). Specific Relationship between Excitatory Inputs and Climbing Fiber Receptive Fields in Deep Cerebellar Nuclear Neurons. *PLoS ONE*, *9*(1), e84616. http://doi.org/10.1371/journal.pone.0084616

Blenkinsop, T. A., & Lang, E. J. (2011). Synaptic Action of the Olivocerebellar System on Cerebellar Nuclear Spike Activity. *Journal of Neuroscience*, *31*(41), 14708–14720. http://doi.org/10.1523/JNEUROSCI.3323-11.2011

Blot, A., & Barbour, B. (2014). Ultra-rapid axon-axon ephaptic inhibition of cerebellar Purkinje cells by the pinceau. *Nature Neuroscience*, *17*(2), 289–95. http://doi.org/10.1038/nn.3624

Brenowitz, S. D., & Regehr, W. G. (2012). Presynaptic Imaging of Projection Fibers by In Vivo Injection of Dextran-Conjugated Calcium Indicators. *Cold Spring Harbor Protocols*, *2012*(4), pdb.prot068551-prot068551. http://doi.org/10.1101/pdb.prot068551

Brochu, G., Maler, L., & Hawkes, R. (1990). Zebrin II: a polypeptide antigen expressed selectively by Purkinje cells reveals compartments in rat and fish cerebellum. *The Journal of Comparative Neurology*, *291*(4), 538–52. http://doi.org/10.1002/cne.902910405

Brodal, P. (2004). *The central nervous system: structure and function*. Oxford University Press.

Brooks, J. X., & Cullen, K. E. (2013). The Primate Cerebellum Selectively Encodes Unexpected Self-Motion. *Current Biology*, *23*(11), 947–955. http://doi.org/10.1016/j.cub.2013.04.029

Buisseret-Delmas, C., & Angaut, P. (1993). The cerebellar olivo-corticonuclear connections in the rat. *Progress in Neurobiology*, *40*(1), 63–87. http://doi.org/10.1016/0301-0082(93)90048-W

Buzsáki, G., & Silva, F. L. da. (2012). High frequency oscillations in the intact brain. *Progress in Neurobiology*, *98*(3), 241–249. http://doi.org/10.1016/j.pneurobio.2012.02.004

Callaway, E. M., & Katz, L. C. (1993). Photostimulation using caged glutamate reveals functional circuitry in living brain slices. *Proceedings of the National Academy of Sciences of the United States of America*, *90*(16), 7661–5. Retrieved from http://www.ncbi.nlm.nih.gov/pubmed/7689225

Canto, C. B., Witter, L., & De Zeeuw, C. I. (2016). Whole-Cell Properties of Cerebellar Nuclei Neurons In Vivo. *PloS One*, *11*(11), e0165887. http://doi.org/10.1371/journal.pone.0165887

Carleton, S. C., & Carpenter, M. B. (1983). Afferent and efferent connections of the medial, inferior and lateral vestibular nuclei in the cat and monkey. *Brain Research*, *278*(1–2), 29–51. Retrieved from http://www.ncbi.nlm.nih.gov/pubmed/6315158

Cerminara, N. L., Lang, E. J., Sillitoe, R. V, & Apps, R. (2015). Redefining the cerebellar cortex as an assembly of non-uniform Purkinje cell microcircuits. *Nature Reviews Neuroscience*, *16*(2), 79–93. http://doi.org/10.1038/nrn3886

Cesana, E., Pietrajtis, K., Bidoret, C., Isope, P., D'Angelo, E., Dieudonné, S., & Forti, L. (2013). Granule cell ascending axon excitatory synapses onto Golgi cells implement a potent feedback circuit in the cerebellar granular layer. *The Journal of Neuroscience : The Official Journal of the Society for Neuroscience*, *33*(30), 12430–46. http://doi.org/10.1523/JNEUROSCI.4897-11.2013

Chan-Palay, V. (1973). A light microscope study of the cytology and organization of neurons in the simple mammalian nucleus lateralis: columns and swirls. *Zeitschrift Für Anatomie Und Entwicklungsgeschichte*, *141*(2), 125–50. Retrieved from http://www.ncbi.nlm.nih.gov/pubmed/4769549

Chan-Palay, V. (1973). On the identification of the afferent axon terminals in the nucleus lateralis of the cerebellum. An electron microscope study. *Zeitschrift Für Anatomie Und Entwicklungsgeschichte*, *142*(2), 149–86. Retrieved from http://www.ncbi.nlm.nih.gov/pubmed/4781861

Chapuis, J., Garcia, S., Messaoudi, B., Thevenet, M., Ferreira, G., Gervais, R., & Ravel, N. (2009). The way an odor is experienced during aversive conditioning determines the extent of the network recruited during retrieval: a multisite electrophysiological study in rats. *The Journal of Neuroscience : The Official Journal of the Society for Neuroscience*, *29*(33), 10287–98. http://doi.org/10.1523/JNEUROSCI.0505-09.2009

Chaumont, J., Guyon, N., Valera, A. M., Dugué, G. P., Popa, D., Marcaggi, P., … Isope, P. (2013). Clusters of cerebellar Purkinje cells control their afferent climbing fiber discharge. *Proceedings of the National Academy of Sciences of the United States of America*, *110*(40), 16223–8. http://doi.org/10.1073/pnas.1302310110

Chen, L., Bao, S., & Thompson, R. F. (1999). Bilateral lesions of the interpositus nucleus completely prevent eyeblink conditioning in Purkinje cell-degeneration mutant mice. *Behavioral Neuroscience*, *113*(1), 204–10. http://doi.org/10.1037/0735-7044.113.1.204

Chen, S., Augustine, G. J., & Chadderton, P. (2016). The cerebellum linearly encodes whisker position during voluntary movement. *eLife*, *5*(JANUARY2016), e10509. http://doi.org/10.7554/eLife.10509

Chen, X., Kovalchuk, Y., Adelsberger, H., Henning, H. a, Sausbier, M., Wietzorrek, G., … Konnerth, A. (2010). Disruption of the olivo-cerebellar circuit by Purkinje neuron-specific ablation of BK channels. *Proceedings of the National Academy of Sciences of the United States of America*, *107*(27), 12323–8. http://doi.org/10.1073/pnas.1001745107

Clement, E. A., Richard, A., Thwaites, M., Ailon, J., Peters, S., & Dickson, C. T. (2008). Cyclic and sleep-like spontaneous alternations of brain state under urethane anaesthesia. *PloS One*, *3*(4), e2004. http://doi.org/10.1371/journal.pone.0002004

Coesmans, M., Weber, J. T., De Zeeuw, C. I., & Hansel, C. (2004). Bidirectional parallel fiber plasticity in the cerebellum under climbing fiber control. *Neuron*, *44*(4), 691–700. http://doi.org/10.1016/j.neuron.2004.10.031

Cohen, D., & Yarom, Y. (2000). Cerebellar on-beam and lateral inhibition: two functionally distinct circuits. *Journal of Neurophysiology*, *83*(4), 1932–40. Retrieved from http://www.ncbi.nlm.nih.gov/pubmed/10758104

Courtemanche, R., Chabaud, P., & Lamarre, Y. (2009). Synchronization in primate cerebellar granule cell layer local field potentials: basic anisotropy and dynamic changes during active expectancy. *Frontiers in Cellular Neuroscience*, *3*(July), 6. http://doi.org/10.3389/neuro.03.006.2009

Courtemanche, R., Robinson, J. C., & Aponte, D. I. (2013). Linking oscillations in cerebellar circuits. *Frontiers in Neural Circuits*, *7*(July), 125. http://doi.org/10.3389/fncir.2013.00125

Cull-Candy, S. G., Brickley, S. G., Misra, C., Feldmeyer, D., Momiyama, A., & Farrant, M. (1998). NMDA receptor diversity in the cerebellum: identification of subunits contributing to functional receptors. *Neuropharmacology*, *37*(10–11), 1369–80. http://doi.org/10.1016/S0028-3908(98)00119-1

Czubayko, U., Sultan, F., Thier, P., & Schwarz, C. (2001). Two types of neurons in the rat cerebellar nuclei as distinguished by membrane potentials and intracellular fillings. *Journal of Neurophysiology*, *85*(5), 2017–29. Retrieved from http://www.ncbi.nlm.nih.gov/pubmed/11353018

D'Angelo, E., & Casali, S. (2012). Seeking a unified framework for cerebellar function and dysfunction: from circuit operations to cognition. *Frontiers in Neural Circuits*, *6*(January), 116. http://doi.org/10.3389/fncir.2012.00116

D'Angelo, E., & De Zeeuw, C. I. (2009). Timing and plasticity in the cerebellum: focus on the granular layer. *Trends in Neurosciences*, *32*(1), 30–40. http://doi.org/10.1016/j.tins.2008.09.007

de Solages, C., Szapiro, G., Brunel, N., Hakim, V., Isope, P., Buisseret, P., … Léna, C. (2008). High-frequency organization and synchrony of activity in the purkinje cell layer of the cerebellum. *Neuron*, *58*(5), 775–88. http://doi.org/10.1016/j.neuron.2008.05.008

De Zeeuw, C. I., & Berrebi, A. S. (1995). Postsynaptic targets of Purkinje cell terminals in the cerebellar and vestibular nuclei of the rat. *The European Journal of Neuroscience*, *7*(11), 2322–33. Retrieved from http://www.ncbi.nlm.nih.gov/pubmed/8563981

De Zeeuw, C. I., Koekkoek, S. K., Wylie, D. R., & Simpson, J. I. (1997). Association between dendritic lamellar bodies and complex spike synchrony in the olivocerebellar system. *Journal of Neurophysiology*, *77*, 1747–58. Retrieved from http://www.ncbi.nlm.nih.gov/pubmed/9114233

De Zeeuw, C. I., Wylie, D. R., DiGiorgi, P. L., & Simpson, J. I. (1994). Projections of individual Purkinje cells of identified zones in the flocculus to the vestibular and cerebellar nuclei in the rabbit. *The Journal of Comparative Neurology*, *349*(3), 428–47. http://doi.org/10.1002/cne.903490308

De Zeeuw, C. I., Wylie, D. R., Stahl, J. S., & Simpson, J. I. (1995). Phase relations of Purkinje cells in the rabbit flocculus during compensatory eye movements. *Journal of Neurophysiology*, *74*(5), 2051–64. Retrieved from http://www.ncbi.nlm.nih.gov/pubmed/8592196

De Zeeuw, C. I., Van Alphen, A. M., Hawkins, R. K., & Ruigrok, T. J. H. (1997). Climbing fibre collaterals contact neurons in the cerebellar nuclei that provide a GABAergic feedback to the inferior olive. *Neuroscience*, *80*(4), 981–986. http://doi.org/10.1016/S0306-4522(97)00249-2

De Zeeuw, C. I., Hoebeek, F. E., & Schonewille, M. (2008). Causes and consequences of oscillations in the cerebellar cortex. *Neuron*, *58*(5), 655–8. http://doi.org/10.1016/j.neuron.2008.05.019

De Zeeuw, C. I., & Ten Brinke, M. M. (2015). Motor learning and the cerebellum. *Cold Spring Harbor Perspectives in Biology*, *7*(9), 1–20. http://doi.org/10.1101/cshperspect.a021683

De Zeeuw, C. I., Hoebeek, F. E., Bosman, L. W. J., Schonewille, M., Witter, L., & Koekkoek, S. K. (2011). Spatiotemporal firing patterns in the cerebellum. *Nature Reviews. Neuroscience*, *12*(6), 327–44. http://doi.org/10.1038/nrn3011

Dean, P., Porrill, J., Ekerot, C.-F., & Jörntell, H. (2010). The cerebellar microcircuit as an adaptive filter: experimental and computational evidence. *Nature Reviews. Neuroscience*, *11*(1), 30–43. http://doi.org/10.1038/nrn2756

Demole, V. (1927). Structure et connection des noyeaux denteles du cervelet. II. *Schweiz Arch Neurol Psychiat*, *20*, 271–294.

Dietrichs, E., & Walberg, F. (1985). The cerebellar nucleo-olivary and olivo-cerebellar nuclear projections in the cat as studied with anterograde and retrograde transport in the same animal after implantation of crystalline WGA-HRP. II. The fastigial nucleus. *Anatomy and Embryology*, *173*(2), 253–61. Retrieved from http://www.ncbi.nlm.nih.gov/pubmed/3002207

Dieudonne, S. (1998). Submillisecond kinetics and low efficacy of parallel fibre-Golgi cell synaptic currents in the rat cerebellum. *The Journal of Physiology*, *510 (Pt 3*, 845–866. http://doi.org/10.1111/j.1469-7793.1998.845bj.x

Ebner, T. J., Hewitt, A. L., & Popa, L. S. (2011). What Features of Limb Movements are Encoded in the Discharge of Cerebellar Neurons? *The Cerebellum*, *10*(4), 683–693. http://doi.org/10.1007/s12311-010-0243-0

Eccles, J. C., Ito, M., & Szentágothai, J. (1967). *The Cerebellum as a Neuronal Machine*. Berlin, Heidelberg: Springer Berlin Heidelberg. http://doi.org/10.1007/978-3-662-13147-3

Ekerot, C. F., & Jörntell, H. (2001). Parallel fibre receptive fields of Purkinje cells and interneurons are climbing fibre-specific. *The European Journal of Neuroscience*, *13*(7), 1303–10. Retrieved from http://www.ncbi.nlm.nih.gov/pubmed/11298790

Ekerot, C.-F., & Jörntell, H. (2003). Parallel fiber receptive fields: a key to understanding cerebellar operation and learning. *Cerebellum (London, England)*, *2*(2), 101–9. Retrieved from http://www.ncbi.nlm.nih.gov/pubmed/12880177

Frederick, A., Bourget-Murray, J., Chapman, C. A., Amir, S., & Courtemanche, R. (2014). Diurnal influences on electrophysiological oscillations and coupling in the dorsal striatum and cerebellar cortex of the anesthetized rat. *Frontiers in Systems Neuroscience*, *8*(September), 145. http://doi.org/10.3389/fnsys.2014.00145

Fredette, B. J., & Mugnaini, E. (1991). The GABAergic cerebello-olivary projection in the rat. *Anatomy and Embryology*, *184*(3), 225–243. http://doi.org/10.1007/BF01673258

Gao, H., Solages, C. de, & Lena, C. (2012). Tetrode recordings in the cerebellar cortex. *Journal of Physiology Paris*, *106*(3–4), 128–136. http://doi.org/10.1016/j.jphysparis.2011.10.005

Gao, Z., Beugen, B. J. van, & Zeeuw, C. I. De. (2012). Distributed synergistic plasticity and cerebellar learning. *Nature Reviews Neuroscience*, *13*(9), 619–635. http://doi.org/10.1038/nrn3312

Gao, Z., Proietti-Onori, M., Lin, Z., Ten Brinke, M. M., Boele, H.-J., Potters, J.-W., … De Zeeuw, C. I. (2016). Excitatory Cerebellar Nucleocortical Circuit Provides Internal Amplification during Associative Conditioning. *Neuron*, *89*(3), 645–57. http://doi.org/10.1016/j.neuron.2016.01.008

Garcia, K. S., Steele, P. M., & Mauk, M. D. (1999). Cerebellar Cortex Lesions Prevent Acquisition of Conditioned Eyelid Responses. *The Journal of Neuroscience*, *19*(24), 10940–10947. Retrieved from http://www.jneurosci.org/content/19/24/10940%5Cnhttp://www.jneurosci.org/content/19/24/10940.full.pdf

Garcia, S., & Fourcaud-Trocmé, N. (2009). OpenElectrophy: An Electrophysiological Data- and Analysis-Sharing Framework. *Frontiers in Neuroinformatics*, *3*, 14. http://doi.org/10.3389/neuro.11.014.2009

Garwicz, M., Apps, R., & Trott, J. R. (1996). Micro-organization of olivocerebellar and corticonuclear connections of the paravermal cerebellum in the cat. *The European Journal of Neuroscience*, *8*(12), 2726–38. Retrieved from http://www.ncbi.nlm.nih.gov/pubmed/8996822

Garwicz, M., Jörntell, H., & Ekerot, C. F. (1998). Cutaneous receptive fields and topography of mossy fibres and climbing fibres projecting to cat cerebellar C3 zone. *Journal of Physiology*, *512*(1), 277–293. http://doi.org/10.1111/j.1469-7793.1998.277bf.x

Gauck, V., & Jaeger, D. (2003). The contribution of NMDA and AMPA conductances to the control of spiking in neurons of the deep cerebellar nuclei. *The Journal of Neuroscience : The Official Journal of the Society for Neuroscience*, *23*(22), 8109–18. http://doi.org/23/22/8109 [pii]

Geurts, F. J., Timmermans, J., Shigemoto, R., & De Schutter, E. (2001). Morphological and neurochemical differentiation of large granular layer interneurons in the adult rat cerebellum. *Neuroscience*, *104*(2), 499–512. http://doi.org/10.1016/S0306-4522(01)00058-6

Goodman, D. C., Hallett, R. E., & Welch, R. B. (1963). Patterns of localization in the cerebellar cortico-nuclear projections of the albino rat. *The Journal of Comparative Neurology*, *121*(1), 51–67. http://doi.org/10.1002/cne.901210106

Groenewegen, H. J., Voogd, J., & Freedman, S. L. (1979). The parasagittal zonation within the olivocerebellar projection. II. Climbing fiber distribution in the intermediate and hemispheric parts of cat cerebellum. *The Journal of Comparative Neurology*, *183*(3), 551–601. http://doi.org/10.1002/cne.901830307

Hamann, M., Rossi, D. J., & Attwell, D. (2002). Tonic and spillover inhibition of granule cells control information flow through cerebellar cortex. *Neuron*, *33*(4), 625–33. http://doi.org/10.1016/S0896-6273(02)00593-7

Hamodeh, S., Baizer, J., Sugihara, I., & Sultan, F. (2014). Systematic analysis of neuronal wiring of the rodent deep cerebellar nuclei reveals differences reflecting adaptations at the neuronal circuit and internuclear levels. *The Journal of Comparative Neurology*, *522*(11), 2481–97. http://doi.org/10.1002/cne.23545

Hara, K., & Harris, R. A. (2002). The anesthetic mechanism of urethane: the effects on neurotransmitter-gated ion channels. *Anesthesia and Analgesia*, *94*(2), 313–8, table of contents. http://doi.org/10.1213/00000539-200202000-00015

Häusser, M., Raman, I. M., Otis, T., Smith, S. L., Nelson, A., du Lac, S., … Yarom, Y. (2004). The beat goes on: spontaneous firing in mammalian neuronal microcircuits. *The Journal of Neuroscience : The Official Journal of the Society for Neuroscience*, *24*(42), 9215–9. http://doi.org/10.1523/JNEUROSCI.3375-04.2004

Hawkes, R., & Leclerc, N. (1989). Purkinje cell axon collateral distributions reflect the chemical compartmentation of the rat cerebellar cortex. *Brain Research*, *476*(2), 279–90. Retrieved from http://www.ncbi.nlm.nih.gov/pubmed/2702469

Heck, D. H., Thach, W. T., & Keating, J. G. (2007). On-beam synchrony in the cerebellum as the mechanism for the timing and coordination of movement. *Proceedings of the National Academy of Sciences of the United States of America*, *104*(18), 7658–7663. http://doi.org/10.1073/pnas.0609966104

Henze, D. a, Borhegyi, Z., Csicsvari, J., Mamiya, a, Harris, K. D., & Buzsáki, G. (2000). Intracellular features predicted by extracellular recordings in the hippocampus in vivo. *Journal of Neurophysiology*, *84*(1), 390–400. http://doi.org/84:390-400

Hirono, M., Saitow, F., Kudo, M., Suzuki, H., Yanagawa, Y., Yamada, M., … Obata, K. (2012). Cerebellar globular cells receive monoaminergic excitation and monosynaptic inhibition from Purkinje cells. *PloS One*, *7*(1), e29663. http://doi.org/10.1371/journal.pone.0029663

Hirota, K., & Lambert, D. G. (1996). Ketamine: its mechanism(s) of action and unusual clinical uses. *British Journal of Anaesthesia*, *77*(4), 441–4. http://doi.org/10.1093/bja/77.4.441

Holdefer, R. N., Miller, L. E., Chen, L. L., & Houk, J. C. (2000). Functional connectivity between cerebellum and primary motor cortex in the awake monkey. *Journal of Neurophysiology*, *84*(1),

585–90. Retrieved from http://www.ncbi.nlm.nih.gov/entrez/query.fcgi?cmd=Retrieve&db=pubmed&dopt=Abstract&list_uids=10899231

Holdefer, R. N., Houk, J. C., & Miller, L. E. (2005). Movement-related discharge in the cerebellar nuclei persists after local injections of GABA(A) antagonists. *Journal of Neurophysiology*, *93*(1), 35–43. http://doi.org/10.1152/jn.00603.2004

Houck, B. D., & Person, A. L. (2015). Cerebellar premotor output neurons collateralize to innervate the cerebellar cortex. *Journal of Comparative Neurology*, *523*(15), 2254–2271. http://doi.org/10.1002/cne.23787

Husson, F., Josse, J., & Pagès, J. (2010). Principal component methods - hierarchical clustering - partitional clustering: why would we need to choose for visualizing data? *Technical Report of the Applied Mathematics Department (Agrocampus)*, (September), 1–17. Retrieved from http://factominer.free.fr/docs/HCPC_husson_josse.pdf

Husson, Z., Rousseau, C. V., Broll, I., Zeilhofer, H. U., & Dieudonne, S. (2014). Differential GABAergic and Glycinergic Inputs of Inhibitory Interneurons and Purkinje Cells to Principal Cells of the Cerebellar Nuclei. *Journal of Neuroscience*, *34*(28), 9418–9431. http://doi.org/10.1523/JNEUROSCI.0401-14.2014

Husson, Z. (2014, September). *Glycinergic neurons and inhibitory transmission in the cerebellar nuclei*. Universit{é} Pierre et Marie Curie - Paris VI. Retrieved from https://tel.archives-ouvertes.fr/tel-01205721

Isope, P., & Barbour, B. (2002). Properties of unitary granule cell-->Purkinje cell synapses in adult rat cerebellar slices. *The Journal of Neuroscience : The Official Journal of the Society for Neuroscience*, *22*(22), 9668–78. http://doi.org/22/22/9668 [pii]

Ito, M. (2008). Control of mental activities by internal models in the cerebellum. *Nature Reviews Neuroscience*, *9*(Box 1), 304–313. http://doi.org/10.1038/nrn2332

Ito, M. (1984). *The Cerebellum and Neural Control*. Raven Press. Retrieved from https://books.google.fr/books?id=Wt1qAAAAMAAJ

Ito, M., & Kano, M. (1982). Long-lasting depression of parallel fiber-Purkinje cell transmission induced by conjunctive stimulation of parallel fibers and climbing fibers in the cerebellar cortex. *Neuroscience Letters*, *33*(3), 253–8. http://doi.org/10.1016/0304-3940(82)90380-9

Ivry, R. B., Keele, S. W., & Diener, H. C. (1988). Dissociation of the lateral and medial cerebellum in movement timing and movement execution. *Experimental Brain Research*, *73*(1), 167–180. http://doi.org/10.1007/BF00279670

Jaeger, D. (2013). Cerebellar Nuclei and Cerebellar Learning. In M. Manto, J. D. Schmahmann, F. Rossi, D. L. Gruol, & N. Koibuchi (Eds.), *Handbook of the Cerebellum and Cerebellar Disorders* (pp. 1111–1130). Dordrecht: Springer Netherlands. http://doi.org/10.1007/978-94-007-1333-8_47

Jaeger, D. (2011). Mini-review: synaptic integration in the cerebellar nuclei--perspectives from dynamic clamp and computer simulation studies. *Cerebellum (London, England)*, *10*(4), 659–66. http://doi.org/10.1007/s12311-011-0248-3

Jakab, R. L., & Hámori, J. (1988). Quantitative morphology and synaptology of cerebellar glomeruli in the rat. *Anatomy and Embryology*, *179*(1), 81–8. Retrieved from http://www.ncbi.nlm.nih.gov/pubmed/3213958

Jansen, J., & Brodal, A. (1940). Experimental studies on the intrinsic fibers of the cerebellum. II. The cortico-nuclear projection. *The Journal of Comparative Neurology*, *73*(2), 267–321. http://doi.org/10.1002/cne.900730204

Jörntell, H. (2016). Cerebellar physiology - links between microcircuitry properties and sensorimotor functions. *The Journal of Physiology*. http://doi.org/10.1113/JP272769

Jörntell, H., & Hansel, C. (2006). Synaptic Memories Upside Down: Bidirectional Plasticity at Cerebellar Parallel Fiber-Purkinje Cell Synapses. *Neuron*, *52*(2), 227–238. http://doi.org/10.1016/j.neuron.2006.09.032

Jueptner, M., & Weiller, C. (1998). A review of differences between basal ganglia and cerebellar control of movements as revealed by functional imaging studies. *Brain : A Journal of Neurology*, *121 (Pt 8*, 1437–49. Retrieved from http://www.ncbi.nlm.nih.gov/pubmed/9712006

Kalil, K. (1979). Projections of the cerebellar and dorsal column nuclei upon the inferior olive in the rhesus monkey: An autoradiographic study. *The Journal of Comparative Neurology*, *188*(1), 43–62. http://doi.org/10.1002/cne.901880105

Kanichay, R. T., & Silver, R. A. (2008). Synaptic and cellular properties of the feedforward inhibitory circuit within the input layer of the cerebellar cortex. *The Journal of Neuroscience : The Official Journal of the Society for Neuroscience*, *28*(36), 8955–67. http://doi.org/10.1523/JNEUROSCI.5469-07.2008

Katoh, A., Shin, S. L., Kimpo, R. R., Rinaldi, J. M., & Raymond, J. L. (2015). Purkinje cell responses during visually and vestibularly driven smooth eye movements in mice. *Brain and Behavior*, *5*(3), e00310. http://doi.org/10.1002/brb3.310

Koekkoek, S. K. E., Hulscher, H. C., Dortland, B. R., Hensbroek, R. A., Elgersma, Y., Ruigrok, T. J. H., & De Zeeuw, C. I. (2003). Cerebellar LTD and learning-dependent timing of conditioned eyelid responses. *Science (New York, N.Y.)*, *301*(5640), 1736–9. http://doi.org/10.1126/science.1088383

Kolkman, K. E., McElvain, L. E., & du Lac, S. (2011). Diverse precerebellar neurons share similar intrinsic excitability. *The Journal of Neuroscience : The Official Journal of the Society for Neuroscience*, *31*(46), 16665–74. http://doi.org/10.1523/JNEUROSCI.3314-11.2011

Korn, H., & Axelrad, H. (1980). Electrical inhibition of Purkinje cells in the cerebellum of the rat. *Proceedings of the National Academy of Sciences of the United States of America*, *77*(10), 6244–7. http://doi.org/10.1073/pnas.77.10.6244

Lainé, J., & Axelrad, H. (2002). Extending the cerebellar Lugaro cell class. *Neuroscience*, *115*(2), 363–74. http://doi.org/10.1016/S0306-4522(02)00421-9

Lang, E. J., Sugihara, I., Welsh, J. P., & Llinás, R. (1999). Patterns of spontaneous purkinje cell complex spike activity in the awake rat. *The Journal of Neuroscience : The Official Journal of the Society for Neuroscience*, *19*(7), 2728–39. Retrieved from http://www.ncbi.nlm.nih.gov/pubmed/10087085

Lang, E. J., Apps, R., Bengtsson, F., Cerminara, N. L., De Zeeuw, C. I., Ebner, T. J., … Xiao, J. (2016). The Roles of the Olivocerebellar Pathway in Motor Learning and Motor Control. A Consensus Paper. *The Cerebellum*, 1–23. http://doi.org/10.1007/s12311-016-0787-8

Lang, E. J., & Blenkinsop, T. A. (2011). Control of Cerebellar Nuclear Cells: A Direct Role for Complex Spikes? *The Cerebellum*, *10*(4), 694–701. http://doi.org/10.1007/s12311-011-0261-6

Lev-Ram, V., Wong, S. T., Storm, D. R., & Tsien, R. Y. (2002). A new form of cerebellar long-term potentiation is postsynaptic and depends on nitric oxide but not cAMP. *Proceedings of the National Academy of Sciences*, *99*(12), 8389–8393. http://doi.org/10.1073/pnas.122206399

Llinás, R., & Sugimori, M. (1980). Electrophysiological properties of in vitro Purkinje cell dendrites in mammalian cerebellar slices. *The Journal of Physiology*, *305*, 197–213. Retrieved from http://www.ncbi.nlm.nih.gov/pubmed/1282967

LLINÁS, R. R., WALTON, K. D., & LANG, E. J. (2004). Cerebellum. In G. M. Shepherd (Ed.), *The Synaptic Organization of the Brain* (pp. 271–310). Oxford University Press. http://doi.org/10.1093/acprof:oso/9780195159561.003.0007

Lu, H., Yang, B., & Jaeger, D. (2016). Cerebellar Nuclei Neurons Show Only Small Excitatory Responses to Optogenetic Olivary Stimulation in Transgenic Mice: In Vivo and In Vitro Studies. *Frontiers in Neural Circuits*, *10*(March), 21. http://doi.org/10.3389/fncir.2016.00021

Malomo, A. O., Idowu, O. E., & Osuagwu, F. C. (2006). Lessons from History: Human Anatomy, from the Origin to the Renaissance. *International Journal of Morphology*, *24*(1), 99–104. http://doi.org/10.4067/S0717-95022006000100018

Manni, E., & Petrosini, L. (2004). A century of cerebellar somatotopy: a debated representation. *Nature Reviews. Neuroscience*, *5*(3), 241–9. http://doi.org/10.1038/nrn1347

Manto, M., Schmahmann, J. D., Rossi, F., Gruol, D. L., & Koibuchi, N. (Eds.). (2013). *Handbook of the Cerebellum and Cerebellar Disorders*. Dordrecht: Springer Netherlands. http://doi.org/10.1007/978-94-007-1333-8

Marr, D. (1969). A theory of cerebellar cortex. *The Journal of Physiology*, *202*(2), 437–470. http://doi.org/10.2307/1776957

Mathy, A., & Clark, B. A. (2013). Dynamics of the Inferior Olive Oscillator and Cerebellar Function. In *Handbook of the Cerebellum and Cerebellar Disorders* (pp. 1059–1078). Dordrecht: Springer Netherlands. http://doi.org/10.1007/978-94-007-1333-8_44

Matsushita, M., & Iwahori, N. (1971). Structural organization of the fastigial nucleus. II. Afferent fiber systems. *Brain Research*, *25*(3), 611–24. http://doi.org/10.1016/0006-8993(71)90464-1

Matsushita, M., & Iwahori, N. (1971). Structural organization of the interpositus and the dentate nuclei. *Brain Research*, *35*(1), 17–36. http://doi.org/10.1016/0006-8993(71)90592-0

Matsushita, M., & Iwahori, N. (1971). Structural organization of the fastigial nucleus. I. Dendrites and axonal pathways. *Brain Research*, *25*(3), 597–610. http://doi.org/10.1016/0006-8993(71)90463-X

Mauk, M. D. (1997). Roles of Cerebellar Cortex and Nuclei in Motor Learning: Contradictions or Clues? *Neuron*, *18*(3), 343–346. http://doi.org/http://dx.doi.org/10.1016/S0896-6273(00)81235-0

McCormick, D. A., & Thompson, R. F. (1984). Neuronal responses of the rabbit cerebellum during acquisition and performance of a classically conditioned nictitating membrane-eyelid response. *The Journal of Neuroscience : The Official Journal of the Society for Neuroscience*, *4*(11), 2811–22. Retrieved from http://www.jneurosci.org/content/4/11/2811%5Cnhttp://libsta28.lib.cam.ac.uk:2378/content/4/11/2811%5Cnhttp://www.jneurosci.org/content/4/11/2811.full.pdf%5Cnhttp://www.ncbi.nlm.nih.gov/pubmed/6502205

McDevitt, C. J., Ebner, T. J., & Bloedel, J. R. (1987). Relationships between simultaneously recorded Purkinje cells and nuclear neurons. *Brain Research*, *425*(1), 1–13. http://doi.org/10.1016/0006-8993(87)90477-X

Medina, J. F., & Khodakhah, K. (2012). Neuroscience: Spikes timed through inhibition. *Nature*, *481*, 446–447. http://doi.org/10.1038/481446a

Medina, J. F., & Lisberger, S. G. (2007). Variation, signal, and noise in cerebellar sensory-motor processing for smooth-pursuit eye movements. *The Journal of Neuroscience : The Official Journal of the Society for Neuroscience*, *27*(25), 6832–42. http://doi.org/10.1523/JNEUROSCI.1323-07.2007

Midtgaard, J. (1992). Membrane properties and synaptic responses of Golgi cells and stellate cells in the turtle cerebellum in vitro. *The Journal of Physiology*, *457*(1), 329–354. http://doi.org/10.1113/jphysiol.1992.sp019381

Molineux, M. L., McRory, J. E., McKay, B. E., Hamid, J., Mehaffey, W. H., Rehak, R., … Turner, R. W. (2006). Specific T-type calcium channel isoforms are associated with distinct burst phenotypes in deep cerebellar nuclear neurons. *Proceedings of the National Academy of Sciences of the United States of America*, *103*(14), 5555–5560. http://doi.org/10.1073/pnas.0601261103

Morishita, W., & Sastry, B. R. (1996). Postsynaptic mechanisms underlying long-term depression of GABAergic transmission in neurons of the deep cerebellar nuclei. *Journal of Neurophysiology*, *76*(1), 59–68. Retrieved from http://www.ncbi.nlm.nih.gov/pubmed/8836209

Mugnaini, E., Sekerková, G., & Martina, M. (2011). The unipolar brush cell: a remarkable neuron finally receiving deserved attention. *Brain Research Reviews*, *66*(1–2), 220–45. http://doi.org/10.1016/j.brainresrev.2010.10.001

Najac, M., & Raman, I. M. (2015). Integration of Purkinje Cell Inhibition by Cerebellar Nucleo-Olivary Neurons. *Journal of Neuroscience*, *35*(2), 544–549. http://doi.org/10.1523/JNEUROSCI.3583-14.2015

Napper, R. M., & Harvey, R. J. (1988). Number of parallel fiber synapses on an individual Purkinje cell in the cerebellum of the rat. *The Journal of Comparative Neurology*, *274*(2), 168–77. http://doi.org/10.1002/cne.902740204

O'Brien, J., & Unwin, N. (2006). Organization of spines on the dendrites of Purkinje cells. *Proceedings of the National Academy of Sciences of the United States of America*, *103*(5), 1575–80. http://doi.org/10.1073/pnas.0507884103

Ohyama, T., Nores, W. L., & Mauk, M. D. (2003). Stimulus generalization of conditioned eyelid responses produced without cerebellar cortex: implications for plasticity in the cerebellar nuclei. *Learning & Memory (Cold Spring Harbor, N.Y.)*, *10*(5), 346–54. http://doi.org/10.1101/lm.67103

Ouardouz, M., & Sastry, B. R. (2000). Mechanisms underlying LTP of inhibitory synaptic transmission in the deep cerebellar nuclei. *Journal of Neurophysiology*, *84*(3), 1414–1421.

Palkovits, M., Mezey, E., Hámori, J., & Szentágothai, J. (1977). Quantitative histological analysis of the cerebellar nuclei in the cat. I. Numerical data on cells and on synapses. *Experimental Brain Research*, *28*(1–2), 189–209. Retrieved from http://www.ncbi.nlm.nih.gov/pubmed/881003

Pantò, M. R., Zappalà, A., Parenti, R., Serapide, M. F., & Cicirata, F. (2001). Corticonuclear projections of the cerebellum preserve both anteroposterior and mediolateral pairing patterns. *European Journal of Neuroscience*, *13*(4), 694–708. http://doi.org/10.1046/j.0953-816x.2000.01442.x

Parenti, R., Zappalà, A., Serapide, M. F., Pantò, M. R., & Cicirata, F. (2002). Projections of the basilar pontine nuclei and nucleus reticularis tegmenti pontis to the cerebellar nuclei of the rat. *Journal of Comparative Neurology*, *452*(2), 115–127. http://doi.org/10.1002/cne.10316

Pedroarena, C. M., & Schwarz, C. (2003). Efficacy and short-term plasticity at GABAergic synapses between Purkinje and cerebellar nuclei neurons. *Journal of Neurophysiology*, *89*, 704–715. http://doi.org/10.1152/jn.00558.2002

Peptides, E. O., & Jacquet, Y. F. (1979). Olov Oscarsson, (June), 143–145. http://doi.org/https://dx.doi.org/10.1016%2F0166-2236%2879%2990057-2

Perrett, S. P., Ruiz, B. P., & Mauk, M. D. (1993). Cerebellar cortex lesions disrupt learning-dependent timing of conditioned eyelid responses. *The Journal of Neuroscience : The Official Journal of the Society for Neuroscience*, *13*(4), 1708–1718.

Person, A. L., & Raman, I. M. (2011). Purkinje neuron synchrony elicits time-locked spiking in the cerebellar nuclei. *Nature*, *481*(7382), 502–505. http://doi.org/10.1038/nature10732

Person, A. L., & Raman, I. M. (2010). Deactivation of l-type ca current by inhibition controls ltp at excitatory synapses in the cerebellar nuclei. *Neuron*, *66*(4), 550–559. http://doi.org/10.1016/j.neuron.2010.04.024

Person, A. L., & Raman, I. M. (2012). Synchrony and neural coding in cerebellar circuits. *Frontiers in Neural Circuits*, *6*(December), 97. http://doi.org/10.3389/fncir.2012.00097

Pijpers, A., Apps, R., Pardoe, J., Voogd, J., & Ruigrok, T. J. H. (2006). Precise Spatial Relationships between Mossy Fibers and Climbing Fibers in Rat Cerebellar Cortical Zones. *Journal of Neuroscience*, *26*(46), 12067–12080. http://doi.org/10.1523/JNEUROSCI.2905-06.2006

Pijpers, A., Voogd, J., & Ruigrok, T. J. H. (2005). Topography of olivo-cortico-nuclear modules in the intermediate cerebellum of the rat. *The Journal of Comparative Neurology*, *492*(2), 193–213. http://doi.org/10.1002/cne.20707

Proville, R. D., Spolidoro, M., Guyon, N., Dugué, G. P., Selimi, F., Isope, P., … Léna, C. (2014). Cerebellum involvement in cortical sensorimotor circuits for the control of voluntary movements. *Nature Neuroscience*, *17*(9), 1233–1239. http://doi.org/10.1038/nn.3773

Pugh, J. R., & Raman, I. M. (2006). Potentiation of Mossy Fiber EPSCs in the Cerebellar Nuclei by NMDA Receptor Activation followed by Postinhibitory Rebound Current. *Neuron*, *51*(1), 113–123. http://doi.org/10.1016/j.neuron.2006.05.021

Pugh, J. R., & Raman, I. M. (2008). Mechanisms of Potentiation of Mossy Fiber EPSCs in the Cerebellar Nuclei by Coincident Synaptic Excitation and Inhibition. *Journal of Neuroscience*, *28*(42), 10549–10560. http://doi.org/10.1523/JNEUROSCI.2061-08.2008

R Core Development Team. (2015). R: a language and environment for statistical computing, 3.2.1. *Document Freely Available on the Internet at: Http://www. R-Project. Org*. Vienna, Austria. http://doi.org/10.1017/CBO9781107415324.004

Racine, R. J., Wilson, D. A., Gingell, R., & Sunderland, D. (1986). Long-term potentiation in the interpositus and vestibular nuclei in the rat. *Experimental Brain Research*, *63*(1), 158–62. Retrieved from http://www.ncbi.nlm.nih.gov/entrez/query.fcgi?cmd=Retrieve&db=PubMed&dopt=Citation&list_uids=3015653

Raman, I. M., Gustafson, A. E., & Padgett, D. (2000). Ionic currents and spontaneous firing in neurons isolated from the cerebellar nuclei. *The Journal of Neuroscience : The Official Journal of the Society for Neuroscience*, *20*(24), 9004–16. http://doi.org/20/24/9004 [pii]

Ros, H., Sachdev, R. N. S., Yu, Y., Sestan, N., & McCormick, D. A. (2009). Neocortical networks entrain neuronal circuits in cerebellar cortex. *The Journal of Neuroscience : The Official Journal of the Society for Neuroscience*, *29*(33), 10309–20. http://doi.org/10.1523/JNEUROSCI.2327-09.2009

Rossi, D. J., & Hamann, M. (1998). Spillover-mediated transmission at inhibitory synapses promoted by high affinity alpha6 subunit GABA(A) receptors and glomerular geometry. *Neuron*, *20*(4), 783–95. http://doi.org/10.1016/S0896-6273(00)81016-8

Roux, S. G., Cenier, T., Garcia, S., Litaudon, P., & Buonviso, N. (2007). A wavelet-based method for local phase extraction from a multi-frequency oscillatory signal. *Journal of Neuroscience Methods*, *160*(1), 135–43. http://doi.org/10.1016/j.jneumeth.2006.09.001

Rowland, N. C., & Jaeger, D. (2005). Coding of tactile response properties in the rat deep cerebellar nuclei. *Journal of Neurophysiology*, *94*(2), 1236–51. http://doi.org/10.1152/jn.00285.2005

Rowland, N. C., & Jaeger, D. (2008). Responses to tactile stimulation in deep cerebellar nucleus neurons result from recurrent activation in multiple pathways. *Journal of Neurophysiology*, *99*(2), 704–17. http://doi.org/10.1152/jn.01100.2007

Ruigrok, T. J. (1997). Cerebellar nuclei: the olivary connection. *Progress in Brain Research*, *114*, 167–92. Retrieved from http://www.ncbi.nlm.nih.gov/pubmed/9193144

Ruigrok, T. J. H. (2011). Ins and outs of cerebellar modules. *Cerebellum*, *10*(3), 464–474. http://doi.org/10.1007/s12311-010-0164-y

Ruigrok, T. J. H., & Teune, T. M. (2014). Collateralization of cerebellar output to functionally distinct brainstem areas. A retrograde, non-fluorescent tracing study in the rat. *Frontiers in Systems Neuroscience*, *8*(February), 23. http://doi.org/10.3389/fnsys.2014.00023

Ruigrok, T. J. H. H., Sillitoe, R. V., & Voogd, J. (2015). Cerebellum and Cerebellar Connections. In G. Paxinos (Ed.), *The Rat Nervous System* (Fourth Edi, pp. 133–205). San Diego: Elsevier. http://doi.org/10.1016/B978-0-12-374245-2.00009-7

Sakamoto, T., & Endo, S. (2010). Amygdala, deep cerebellar nuclei and red nucleus contribute to delay eyeblink conditioning in C57BL/6 mice. *European Journal of Neuroscience*, *32*(9), 1537–1551. http://doi.org/10.1111/j.1460-9568.2010.07406.x

Sakamoto, T., & Endo, S. (2013). Deep cerebellar nuclei play an important role in two-tone discrimination on delay eyeblink conditioning in C57BL/6 mice. *PloS One*, *8*(3), e59880. http://doi.org/10.1371/journal.pone.0059880

Shambes, G. M., Beermann, D. H., & Welker, W. (1978). Multiple tactile areas in cerebellar cortex: another patchy cutaneous projection to granule cell columns in rats. *Brain Research*, *157*(1), 123–128. http://doi.org/10.1016/0006-8993(78)91000-4

Shin, S.-L., Hoebeek, F. E., Schonewille, M., De Zeeuw, C. I., Aertsen, A., & De Schutter, E. (2007). Regular patterns in cerebellar Purkinje cell simple spike trains. *PloS One*, *2*(5), e485. http://doi.org/10.1371/journal.pone.0000485

Shinoda, Y., Sugihara, I., Wu, H. S., & Sugiuchi, Y. (2000). The entire trajectory of single climbing and mossy fibers in the cerebellar nuclei and cortex. *Progress in Brain Research*, *124*, 173–86. http://doi.org/10.1016/S0079-6123(00)24015-6

Soteropoulos, D. S., & Baker, S. N. (2006). Cortico-cerebellar coherence during a precision grip task in the monkey. *Journal of Neurophysiology*, *95*(2), 1194–1206. http://doi.org/10.1152/jn.00935.2005

Sugihara, I., Wu, H., & Shinoda, Y. (1999). Morphology of single olivocerebellar axons labeled with biotinylated dextran amine in the rat. *The Journal of Comparative Neurology*, *414*(2), 131–48. Retrieved from http://www.ncbi.nlm.nih.gov/pubmed/10516588

Sugihara, I., Fujita, H., Na, J., Quy, P. N., Li, B.-Y., & Ikeda, D. (2009). Projection of reconstructed single purkinje cell axons in relation to the cortical and nuclear aldolase C compartments of the rat cerebellum. *The Journal of Comparative Neurology*, *512*(2), 282–304. http://doi.org/10.1002/cne.21889

Sugihara, I., & Shinoda, Y. (2004). Molecular, topographic, and functional organization of the cerebellar cortex: a study with combined aldolase C and olivocerebellar labeling. *The Journal of Neuroscience : The Official Journal of the Society for Neuroscience*, *24*(40), 8771–85. http://doi.org/10.1523/JNEUROSCI.1961-04.2004

Sugihara, I., & Shinoda, Y. (2007). Molecular, topographic, and functional organization of the cerebellar nuclei: analysis by three-dimensional mapping of the olivonuclear projection and aldolase C labeling. *The Journal of Neuroscience : The Official Journal of the Society for Neuroscience*, *27*(36), 9696–9710. http://doi.org/10.1523/JNEUROSCI.1579-07.2007

Sultan, F., Augath, M., Hamodeh, S., Murayama, Y., Oeltermann, A., Rauch, A., & Thier, P. (2012). Unravelling cerebellar pathways with high temporal precision targeting motor and extensive sensory and parietal networks. *Nature Communications*, *3*(May), 924. http://doi.org/10.1038/ncomms1912

Sultan, F., König, T., Möck, M., & Thier, P. (2002). Quantitative organization of neurotransmitters in the deep cerebellar nuclei of the Lurcher mutant. *The Journal of Comparative Neurology*, *452*(4), 311–23. http://doi.org/10.1002/cne.10365

Szapiro, G., & Barbour, B. (2007). Multiple climbing fibers signal to molecular layer interneurons exclusively via glutamate spillover. *Nature Neuroscience*, *10*(6), 735–42. http://doi.org/10.1038/nn1907

Szoboszlay, M., Lőrincz, A., Lanore, F., Vervaeke, K., Silver, R. A., & Nusser, Z. (2016). Functional Properties of Dendritic Gap Junctions in Cerebellar Golgi Cells. *Neuron*, *90*(5), 1043–1056. http://doi.org/10.1016/j.neuron.2016.03.029

Tadayonnejad, R., Anderson, D., Molineux, M. L., Mehaffey, W. H., Jayasuriya, K., & Turner, R. W. (2010). Rebound discharge in deep cerebellar nuclear neurons in vitro. *Cerebellum (London, England)*, *9*(3), 352–74. http://doi.org/10.1007/s12311-010-0168-7

Tang, T., Suh, C. Y., Blenkinsop, T. A., & Lang, E. J. (2016). Synchrony is Key: Complex Spike Inhibition of the Deep Cerebellar Nuclei. *Cerebellum*, *15*(1), 10–13. http://doi.org/10.1007/s12311-015-0743-z

Telgkamp, P., & Raman, I. M. (2002). Depression of inhibitory synaptic transmission between Purkinje cells and neurons of the cerebellar nuclei. *The Journal of Neuroscience : The Official Journal of the Society for Neuroscience*, *22*(19), 8447–8457.

Teune, T. M., van der Burg, J., de Zeeuw, C. I., Voogd, J., & Ruigrok, T. J. (1998). Single Purkinje cell can innervate multiple classes of projection neurons in the cerebellar nuclei of the rat: a light microscopic and ultrastructural triple-tracer study in the rat. *The Journal of Comparative Neurology*, *392*(2), 164–78. Retrieved from http://www.ncbi.nlm.nih.gov/pubmed/9512267

Teune, T. M., der Burg, J., & Ruigrok, T. J. H. (1995). Cerebellar projections to the red nucleus and inferior olive originate from separate populations of neurons in the rat: a non-fluorescent double labeling study. *Brain Research*, *673*(2), 313–319. http://doi.org/10.1016/0006-8993(94)01431-G

Thach, W. T. (1968). Discharge of Purkinje and cerebellar nuclear neurons during rapidly alternating arm movements in the monkey. *Journal of Neurophysiology*, *31*(5), 785–97. Retrieved from http://www.ncbi.nlm.nih.gov/pubmed/4974877

Thach, W. T., Goodkin, H. P., & Keating, J. G. (1992). The cerebellum and the adaptive coordination of movement. *Annual Review of Neuroscience*, *15*, 403–42. http://doi.org/10.1146/annurev.ne.15.030192.002155

Thier, P., Dicke, P. W., Haas, R., & Barash, S. (2000). Encoding of movement time by populations of cerebellar Purkinje cells. *Nature*, *405*(6782), 72–6. http://doi.org/10.1038/35011062

Tolbert, D. L., Bantli, H., & Bloedel, J. R. (1976). Anatomical and physiological evidence for a cerebellar nucleo-cortical projection in the cat. *Neuroscience*, *1*(3), 205–17. Retrieved from http://www.ncbi.nlm.nih.gov/pubmed/11370232

Trott, J. R., Apps, R., & Armstrong, D. M. (1998). Zonal organization of cortico-nuclear and nucleo-cortical projections of the paramedian lobule of the cat cerebellum. 2. the C2 zone. *Experimental Brain Research*, *118*(3), 316–30. Retrieved from http://www.ncbi.nlm.nih.gov/pubmed/9497139

Trott, J. R., Apps, R., & Armstrong, D. M. (1998). Zonal organization of cortico-nuclear and nucleo-cortical projections of the paramedian lobule of the cat cerebellum. 1. the C1 zone. *Experimental Brain Research*, *118*(3), 298–315. Retrieved from http://www.ncbi.nlm.nih.gov/pubmed/9497138

Tyrrell, T., & Willshaw, D. (1992). Cerebellar cortex: its simulation and the relevance of Marr's theory. *Philosophical Transactions of the Royal Society of London. Series B, Biological Sciences*, *336*(1277), 239–57. http://doi.org/10.1098/rstb.1992.0059

Uusisaari, M., & Knöpfel, T. (2008). GABAergic synaptic communication in the GABAergic and non-GABAergic cells in the deep cerebellar nuclei. *Neuroscience*, *156*(3), 537–49. http://doi.org/10.1016/j.neuroscience.2008.07.060

Uusisaari, M. Y., & Knöpfel, T. (2012). Diversity of neuronal elements and circuitry in the cerebellar nuclei. *Cerebellum*, *11*(2), 420–421. http://doi.org/10.1007/s12311-011-0350-6

Uusisaari, M. Y., & Knöpfel, T. (2013). Neurons of the Deep Cerebellar Nuclei. In M. Manto, J. D. Schmahmann, F. Rossi, D. L. Gruol, & N. Koibuchi (Eds.), *Handbook of the Cerebellum and Cerebellar Disorders* (pp. 1101–1110). Dordrecht: Springer Netherlands. http://doi.org/10.1007/978-94-007-1333-8_46

Uusisaari, M., & De Schutter, E. (2011). The mysterious microcircuitry of the cerebellar nuclei. *The Journal of Physiology*, *589*(Pt 14), 3441–57. http://doi.org/10.1113/jphysiol.2010.201582

Uusisaari, M., & Knöpfel, T. (2010). GlyT2+ neurons in the lateral cerebellar nucleus. *Cerebellum (London, England)*, *9*(1), 42–55. http://doi.org/10.1007/s12311-009-0137-1

Uusisaari, M., & Knöpfel, T. (2011). Functional classification of neurons in the mouse lateral cerebellar nuclei. *Cerebellum (London, England)*, *10*(4), 637–46. http://doi.org/10.1007/s12311-010-0240-3

Uusisaari, M., Obata, K., & Knöpfel, T. (2007). Morphological and electrophysiological properties of GABAergic and non-GABAergic cells in the deep cerebellar nuclei. *Journal of Neurophysiology*, *97*(1), 901–911. http://doi.org/10.1152/jn.00974.2006

Valera, A. M., Binda, F., Pawlowski, S. A., Dupont, J.-L., Casella, J.-F., Rothstein, J. D., … Isope, P. (2016). Stereotyped spatial patterns of functional synaptic connectivity in the cerebellar cortex. *eLife*, *5*, 1–22. http://doi.org/10.7554/eLife.09862

van der Want, J. J. L., & Voogd, J. (1987). Ultrastructural identification and localization of climbing fiber terminals in the fastigial nucleus of the cat. *The Journal of Comparative Neurology*, *258*(1), 81–90. http://doi.org/10.1002/cne.902580106

van Kan, P. L., Gibson, A. R., & Houk, J. C. (1993). Movement-related inputs to intermediate cerebellum of the monkey. *Journal of Neurophysiology*, *69*(1), 74–94. Retrieved from http://www.ncbi.nlm.nih.gov/pubmed/8433135

Vervaeke, K., Lorincz, A., Nusser, Z., & Silver, R. A. (2012). Gap junctions compensate for sublinear dendritic integration in an inhibitory network. *Science (New York, N.Y.)*, *335*(6076), 1624–8. http://doi.org/10.1126/science.1215101

Villette, V., Poindessous-Jazat, F., Simon, A., Léna, C., Roullot, E., Bellessort, B., … Stéphan, A. (2010). Decreased rhythmic GABAergic septal activity and memory-associated theta oscillations after hippocampal amyloid-beta pathology in the rat. *The Journal of Neuroscience : The Official Journal of the Society for Neuroscience*, *30*(33), 10991–1003. http://doi.org/10.1523/JNEUROSCI.6284-09.2010

von Holst, E. (1954). Relations between the central Nervous System and the peripheral organs. *The British Journal of Animal Behaviour*, *2*(3), 89–94. http://doi.org/10.1016/S0950-5601(54)80044-X

Voogd, J., & Glickstein, M. (1998). The anatomy of the cerebellum. *Trends in Neurosciences*, *21*(9), 370–5. Retrieved from http://www.ncbi.nlm.nih.gov/pubmed/9735944

Voogd, J., Pardoe, J., Ruigrok, T. J. H., & Apps, R. (2003). The distribution of climbing and mossy fiber collateral branches from the copula pyramidis and the paramedian lobule: congruence of climbing fiber cortical zones and the pattern of zebrin banding within the rat cerebellum. *The Journal of Neuroscience*, *23*(11), 4645–56. http://doi.org/23/11/4645 [pii]

Voogd, J., & Ruigrok, T. J. H. (2004). The organization of the corticonuclear and olivocerebellar climbing fiber projections to the rat cerebellar vermis: the congruence of projection zones and the zebrin pattern. *Journal of Neurocytology*, *33*(1), 5–21. http://doi.org/10.1023/B:NEUR.0000029645.72074.2b

Voogd, J., Shinoda, Y., Ruigrok, T. J. H., & Sugihara, I. (2013). Cerebellar Nuclei and the Inferior Olivary Nuclei: Organization and Connections. In M. Manto, J. D. Schmahmann, F. Rossi, D. L. Gruol, & N. Koibuchi (Eds.), *Handbook of the Cerebellum and Cerebellar Disorders* (pp. 377–436). Dordrecht: Springer Netherlands. http://doi.org/10.1007/978-94-007-1333-8_19

Wada, N., Kishimoto, Y., Watanabe, D., Kano, M., Hirano, T., & Funabiki, K. (2007). Conditioned eyeblink learning is formed and stored without cerebellar granule cell transmission, *104*(42). http://doi.org/10.1073?pnas.0708165104

Wassef, M., Simons, J., Tappaz, M. L., & Sotelo, C. (1986). Non-Purkinje cell GABAergic innervation of the deep cerebellar nuclei: a quantitative immunocytochemical study in C57BL and in Purkinje cell degeneration mutant mice. *Brain Research*, *399*(1), 125–35. http://doi.org/10.1016/0006-8993(86)90606-2

Witter, L., Canto, C. B., Hoogland, T. M., de Gruijl, J. R., & De Zeeuw, C. I. (2013). Strength and timing of motor responses mediated by rebound firing in the cerebellar nuclei after Purkinje cell activation. *Frontiers in Neural Circuits*, *7*(August), 133. http://doi.org/10.3389/fncir.2013.00133

Witter, L., De Zeeuw, C. I., Ruigrok, T. J. H., & Hoebeek, F. E. (2011). The cerebellar nuclei take center stage. *Cerebellum (London, England)*, *10*(4), 633–6. http://doi.org/10.1007/s12311-010-0245-y

Wolpert, D. M., Miall, R. C., & Kawato, M. (1998). Internal models in the cerebellum. *Trends in Cognitive Sciences*, *2*(9), 338–47. Retrieved from http://www.ncbi.nlm.nih.gov/pubmed/21227230

Yamamoto, F., Sato, Y., & Kawasaki, T. (1986). The neuronal pathway from the flocculus to the oculomotor nucleus: an electrophysiological study of group y nucleus in cats. *Brain Research*, *371*(2), 350–4. Retrieved from http://www.ncbi.nlm.nih.gov/pubmed/3697763

Ylinen, A., Bragin, A., Nádasdy, Z., Jandó, G., Szabó, I., Sik, A., & Buzsáki, G. (1995). Sharp wave-associated high-frequency oscillation (200 Hz) in the intact hippocampus: network and intracellular mechanisms. *The Journal of Neuroscience : The Official Journal of the Society for Neuroscience*, *15*(1 Pt 1), 30–46. Retrieved from http://www.ncbi.nlm.nih.gov/pubmed/7823136

Zanjani, H. S., Vogel, M. W., Delhaye-Bouchaud, N., Martinou, J. C., & Mariani, J. (1996). Increased cerebellar Purkinje cell numbers in mice overexpressing a human bcl-2 transgene. *The Journal of Comparative Neurology*, *374*(3), 332–41. http://doi.org/10.1002/(SICI)1096-9861(19961021)374:3<332::AID-CNE2>3.0.CO;2-2

Zeilhofer, H. U., Studler, B., Arabadzisz, D., Schweizer, C., Ahmadi, S., Layh, B., … Fritschy, J. M. (2005). Glycinergic neurons expressing enhanced green fluorescent protein in bacterial artificial chromosome transgenic mice. *Journal of Comparative Neurology*, *482*(2), 123–141. http://doi.org/10.1002/cne.20349

Zhang, X.-Y., Wang, J.-J., & Zhu, J.-N. (2016). Cerebellar fastigial nucleus: from anatomic construction to physiological functions. *Cerebellum & Ataxias*, *3*(1), 9. http://doi.org/10.1186/s40673-016-0047-1

Zhou, H., Lin, Z., Voges, K., Ju, C., Gao, Z., Bosman, L. W. J., … Schonewille, M. (2014). Cerebellar modules operate at different frequencies. *eLife*, *2014*(3), 1–18. http://doi.org/10.7554/eLife.02536

7 Résumé de thèse en français

1. Introduction

Le cervelet est une structure du système nerveux central, qui joue un rôle essentiel dans l'intégration sensorielle et motrice chez les vertébrés. Historiquement, des observations cliniques ont démontré son implication dans le contrôle musculaire. En effet, chez de nombreux patients, des lésions du cervelet étaient associées à des faiblesses musculaires et des contractions anormales. Ultérieurement, de nombreuses découvertes ont confirmé l'implication du cervelet dans le contrôle mais également dans l'apprentissage et la coordination musculaire à l'origine des mouvements du corps. Ces mouvements peuvent être très complexes et requièrent une coopération dans le temps de nombreux muscles en fonction de l'état du corps. Pour ce faire, le cervelet intègre des informations somato-sensorielles, vestibulaires, visuelles et auditives ainsi que les commandes motrices. Puisque les mouvements complexes se décomposent en plusieurs étapes, le cervelet prédit en séquence les futurs états sensoriels du corps. Cette prédiction est comparée avec le retour sensoriel immédiat (rétrocontrôle sensoriel) permettant la détection d'éventuelles erreurs (Wolpert et al., 1998; Bastian, 2006). Le calcul d'erreurs de prédiction permet d'assurer un meilleur contrôle du mouvement au cours de son exécution (Thach et al., 1992; Jueptner & Weiller, 1998). Par conséquent, on peut considérer le cervelet comme un co-processeur fonctionnant en parallèle du reste du cerveau (D'Angelo & Casali, 2012). De ce fait, il serait impliqué dans une multitude de tâches opérant en boucles d'interactions avec d'autres parties spécifiques du cerveau ce qui le rend non seulement impliqué dans la coordination motrice mais aussi dans des tâches cognitives.

Bien que l'on connaisse le fonctionnement du cervelet dans ses grandes lignes, les mécanismes du traitement des informations par les réseaux du cervelet sont encore méconnus. Les entrées extra-cérébelleuses, composées des fibres moussues, en provenances de divers noyaux pré cérébelleux, et les fibres grimpantes issues de l'olive inférieure se connectent au cortex cérébelleux et aux noyaux cérébelleux profonds (DCN). La connectivité fonctionnelle des entrées sensorielles du cortex cérébelleux (Valera et al. 2016) permet un traitement sélectif de ces informations au sein de micro-zones (Voogd & Glickstein, 1998; De Zeeuw et al., 2011). L'information ainsi traitée converge vers les cellules principales du cortex cérébelleux, les cellules de Purkinje (PC), des cellules inhibitrices

constituant l'unique voie de sortie du cortex cérébelleux. Les DCN représentent le point de convergence de toutes les informations, et constituent la sortie du cervelet. Cependant, contrairement au cortex cérébelleux, la connectivité fonctionnelle au sein des DCN est peu décrite et les mécanismes de traitement de l'information nerveuse restent encore inconnus.

Les DCN représentent une faible partie du volume total du cervelet, mais du à un grand taux de convergences de projections, reçoivent une importante quantité de connexion synaptiques. Le traitement de l'information par les cellules des DCN a été caractérisé dans quelques études princeps (Rowland & Jaeger, 2008; Hoebeek et al., 2010; Blenkinsop & Lang, 2011 and Bengtsson & Jörntell, 2014) montrant des réponses complexes issues de la double intégration inhibitrice (du cortex cérébelleux) et excitatrice (des entrées extra-cerebelleuses). Remarquablement, d'autres études ont décrit plusieurs modes opérationnels des PC démontrant ainsi un codage temporel précis allant de l'occurrence et la synchronisation temporelle (Person & Raman, 2012) à une modulation codée en fréquence (Armstrong & Edgley, 1984; Thach, 1968). Néanmoins, l'interaction de ces deux modes de codage dans un environnement physiologiques reste méconnue.

Afin de comprendre le fonctionnement physiologique des DCN, il est capital de caractériser ses différents sous-types neuronaux. En plus des cellules principales de sortie, plusieurs études in-vitro ont identifié d'autres groupes de neurones au sein des DCN. Par exemple, une étude récente a identifié une sous-population de cellules nucleo-corticales possédant des connexions collatérales locales (Ankri et al., 2015). Ces neurones ont un énorme poids inhibiteur sur autres cellules locales (Husson et al., 2014) et affectent dramatiquement le traitement de l'information en sortie des DCN. Par conséquent, étudier comment les différents éléments neuronaux des DCN fonctionnent de concert in-vivo est capital pour comprendre comment le cervelet transforme le message sensori-moteur à sa sortie.

2. Objectifs and technique

Dans le cadre de mon projet, nous avons caractérisé in vivo les différents types cellulaires qui composent les DCN, ainsi que la modulation assurée par les PC sur ces cellules. Nous avons utilisé une souche murine génétiquement modifiée (L7-ChR2) développée dans notre laboratoire (Chaumont et al, 2013), et qui permet une stimulation optogénétique efficace des CP qui expriment de manière spécifique la ChannelRhodopsine2. Des stimulations lumineuses de différentes intensités et fréquences nous on permit d'augmenter progressivement la fréquence de décharge des PC in vivo. Grâce à l'enregistrement électrophysiologique multi unitaire, nous avons enregistré les deux zones du cervelet simultanément : le cortex et les DCN. Différents niveaux d'excitation des PC ont été

enregistrés, de même que différents niveaux d'inhibition dans les DCN. Les électrodes d'enregistrement utilisées, formées de 4 tétrodes, nous on permis d'enregistrer plusieurs cellules simultanément.

3. Résultants

Nous avons ainsi enregistré 39 cellules provenant de la partie médiane des DCN (13 animaux, 25 sites d'enregistrement), regroupées en 2 groupes après analyse selon des différences significatives dans la forme des potentiels d'action et de fréquence de décharge. Ces différences sont corrélées à l'identité neurochimique des cellules composant les DCN (GABAergiques vs non-GABAergiques) caractérisées in vitro (Uusisaari et al, 2007). 56% des cellules enregistrées dans les DCN (groupe 1) présentaient des potentiels d'action rapides (0,18+/-0,01ms) couplés à une fréquence de décharge élevée (63,9+/-5,0Hz), et représentent potentiellement les cellules non-GABAergiques, principales composantes des DCN. Les autres cellules enregistrées (groupe 2) possèdent des potentiels d'action plus lents (0,22+/-0,02ms) et une fréquence de décharge plus faible (23,2+/-4,7Hz) que les cellules du groupe 1. Ce deuxième groupe représenterait les cellules GABAergiques des DCN (cellules nucléo-olivaires et nucléo-corticales). Ces 2 groupes, au mieux de notre connaissance, représentent le premier enregistrement simultané et la première discrimination in vivo des différentes cellules composant les DCN.

Les différences de taux de décharge enregistrés *in vivo* et *in vitro* peuvent être la conséquence de la coupe des afférences (en tranche) ou de l'exposition à la température ambiante. Les largeurs de potentiel d'action *in vivo* ont été estimées en somme des demi-largeurs des pics positifs et négatifs des formes d'onde extracellulaires qui étaient plus faibles mais proportionnelles aux largeurs de potentiel d'action obtenues *in vitro*. Des études *in vitro* antérieures ont défini cinq types différents de cellules appartenant aux DCN, qui se répartissent en deux groupes principaux mentionnés ci-dessus. Le premier groupe était les cellules non-GABAergiques, majoritaires et projetant vers le cortex pré moteur. On trouve également des cellules glycinergiques (Bagnall et al., 2009) et des interneurones non inhibiteurs (Uusisaari et al., 2007) qui restent peu étudiés à ce jour. Le second groupe est quant à lui composé des cellules DCN GABAergiques (voir Introduction, section 1.5.3).

Dans mes enregistrements des DCN, les oscillations détectées ont été moyennées par cellule (n=39) et compares par séquences de 250 secondes d'enregistrement (exprimées en pourcentage, voir Figure 28 D). De manière intéressante, la durée d'oscillation la plus longue a été observée dans la bande delta et thêta ; cette bande comprenant des basses fréquences allant jusqu'à 10Hz. Des fréquences d'oscillation plus élevées ont été détectées, mais uniquement pour des oscillations plus courtes allant

au maximum jusqu'à 5% du temps d'enregistrement. La durée de ces oscillations est significativement différente d'une bande de fréquence à l'autre (p-value <0.05) sauf pour les bandes beta et gamma (Figure 28 D). Le pourcentage médian de la durée des oscillations des bandes beta et gamma sont respectivement de 1.73% et 1.18% sans différence significative entre ces deux groupes (Mann–Whitney $U = 404.0$, n1 = n2 = 29, $P = 0.40$). Il n'y a pas de synchronisation de phase dans l'activité des DCN sur ces deux bandes de fréquence. La littérature rapporte que ces oscillations sont liées à la communication des DCN avec d'autres aires cérébrales (Ros et al., 2009, Courtemanche et al., 2013). Ainsi, l'absence de synchronisation de phase des oscillations lentes dans le DCN n'est pas surprenante. Grace aux enregistrements multiélectrode j'ai pu mesurer des oscillations provenant de deux tétrodes distinctes implantées directement dans le DCN. Ces tétrodes ayant un écart maximal de 300µm, mes enregistrements électriques se situent à une échelle intermédiaire au sein de cette structure.

Un plus grand pourcentage de cellules était en relation de phase avec les oscillations des bandes à haute fréquence et de la bande gamma (Groupe 1 :65% et 88%, Groupe 2 : 83% et 67% respectivement). Contrairement aux basses fréquences, ces oscillations sont décrites comme étant des interactions locales transitoires (Buzsáki and Silva, 2012) qui, en accord avec mes conditions d'enregistrement, sont très locales (entre les tetrodes espacées de de 300µm). Comme prévu, les oscillations enregistrées dans les bandes gamma et autres hautes fréquences étaient de courte durée (entre 2 et 5% du temps total respectivement) et transitoires. A l'avenir, d'autres analyses devront concerner des conditions ou les deux groupes de cellules sont en synchronisation de phase avec les oscillations de champ à haute fréquence.

La synchronisation de la décharge des PC est connue pour induire l'activité synchrone des DCN par l'inhibition corticale, qui peut déterminer la sortie du cervelet. Cependant, dans une étude précédente (Pearson et Raman, 2012), aucune distinction entre les cellules des DCN n'était possible. Nous avons étudié cet effet dans les deux groupes de cellules décrits précédemment : la stimulation à fréquence fixe des PC inhibe 95% des cellules des DCN. De manière surprenante, 100% des cellules du non-GABAergiques (groupe 1) déchargent de manière synchrone avec la stimulation des PC, contre seulement 24% des cellules GABAergiques (groupe 2, test de Rayleigh de distribution non uniforme, p<0,01). Nos résultats montrent également que l'inhibition corticale par les PC assure un contrôle inhibiteur progressif sur la fréquence de décharge des DCN mais ne contrôle pas de manière temporelle les cellules GABAergiques qui assurent l'inhibition locale vers les cellules principales. Ainsi, nous postulons que les mêmes entrées corticales, les PC, contrôlent les cellules de projection principale via un codage temporel et de fréquence alors que l'inhibition locale ne le fait que par la

fréquence. Néanmoins, les cellules GABAergiques semblent être dirigées de manière plus précise par les entrées extra cérébelleuses, plutôt que par l'inhibition locale.

Une autre distinction entre les cellules GABAergiques et non-GABAergiques in vitro est leur capacité à décharger dans une large gamme de fréquences. Des injections de courant peuvent entrainer une décharge à 200Hz des cellules non-GABAergiques tandis que les cellules GABAergiques ne peuvent décharger qu'à 50 Hz maximum (Uusisaari et Knöpfel, 2008). Ce comportement a été testé *in vivo* par des stimulations aléatoires suivant une loi de Poisson. Ce protocole comprenait des impulsions de stimulation entre 5 Hz et 210 Hz et les capacités des cellules DCN à répondre dans ces fréquences ont été testées. Sur la figure 35 A-B, on a représenté des histogrammes de fréquence de déclenchement instantanée normalisée (IFF) pour 2 exemples (cellule A et cellule B, en rouge et en bleu), recouvert par l'histogramme des fréquences de stimulation PC en gris. La cellule A peut se décharger sur une large gamme de fréquences allant jusqu'à 200 Hz (Figure 35 A, rouge), tandis que la Cellule B décharge seulement dans une bande étroite jusqu'à 50 Hz (Figure 35 B, bleue). On a observé les mêmes résultats dans le graphique de répartition cumulative (figure 35 C), où les fréquences de décharge instantanées de la cellule A (rouge) étaient similaires aux fréquences de stimulation (noire) et la cellule B n'avaient que des basses fréquences. Dans l'étape suivante, les histogrammes de fréquence de décharge instantanés normalisés de cellules ont été comparés avec l'histogramme de la stimulation en utilisant un test de Kolmogorov-Smirnov. La cellule A ne montre pas de distribution IFF significativement différente par rapport à la stimulation attendue ($p = 0,14$) alors que la cellule B présente une différence significative ($p < 0,01$). Comme pour la cellule A, la plupart des cellules du groupe 1 (16 sur 22) ont atteint un pic à des fréquences similaires avec la fréquence de stimulation (figure 35 D). La plupart des cellules du groupe 2, comme cela a été observé pour la cellule B, d'autre part, n'ont pas augmenté à ces fréquences et le test de Kolmogorov-Smirnov a été rejeté ($p < 0,01$), (figure 35 D). Les cellules du groupe 1 peuvent suivre la synchronisation des PC jusqu'à 200 Hz et les cellules du groupe 2 ne peuvent pas suivre l'activité du PC. Il est intéressant de noter qu'une telle stimulation à haute fréquence de PC peut encore évoquer un accrochage temporisé dans leurs cellules DCN efférentes, principalement les cellules de projection principales représentées dans le groupe 1.

Dans mes expériences, 22 paires de cellules ont été enregistrées simultanément. Malheureusement, seulement trois d'entre elles concernaient des cellules provenant des différents groupes (Une cellule du groupe 1 et une du groupe 2). Deux paires provenaient de la même tétrode et une de deux tetrodes adjacentes (avec 150µm d'écart). Afin d'étudier des possibles relations de décharge entre ces cellules nous avons effectué des analyses de cross-corrélation de leur activité. Nous espérions tout particulièrement mettre en évidence des connexions inhibitrices locales sur les cellules principales du

DCN (Groupe 1) depuis les cellules nucléo-corticales (Groupe2). Malheureusement, aucune relation n'a été tirée des cross-corrélations que ce soit dans les conditions de ligne de base ou après les différents protocoles de stimulation (une paire est donnée Figure 36). Les cellules enregistrées simultanément n'ayant pas d'activité corrélée, nous discuterons de cette absence de corrélation en discussion.

4. Conclusion

Par conséquence, ceci suggère un mécanisme compétitif entre le codage par fréquence de l'inhibition corticale et le codage temporel des entrées extra cérébelleuses. D'autres pistes doivent être explorées pour comprendre la contribution de l'inhibition locale à la formation du message de sortie du cervelet. Cette étude démontre l'importance des circuits neuronaux des DCN, en démontrant l'existence de différents mécanismes de codage de l'information propres aux différentes cellules des DCN. Les entrées synaptiques sont ainsi intégrées de manière différentielle pour générer le signal de sortie des DCN.

L'absence de contrôle temporel des cellules GABAergiques au sein du DCN renforce la synchronicité de l'activité de décharge des cellules non-GABAergiques. Puisque les cellules nucléo-corticales (GABAergiques) ne sont pas contrôlées dans le temps, leur inhibition locale n'est pas « *time-locked* » (Figure 37B). Ainsi, les cellules principales (non-GABAergiques), en sortie des DCN, ne sont pas contrôlées par l'inhibition suite à une stimulation. Cependant, l'inhibition locale peut être réduite via l'activation des PC en entrée du DCN. Cette levée d'inhibition est capable de renforcer la capacité des cellules principales à coder une information dans le temps.

Characterization of the Purkinje cell to nuclear cell connections in mice cerebellum

Orçun Orkan ÖZCAN

PhD Thesis Summary

The cerebellum integrates motor commands with somatosensory, vestibular, visual and auditory information for motor learning and coordination functions. The deep cerebellar nuclei (DCN) generates the final output by processing inputs from Purkinje cells (PC), mossy and climbing fibers. We investigated the properties of PC connections to DCN cells using optogenetic stimulation in L7-ChR2 mice with *in vivo* multi electrode extracellular recordings in lobule IV/V of the cerebellar cortex and in the medial nuclei. DCN cells discharged phase locked to local field potentials in the beta, gamma and high frequency bands. We identified two groups of DCN cells with significant differences in action potential waveforms and firing rates, matching previously discriminated *in vitro* properties of GABAergic and non-GABAergic cells. PCs inhibited the two group of cells gradually (rate coding), however spike times were controlled for only non-GABAergic cells. Our results suggest that PC inputs temporally control the output of cerebellum and the internal DCN circuitry supports this phenomenon since GABAergic cells do not induce a temporal effect through local inhibition.

Keywords: Cerebellum, optogenetic stimulation, deep cerebellar nuclei, Purkinje cells, local inhibition, GABAergic interneurons, Glutamatergic projection cells, in vivo electrophysiology, rate coding, temporal coding, L7-ChR2 mice

Résumé

Le cervelet permet l'apprentissage moteur et la coordination des mouvements fins. Pour ce faire, il intègre les informations sensorielles provenant de l'ensemble du corps ainsi que les commandes motrices émises par d'autres structures du système nerveux central. Les noyaux cérébelleux profonds (DCN) constituent la sortie du cervelet et intègre les informations provenant des cellules de Purkinje (PC), des fibres moussues et des fibres grimpantes. Nous avons étudié les connexions fonctionnelles entres les PC et les DNC *in vivo*, grâce à une stimulation optogénétique des lobules IV/V du cortex cérébelleux et à l'enregistrement multi unitaire du noyau médian. Nous avons ainsi identifié deux groupes de cellules au sein des DCN, présentant des caractéristiques propres au niveau de leur fréquence de décharge et de la forme des potentiels d'action, en accord avec la dichotomie établie par une précédente étude *in vitro* permettant de séparer les neurones GABAergiques des autres neurones. Nos résultats suggèrent que les PC contrôlent la sotie du cervelet d'un point de vue temporel. De plus, la ciruiterie interne des DCN conforte ce résultat de part le fait que les cellules GABAergiques ne produisent pas d'effet temporel au travers de l'inhibition locale.

Mots clés: Cervelet, optogénétique, Noyaux cérébelleux profonds, cellules de Purkinje, inhibition locale, inter neurones GABAergiques, Cellules de projection glutamatergiques, électrophysiologie *in vivo*, codage temporel, codage de fréquence, souris transgénique L7-ChR2